

BULGARIAN CHEMICAL COMMUNICATIONS

2021 Volume 53 / Special Issue D

Selected papers from the International Chemical Engineering Conference 2021
“100 Glorious Years of Chemical Engineering & Technology”, Department of
Chemical Engineering, Dr. B. R. Ambedkar National Institute of Technology,
Jalandhar, Punjab, India, September 16 to 19, 2021

*Journal of the Chemical Institutes
of the Bulgarian Academy of Sciences
and of the Union of Chemists in Bulgaria*

Review of lead flows in the anthropogenic environment

M. Gupta, A. Kumar*, S. Kumar

Malaviya National Institute of Technology Jaipur, Jaipur-302017, India

Received: November 11, 2021; Revised: January 01, 2022

MFA (material flow analysis) is a common approach for assessing stocks and fluxes of material and substances in the environment. MFA has demonstrated over the last many years that it improves understanding of the sources and sinks of the metal-containing goods. This article shows the in-depth analysis of the literature related to flow of lead in the environment. The review describes the significant inflows, outflows, and stocks of lead, based upon eighteen MFA studies done at various geographical levels throughout the world. The information compiled on major fluxes and stocks at various geographical scales may be used to improve future studies aimed at quantifying flows of lead. The insights presented in here may also guide the policy and management choices for lead for a city or region. [copyright information to be updated in production process].

Keywords: Material flow analysis; lead; flow; stock

INTRODUCTION

Lead is a naturally occurring substance and the world's lead deposits have been estimated to be 90 million tons by lead content [1]. Australia controls 40% of the world's reserves, followed by China (20%), Russia and Peru (7% each), Mexico and the United States (6% each), and so on [2]. According to [1], worldwide production of lead in terms of metal composition was around 4.8 million tons in 2018, which is roughly identical to the amount produced in 2017. The country with the greatest production capacity is China, having an estimated yearly production of 2.28 million tons (48 % of world production). They are followed by Australia (9%), Peru (6%), the United States and Mexico (5% each), Russia and India (4% each) [1].

India is home to large lead reservoirs with its annual production of 265,651 tons of lead concentrates in the year 2019. Rajasthan is the only state responsible for whole lead production in India (IBM, 2020). Till 2018, India was the net importer of lead [1]. In 2019, India has started exporting lead because of the increase in mining activities in the country [3]. Lead is totally recyclable and retains its qualities after recycling. Lead recycling is a growing sector in the country. However, because informal lead recycling poses a health concern, the lead recyclers are required to obtain permit from Central Pollution Control Board to assure compliance with environmental standards.

Lead is a heavy metal that has been linked to cancer in humans. Anemia, weakness, renal and brain damage are just a few of the adverse

consequences that occur in individuals exposed to extremely high levels of lead. Lead exposure at exceptionally higher levels can be lethal. As lead may cross the placental barrier, pregnant women exposed to it risk harming their unborn child as well. Lead is hazardous to an infant's developing nervous system [4, 5].

So, lead is widely used in a number of products and has the potential of affecting the human health and the environment. As a result, it becomes important to understand the flow of Pb. However, there has not been any systematic review elaborating on lead flows in the anthropogenic environment. This study attempts to fill this gap in literature.

The objective of the study is to critically review the flows of lead in the environment. The study aims to identify the key sectors, key inflows and outflows and key stocks important for the studies of Pb flow.

Materials and methods

This study is based on the review of the literature published till May 2021. For the literature, the search was made on the websites of the following publishers: Elsevier, Wiley, and SAGE Publications. The searches were also made on Google Scholar platform. Eighteen studies related to Pb flow were finally chosen for this assessment based on the following criteria: (i) studies using MFA as a method; (ii) studies being conducted at any spatial scale; (iii) studies estimating lead flows over one or more than one year of time-period. There were mainly three geographical scales found among these studies: (i) smaller system (e.g. a waste treatment plant), (ii) city level and, (iii) region level.

* To whom all correspondence should be sent:
E-mail: amitrathi.ucf@gmail.com

RESULTS AND DISCUSSION

Critical sectors of Pb flow

Any Pb flow analysis will produce a result based on how the system is described in terms of the spatial scale and the main sectors responsible for Pb flow. The critical sectors for Pb flow vary at different geographical scales (Table 1). The different geographical levels may be smaller system, city level, region level.

Based on the assessment of the literature, a smaller system may consist of a university campus, treatment units (e.g., wastewater treatment plants and solid waste treatment facilities), and waste utilization units (composting units, smelting plants). In smaller systems, primary sectors may vary

depending upon type of the treatment facilities. At the city scale, the primary sectors of Pb flow are private residences, waste treatment units (wastewater treatment plants or solid waste treatment facilities), landfills, and various categories of soil (e.g. agriculture soil, urban soil).

The region scale is much larger than the city level and often encompasses Pb mining and import sectors. At regional level, the key sectors include housing, agriculture, and industry along with Pb mining and import sectors. On a region level, the production of Pb *via* mining ores is a critical sector, and the primary distinction between city and region scales is the presence of this field. However, sometimes production sector is included at the city-level as the production units are in the city.

Table 1. Multiple diverse sectors across various geographical scales

Geographical Scale (Ref.)	Location, Country	Type of system	Year of flow	Key Sectors
Smaller System [4]	MNIT Jaipur, India	Anthropogenic System	2019	Public Household, WWTP
Smaller System [6]	Smelting Plant, China	Anthropogenic System	2013	Palletisation, Blast furnace, Primary Smelting
Smaller System [7]	Avedore WWTP, Denmark	Wastewater system	2011	Pre-treatment, Primary treatment, anaerobic digester
City [9]	Hitachi, Japan	WEEE management	2010	Agriculture soil, Forest soil, Urban soil, Households, Landfill, Industry
City [10]	Norrkoping, Sweden	Recovered Waste wood Management	2002	Biofuel boiler, Waste Incinerators
Region [8]	Swiss region, Switzerland	Anthropogenic System	1987	Household, Industry, Agriculture soil
Region [11]	Malaysia	Wastewater system	2019	Klang River, Treatment Plant
Region [12]	China	Lead Acid Batteries	2018	Lead Rod/Mixer factory, Battery factory, Customer, All collection
Region [13]	China	Anthropogenic System	2015	Primary lead, Batteries, Old scrap
Region [14]	China	Anthropogenic System	2014	Lead Acid Batteries (LAB) production, LAB use, recycling
Region [2]	Korea	Anthropogenic System	2014	Lead ore
Region [15]	China	Anthropogenic System	2010	Production, Use
Region [16]	China	Anthropogenic System	2010	Production, Use
Region [17]	Japan	Anthropogenic System	2007	Raw material, Material production, recycling
Region [18]	Austria	Anthropogenic System	2005	Industry business service, PHH, Waste management
Region [19]	China	Anthropogenic System	1999	Lead concentration, Refined lead, Manufacturing of LAB
Region [20]	Denmark	Anthropogenic System	1994	Batteries, building materials, cable sheets
Region [21]	Switzerland	Waste Management System	1988	Agriculture soil, Forest soil, Urban soil, Households, Landfill, Industry

Key inflows

It is crucial to know the major inflows at various geographical scales to establish the priorities for control of Pb. Table 2 summarizes this information in terms of geographical and temporal dimensions, system type, total inflow, important inflows, and sectors receiving the inflows.

The largest Pb influx to the city scale happens because of imported commodities. In a city-scale study that examined the Pb flow through the WEEE system in Hitachi (Japan) for 2010 [9], it was found that nearly 90% of the total Pb inflow is from used cars and scrap metals. For Pb contaminant fluxes in cities, the private residences and industries are the two important contributors to the influx of Pb. This highlights the importance of understanding all the Pb consumption scenarios, including any household-level emissions. At the household level, the input flow is generally computed from the mass balance using the emissions through wastewater and solid waste. In this approach, the stocks of Pb in the public household are neglected in almost all the studies.

While global trade for consumer products and used automobiles is a significant contributor to the Pb inputs to the environment, other key Pb input pathways occur at a regional scale. As an example, in a research conducted on Swiss area (Switzerland)

which focused on the industrial sector, as well as the products consumption sector, over 97% of the total inflow was found to occur through used automobiles [8]. According to the results of [2], about 67% of the overall intake in the Pb flow occur through the anthropogenic system originating from mineral ore in the territory of Korea. In China, a countrywide scale study on the lead acid batteries management system [12], lead rod has been found as the primary input, where it accounts for almost 100% of the overall input in 2018. This study did not consider other important sectors, e.g. public household. It can be inferred that in the absence of availability of mineral ore for Pb production, the predominant Pb inflow to the country is either lead rods or used automobiles, whereas the presence of mineral ore in a country makes it the predominant Pb inflow.

Key outflows

Table 3 depicts an analysis of the major outflows of lead at various geographical scales. Industry-related products accounted for about 82 percent of output in Hitachi (Japan) in 2010 [9]. Outflow of lead emissions to air, water and soil from industrial production is unproductive and may be posing a serious public health concern for the people in the surrounding environment.

Table 2. Key inflows across various geographical scales

Geographical Scale (Ref.)	Measuring units	Total inflow quantity	Key inflows	% of total inflow
Smaller System [4]	Kg/year	53	Import of Private households and Inflow to sewer system	100%
Smaller System [6]	Tons/ton of product	1.2472	Palletization	87%
Smaller System [7]	Ton/day	0.000926	Influent to Pre-treatment	100%
City [9]	Tons	338	Used cars and scrap metals	88%
City [10]	Kg	24000	RWW	55%
Region [8]	Tons/year	340	Consumer goods, used cars	100%
Region [11]	Kg/year	3817547	Penchala River	62%
Region [12]	Tons/year	161050	Lead Rod/Mixer Factory	100%
Region [13]	Kt	4073	Ore to concentrate, Import to concentrate	90%
Region [14]	Tons	308.86	Lithosphere to mining, import to smelting	100%
Region [2]	Tons	96845	Import of lead ore, metal products	65%
Region [15]	Kt	3880.8	Lithosphere to production	100%
Region [16]	Kt	3137	Lithosphere to production	59%
Region [17]	Kt	242.4	Import to Raw Material and Interim product production	77%
Region [18]	Kt/year	49	Industry business service	100%
Region [19]	Kt	553.54	Lead ore	100%
Region [20]	Tons/year	15500	Raw material	60%
Region [21]	Tons/year	338	Used cars and scrap metals	88%

So, from these results, it can be concluded that the industrial sector is important in terms of Pb discharge at the city. In order to meet better Pb management goals, greater attention should be paid to the recovery and recycling of Pb from environmental emissions. It has been shown that the major outflow of Pb occurs as Pb from industrial production.

Accordingly, municipal solid waste (MSW) from private households has been recognized as the second-largest source of lead discharge in the Swiss area (Switzerland) [8]. At the region level, the type and amount of significant Pb outflows have been documented to differ significantly between countries. According to nine out of the thirteen region scale evaluations, industrial products has been identified as the most significant outflow. For example, emissions and outmoded cables account for around 34% and 46% of the total yearly outflow in China in 2014 [14] and 1999, respectively [19]. On the opposite side of the scale, 16% of the overall outflow is the export-oriented transport equipment and battery items in Korea [2]. The findings are from a region scale study [2], which examined domestic Pb flow for the year 2014 in South Korea. In 2011,

ash from incinerators being disposed of in landfills constituted a major flow of Pb in Denmark[7]. Pb emissions to air, water and soil were found to be quite significant in Sweden in 2002 [10], and in China in 2014 [14]. A comparative assessment of main Pb outflows at different geographical scales demonstrated that large quantities of Pb leave the system as industrial products and other commodities.

Key stocks

As can be seen from Table 4, the stock quantities of Pb in the system at all three levels (smaller system, city and region) account for a large percentage of the overall amount of P that entered the system. In all city-scale assessments, it was discovered that the system stores more than 50% of the entire influx of Pb. At this scale, landfills and soil have been recognized as the primary processes for Pb stocks. About 65% of the total intake of Pb has been shown to be retained within the system in six of the thirteen region scale investigations. As discussed before, it demonstrates that the end-user consumption is the primary driver of Pb stocks at the region scale.

Table 3. Key outflows across various geographical scales

Geographical Scale (Ref.)	Measuring units	Total Outflow	Key Outflows	% of total outflow
Smaller System [4]	Kg/year	28	MSW from households, outflow from storm water drain	53%
Smaller System [6]	Tons/ton of product	1	Lead Ingot from casting	81%
Smaler System [7]	Ton/day	0.000034	Ash from incinerator	4%
City [9]	Tons	277	Products from industry	82%
City [10]	Kg	400	Emission to air and water	2%
Region [8]	Tons/year	280	Products from industry	83%
Region [11]	Kg/year	3817546	Other purposes	100%
Region [12]	Tons/year	156645	Lead acid battery and unknown products	98%
Region [13]	Kt	898	Export, Products	23%
Region [14]	Tons	103.39	Products and emissions	34%
Region [2]	Tons	15101	Transportation equipment, battery and metal products	16%
Region [15]	Kt	3207.1	Production to export, Fabrication and manufacturing to export	83%
Region [16]	Kt	2153	Production to export, Fabrication and manufacturing to export	69%
Region [17]	Kt	152.8	Export from final product production	64%
Region [18]	Kt/year	46	Industry business service to PHH	94%
Region [19]	Kt	253	Obsolete cable and construction materials	46%
Region [20]	Tons/year	2610	Semi manufactures and manufactured products, scrap and other waste products	17%
Region [21]	Tons/year	280	Steel and filter products	83%

Table 4. Key outflows across various geographical scales

Geographical Scale (Ref.)	Measuring units	Total stocks	% of total inflow	Key stocks
Smaller System [4]	Kg/year	25	47%	Soil
Smaller System [6]	Tons/ton of product	0.1228	10%	N/A
Smaller System [7]	Ton/day	N/A	N/A	N/A
City [9]	Tons	N/A	N/A	Landfill and soil
City [10]	Kg	N/A	N/A	N/A
Region [8]	Ton/year	60	18%	Agriculture soil, Forest soil, Landfill
Region [11]	Kg/year	N/A	N/A	N/A
Region [12]	Tons/year	N/A	N/A	N/A
Region [13]	Kt	N/A	N/A	N/A
Region [14]	Ton	91.84	30%	Lead in use stock
Region [2]	Ton	N/A	N/A	N/A
Region [15]	Kt	1758	45%	Production and In use
Region [16]	Kt	1996	64%	Production and In use
Region [17]	Kt	N/A	N/A	N/A
Region [18]	Kt/year	2.7	6%	PHH, Waste Management
Region [19]	Kt	483.62	87%	Chemical products, LABs, Construction material and cables
Country [20]	NA	NA	NA	N/A
Region [21]	Tons/year	N/A	N/A	Landfill and soil

In China, about 64% of the entire annual influx of Pb remained inside the industrial production sector, while the other 36% of the total annual inflow of Pb ended up being exported in China in 2010 [15, 16]. Large amounts of lead are buried in landfills and land soils in Switzerland [8]. In Austria, a mass bulk of the Pb was held in private households [18]. It is obvious that on a regional and city scale, landfill and soil make up a major percent of the overall stock every year. The buildup of Pb in this manner over the course of many years might result in the soil having an excessive amount of Pb. A further complication to this problem is that runoff water can leach Pb into groundwater. Thus, rather than allowing any lead to be deposited in soil or landfill, it is preferable to recycle the substance [22]. An additional benefit of using soil Pb stockpiles for production is that it will minimize the demand for mineral lead input, which eventually helps to alleviate the problem of mineral lead shortages. As a result, future choices on Pb management at the regional and region levels should place greater emphasis on determining the Pb stock in the soil.

CONCLUSION

This study has effectively identified major Pb inflows, outflows and stocks. Our study shows that at city scale, the largest Pb influx happens as a result of imported commodities and at the region level, major inflow of lead occurs through the lead ore. At

city scale as well as region scale, landfill and soil have been identified as the major stocks of Pb.

Acknowledgement: To be presented at the *International Chemical Engineering Conference on “100 Glorious Years of Chemical Engineering & Technology” from September 17 to 19, 2021, organized by the Department of Chemical Engineering at D. B. R. Ambedkar NIT Jalandhar, Punjab, India (Organizing Chairman: Dr. Raj Kumar Arya & Organizing secretary: Dr. Anurag Kumar Tiwari).*

REFERENCES

1. IBM, Indian Minerals Yearbook 2019, Part II, 2020.
2. K. P. Jeong J. G. Kim, *J. Mater. Cycles Waste Manag.*, **20** (2), 1348 (2018), doi: 10.1007/s10163-017-0649-6.
3. USGS, Lead in February 2021, 2021.
4. A. Agarwal, A. Kumar, S. Dangayach, in: *Advances in Energy and Environment. Lecture Notes in Civil Engineering*, vol. **142**, R. Al Khaddar, N. D. Kaushik, S. Singh, R. K. Tomar (eds.) Springer, Singapore, 2021.
5. J. Johnson, L. Schewel, T. E. Graedel, *Environ. Sci. Technol.*, **40**(22), 7060 (2006), doi: 10.1021/es060061i.
6. L. Bai, Q. Qiao, Y. Li, M. Xie, S. Wan, Q. Zhong, *J. Clean. Prod.*, **104**, 502 (2015), doi: 10.1016/j.jclepro.2015.05.020.
7. H. Yoshida, T. H. Christensen, T. Guildal, C. Scheutz, *Chemosphere*, **138**, 874 (2015), doi: 10.1016/j.chemosphere.2013.09.045.

8. P. H. Brunner, H. Rechberger, Practical handbook of material flow analysis, Boca Raton, FL, USA: Lewis Publishers, 2016.
9. M. Oguchi, H. Sakanakura, A. Terazono, H. Takigami, *Waste Manag.*, **32**(1), 96 (2012), doi: 10.1016/j.wasman.2011.09.012.
10. J. Krook, A. Mårtensson, M. Eklund, *Resour. Conserv. Recycl.*, **52**(1), 103 (2007), doi: 10.1016/j.resconrec.2007.03.002.
11. N. R. Shahbudin, N. A. Kamal, *Ain Shams Eng. J.*, (2020), doi: 10.1016/j.asej.2020.10.009.
12. W. Suriyanon, N. Jakrawatana, N. Suriyanon, *Material Flow Analysis of Lead in Lead Acid Batteries Supply Chain Toward Circular Economy*, **34**(3), 55 (2020).
13. W. Liu, Z. Cui, J. Tian, L. Chen, *J. Clean. Prod.*, **205**, 86 (2018), doi: 10.1016/j.jclepro.2018.09.088.
14. S. Chen et al., *Energies*, **10**(12) (2017), doi: 10.3390/en10121969.
15. J. Liang, J. S. Mao, *Trans. Nonferrous Met. Soc. China, English Ed.*, **24**(4), 1125 (2014), doi: 10.1016/S1003-6326(14)63171-X.
16. J. Liang, J. S. Mao, *Trans. Nonferrous Met. Soc. China, English Ed.*, **25**(4), 1262 (2015), doi: 10.1016/S1003-6326(15)63724-4.
17. Sh. Ando, S. Murakami, J. Yamatomi, *Journal MMIJ*, **126**(8), 6 (2010).
18. H. Reisinger et al., *Österr. Wasser- und Abfallwirtschaft*, **61**(5–6), 63 (2009), doi: 10.1007/s00506-009-0080-x.
19. J. S. Mao, Z. F. Yang, Z. W. Lu, *Trans. Nonferrous Met. Soc. China, English Ed.*, **17**(2), 400 (2007), doi: 10.1016/S1003-6326(07)60106-X.
20. E. Hansen, C. Lassen, *J. Ind. Ecol.*, **6**(3–4), 201 (2003), doi: 10.1162/108819802766269601.
21. P. H. Brunner, H. Rechberger, Practical Handbook of Material Flow Analysis, Boca Raton, FL, USA: Lewis Publishers, 2004.
22. T. E. Graedel et al., UNEP (2011) Recycling Rates of Metals – A Status Report, 2011.

Enhancement of low-temperature impact toughness of polycarbonate by hydroxyl terminated siloxanes and its concomitant effects on other properties

J. N. Srivastava^{1,2*}, S. K. Gupta²

¹Defence Materials and Stores Research & Development Establishment, GT Road, Kanpur (UP), India-208013

²Harcourt Butler Technical University, Nawabganj, Kanpur (UP), India-208002

Received: October 13, 2021; Revised: January 07, 2022

Modification of commercial grades of polycarbonate (PC) to the specific grades required for a particular end application along with optimized processing conditions has now become inevitable keeping in view the present cost, time and technological challenges. An effective and simpler method has been developed to enhance the properties of PC by reactive blending with siloxanes terminated with a reactive group. The work presented here has very good results with respect to enhancement of low-temperature (-30°C) impact strength of PC by incorporating hydroxyl terminated poly dimethyl siloxane (PDMSOH). PC after reactive blending with PDMSOH at certain processing conditions changes properties as concentration and viscosity of PDMSOH is varied. It was observed that modification of impact toughness by this method also had concomitant effects on other properties, e.g. tensile strength, tensile modulus, optical transmittance and haze. Dependence of change in properties on both or either viscosity and concentration of PDMSOH was also observed. Impact toughness at low temperature was improved up to 655 J/m at -30°C, i.e. up to 428% by increasing both concentration and viscosity of PDMSOH whereas tensile strength and tensile modulus showed a peculiar behaviour. Optical transmittance and haze were however influenced by only < 7% and < 5%, respectively, just by changing the concentration of PDMSOH and there was hardly any change with respect to its viscosity. Results obtained may be useful in selecting and modifying PC for an end application at sub-zero temperature. The material was characterised by Izod impact tester, SEM, capillary viscometer, tensile tester, transmittance and haze tester.

Keywords: Impact toughness, Sub-zero temperature, Polycarbonate, Tensile strength, Transmittance

INTRODUCTION

Polycarbonate (PC) is a widely used engineering thermoplastic having excellent impact resistance, high optical transmittance [1] and good thermal stability. The material however starts losing its impact toughness at around -20°C temperature [2]. Enhancement of properties by blends and copolymers of PC have been extensively studied in the past few decades [3-8]. Impact modification for low temperature of PC has been attempted by researchers using different methods but they generally lead to some adverse effects on other mechanical, optical and thermal properties [9-12]. Copolymerising bisphenol-A with siloxanes of different molecular weight by interfacial copolymerisation using phosgene, had been traditionally done and a few grades of such copolymers are commercially available. These block copolymers though enhanced the impact strength of PC at sub-zero temperature because of strong separation of micro-phases of polycarbonate and siloxane blocks but there was a considerable reduction in tensile strength. Such commercially available copolymers are there only with a very few grades, probably because their requirements are quite specific and lower in volume. First reactive blending of siloxane with polycarbonate in melt state

was done by Hawkins *et al.* using carboxylic acid terminated siloxanes [11]. Later siloxanes functionalised with aryl amino group and hydroxyl aryloxy terminated PDMS were also used for reactive blending with polycarbonate [13,14]. Physical blending of siloxane with PC results in formation of larger domains of siloxane of size bigger than 10 µm whereas in reactive blending siloxane domains are much smaller and are in the size range of less than 3 µm to sub-micron sizes. Larger domain size clearly indicates the immiscibility of the two materials and the same is reflected in the end properties of the blended PC. Solubility of siloxanes in PC is very low, hence there is a clearly visible phase separation in the physical blends that can even be observed as a layer of silicon oil on the surface of PC. Miscible and immiscible blends can thus be distinguished by the morphology and domain size of siloxane blocks. Though the researchers have made good progress in reactive blending, yet there is ample scope of further work with respect to development of structure-property relationship, optimised conditions and reaction mechanism. Reactive blending as compared with conventional interfacial copolymerisation is a much simpler, less complex and efficient method to modify the properties of polycarbonate. It is also

* To whom all correspondence should be sent:

E-mail: jn_sri@rediffmail.com

a very useful and cost-effective method for converting smaller volumes of PC to a grade having desired properties, as manufacturers of PC are generally conservative in developing the copolymers PC and siloxanes required in smaller quantities.

It is therefore essentially required to develop such methods that can enhance the property of a commercially available grade of PC meeting the requirement of processing and end application. Blending of PC with other polymers and additives using a compatibilizer could be one way of doing such modification but it is observed that blends of PC have adverse effects on other properties, e.g. optical transmittance, tensile strength and surface finish, etc. Phase stability and miscibility in PC blends is also very limited and generally adequate only to some extent to meet the requirement of desired property enhancement [15-17]. PC-EMA (ethylene methyl acrylate) copolymer and PC-PBT (poly butylene terephthalate) blend using different compatibilizers were studied for their mechanical and flow properties [18,19]. Impact toughening could be achieved by all these methods but at the cost of adverse effects on other properties specially the optical transmittance. Nano-fillers were incorporated in PC blends to increase the toughening by making nano-composites [20-23]. Processing of such nano-composites into a product by conventional cost-effective techniques though have some technical challenges to overcome. PC being an engineering material of vast application owing to its excellent properties as mentioned before, therefore need of an appropriate method that can take care of all the desired properties becomes imperative.

In the work presented here, PC is chemically modified by siloxanes to improve its low-temperature impact strength. Different viscosity and concentrations of PDMSOH are used to modify PC and very useful observations are found with respect to low-temperature impact, tensile and optical properties. Tensile strength that generally reduces in block copolymers of PC and siloxane produced through interfacial copolymerisation interestingly gets enhanced in the PC modified by reactive blending with siloxane. The transesterification reaction that takes place between the hydroxyl group of PDMSOH and the carbonyl group of

polycarbonate is also influenced by the concentration of the catalyst KOH. Low-viscosity PDMSOH, i.e. lower molecular weight siloxane used in the reactive blending has a comparatively larger number of terminated hydroxyl groups, thus concentration of catalyst becomes important and needs to be optimised.

MATERIALS AND METHODS

Materials

Polycarbonate (PC) from the SABIC Company of grade LEXAN 144R was used for the experimental work. Two grades of hydroxyl terminated polydimethyl siloxane (PDMSOH) of viscosity 750 cSt and 3500 cSt were used of Aldrich Chemicals. Different-viscosity compositions of PDMSOH were prepared by mixing the two different grades of PDMSOH in different proportions as described in Table.1 to determine the effect of viscosity of PDMSOH on the impact strength of PC. Kinematic viscosity of PDMSOH compositions was measured at 23°C by a glass capillary U tube viscometer as per the method ASTM D445.

Sample Preparation

Reactive blending between PC and PDMSOH was done in an agitated glass reactor at 260°C in presence of KOH catalyst at 0.1 wt% concentration under an inert atmosphere of nitrogen for about 40 minutes. Both, viscosity and concentration of PDMSOH were varied to observe their impact on various properties. Viscosity variation from 750 to 3500 cSt was done by making a total of six compositions, i.e. PDMS750, A, B, C, D and PDMS3500 as shown in Table 1. Concentration of PDMSOH was changed from 0.5 to 3.0 wt% at an increment of 0.5 wt%. Physical melt blend of PC and PDMSOH (3.0 wt%) was also prepared at 260°C to compare it with reactive blended samples.

Physically blended sample (PC+PDMSOH) was prepared without KOH catalyst and mixing time was about 10 minutes to ensure a thorough mixing of the two phases. Since the reaction mass was highly viscous, both physical and reactive blending was done using pitch blade agitator at a speed of 150 to 200 rpm.

Table 1. Compositions of PDMSOH having different viscosities

Hydroxy terminated PDMS	PDMS 750	PDMS-A	PDMS-B	PDMS-C	PDMS-D	PDMS 3500
Composition [% PDMS750 : %PDMS3500]	100:0	80:20	60:40	40:60	20:80	0:100
Viscosity [cSt]	750	1210	1870	2560	3070	3500

A gas sensor was also provided at the vent of the reactor to observe the generation of CO₂ gas during reactive blending.

Characterisation

Izod impact tester was used to measure impact strength both at room temperature and at -30°C. Notched samples were prepared of size 64×12.7×3.2 mm as per ASTM-D256. Tensile strength and modulus were measured by a universal testing machine (UTM) of make Instron as per ASTM - D638. Scanning Electron Microscope of make Tescan MIRA-3 was used to observe the phase compatibility of PC and PDMSOH. UV-VIS spectrophotometer of make Chemito, India was used to characterise covalent bonding between PC and PDMSOH. Samples were dissolved in Methylene dichloride and filled in the quartz cell to characterise them by the UV-Vis spectrophotometer. Optical transmittance and haze of modified PC were measured as per ASTM-D1003.

RESULTS AND DISCUSSION

Reactive Blending with Siloxanes

Reaction between PDMSOH and PC chains is characterised by the Red Shift obtained in UV-VIS spectra as shown in Fig. 1. The covalent bonding between the two polymeric chains is verified in π - π^* transition of aromatic fragments of PC in the UV-VIS spectra. It can be seen that the characteristic peak of PC in UV-Vis spectra at 262 nm is not changed in the physically blended sample (PC+PDMSOH). However, for the reactive blended sample (PC/PDMSOH), there is an appreciable shift of 8 nm and the peak is found at 268 nm. The difference in the spectra of physically blended (PC+PDMSOH) and reactively blended (PC/PDMSOH) is indicative of the chemical binding between the two polymeric chains. This observation is in agreement with the results reported elsewhere [24,25]. The transesterification reaction between the carbonyl group of PC and the hydroxyl group of PDMSOH in presence of catalyst KOH takes place as shown in the proposed mechanism in Fig. 2 [12,24,25], The mechanism is also supported by the observation of an increase in the concentration of CO₂ gas in the vent of the reactor during reactive blending measured by a chemical sensor.

Influence on Low-Temperature Impact Strength

Modified Izod impact strength values of PC grade Lexan 144 R used in the experiment are tabulated in Table 2. Impact strength of the unmodified base PC resin at room temperature is 754

J/m which is drastically reduced to 124 J/m at -30°C temperature.

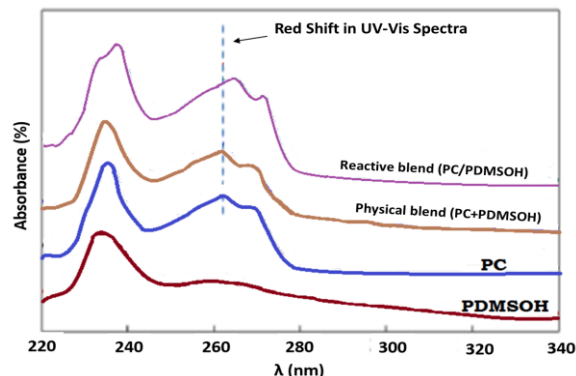


Fig. 1. UV-Vis spectra of PC, PDMSOH and their physical (PC+PDMSOH) and reactive (PC/PDMSOH) blends.

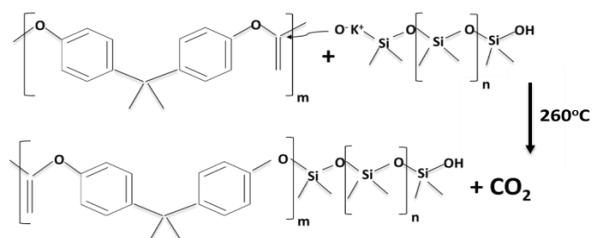


Fig. 2. Proposed mechanism of the reaction between PC and PDMSOH with KOH catalyst.

After the reactive blending with siloxane at the reaction conditions mentioned before, the impact strength at -30°C temperature increases with both concentration and viscosity of the PDMSOH, as shown in Table 2. Maximum impact strength of PC at -30°C temperature was achieved as 655 J/m at 3.0 wt% concentration and 3500 cSt kinematic viscosity of PDMSOH. The enhancement in impact strength from 124 J/m to 655 J/m is quite appreciable and is better than the values that can be achieved by interfacial copolymerization. The different impact strength values reported in Table 2 provide a range of 162 J/m to 655 J/m achieved at different concentrations and viscosities of PDMSOH. Keeping in view the effect of impact modification on other properties, specially the mechanical properties like tensile strength and modulus, an appropriate composition of the reactive blend can be selected from the reported data as may be required for a particular end application of polycarbonate. Since both viscosity and concentration of PDMSOH play role in changing the different properties of PC, data reported in this paper can be usefully applied in selection of the grade of PC. The concentration of PDMSOH beyond 3.0 wt% is not stable and it leads to phase separation. As can be seen in the SEM micrographs of Fig. 3, uniformly dispersed phases of PDMSOH are seen at 0.5 and 3.0 wt% concentration

in Fig. 3(a) and 3(b), respectively, whereas phase separation is observed in Fig. 3(c) at 3.5 wt% concentration. Uniformly dispersed siloxane domains from 2 μm to sub-micron sizes are seen in Fig. 3(a) which are miscible with the reactive blend of PC and PDMSOH. This phenomenon occurs upto the concentration of 3.0 wt%. As shown in Fig. 3(b), domain sizes of 1 to 3 μm are found uniformly dispersed in the bulk PC blend. Unevenly dispersed siloxane domains of sizes bigger than 10 μm are shown in Fig. 3(c) at 3.5 wt% concentration which verifies that siloxane is immiscible and unstable beyond 3.0 wt% concentration. Immiscibility of siloxanes could also be seen visually as an oil-like layer on the surface of PC as a separated phase at higher concentrations of PDMSOH.

The mechanism of impact toughening can be understood by the fact that siloxanes have extremely low glass transition temperature and also they are much softer material compared to the base PC resin.

Impact stress on PC is transferred to the softer siloxane modifier that results in enhanced toughness and also low temperature ductility due to the sub-zero glass transition temperature of PDMSOH. Incorporation of siloxane in the PC matrix with uniformly dispersed phases, good compatibility and adherence are a few factors that result in appreciable modification in low-temperature impact strength and it could only be achieved by reactive blending between the two phases.

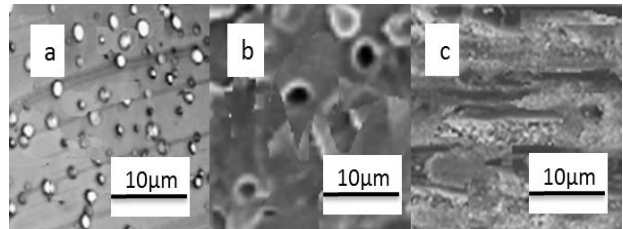


Fig. 3. SEM of PDMSOH-PC blend (a) 0.5 wt% (b) 3.0 wt% (c) 3.5 wt%.

Table 2. Change in Izod impact strength at different concentrations and viscosities of PDMSOH

PDMSOH concentration [wt %]	Izod Impact Strength [J/m] at -30°C					
	PDMSOH 750	A	B	C	D	PDMSOH 3500
0.5	162	170	174	178	181	185
1.0	220	223	226	228	232	235
1.5	316	321	331	339	346	355
2.0	395	406	414	428	446	460
2.5	415	426	440	477	508	540
3.0	445	490	525	585	615	655

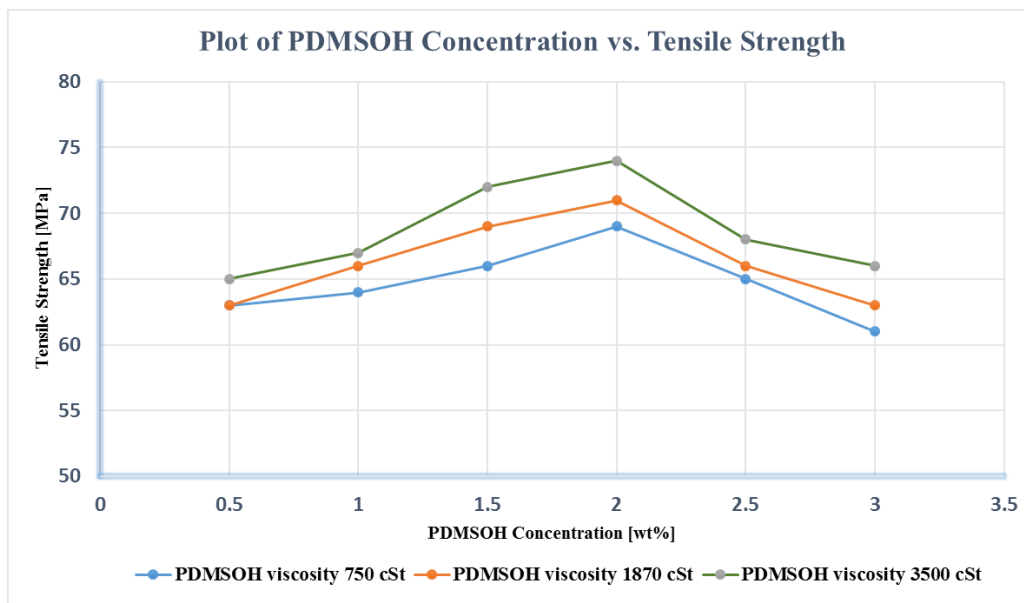


Fig. 4. Effect of PDMSOH concentration on tensile strength of PC

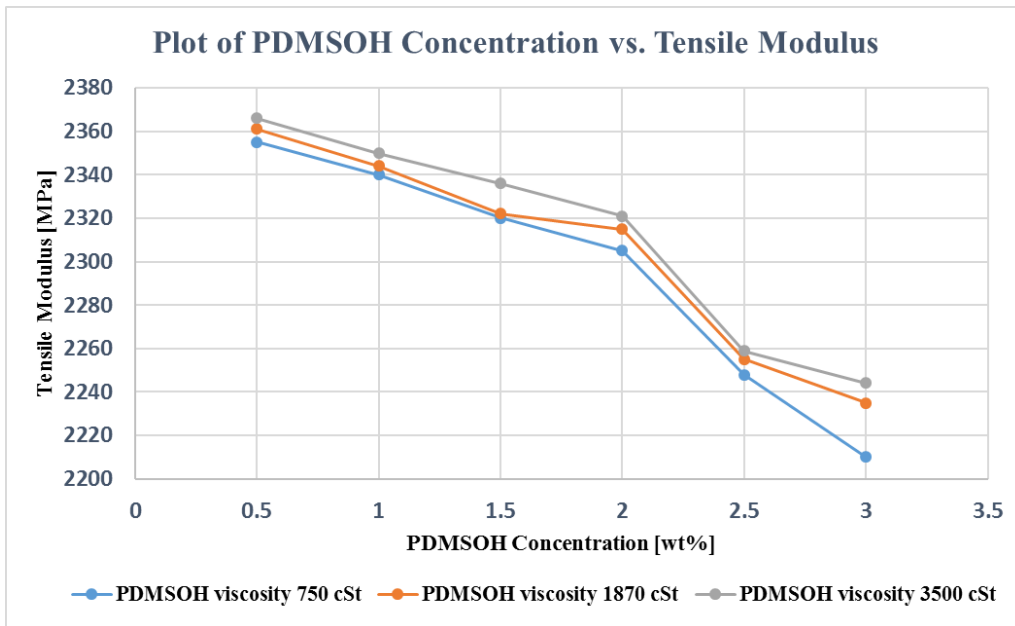


Fig. 5. Tensile modulus of PC at different concentrations and viscosity of PDMSOH

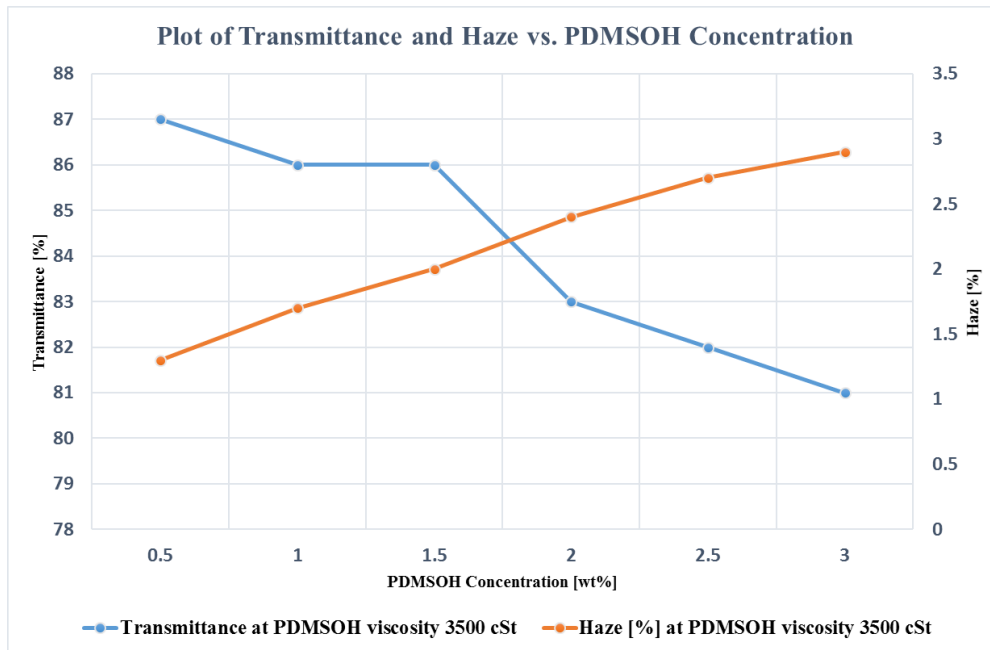


Fig. 6. Influence of PDMSOH concentration on transmittance and haze

Concomitant Effects on Other Properties

Tensile strength and modulus are also very important mechanical properties required for a particular application of PC. While modifying PC it is essentially required to observe the influence of modifier on these properties. As shown in Fig. 4, tensile strength of modified PC initially increases upto 2.0 wt% concentration of PDMSOH and then keeps decreasing upto 3.0 wt%. Improvement in tensile strength is achieved by the enhanced adhesion between the polymer chains by PDMSOH. Lower molecular weight chains of siloxanes in PDMSOH of viscosity 750 cSt are more evenly dispersed in the

base polycarbonate resin which results to maximum enhancement in tensile strength. However, as the molecular weight of PDMSOH chains increases with the higher viscosity, dispersion is adversely affected, probably due to the tendency of polymer chains to clutter and entangle more with the longer chain lengths. Beyond 2.0 wt% concentration of PDMSOH, there is reduction in tensile strength due to the weakening of interface beyond a certain concentration of the siloxane modifier in PC, however, at lower concentrations it improves the inter-chain binding in PC. Higher viscosity has a lesser impact on tensile strength as shown in Fig. 4 as

PDMS molecules of longer chain lengths tend to lump instead of adhering on PC chains whereas siloxane molecules of shorter chain lengths spread more evenly and uniformly at the PC-PDMS interface. Contrary to tensile strength, tensile modulus slightly decreases up to 2.0 wt% concentration of PDMSOH as shown in Fig. 5. This mechanical behaviour is attributed to incorporation of a softer material, i.e. siloxane in PC which increases the strain as the material loses its stiffness. Modulus further sharply decreases up to 3.0 wt% concentration of PDMSOH as shown in Fig. 4. Decrease in tensile strength and increase in strain at higher concentrations of siloxanes are the main cause of the substantial reduction in the tensile modulus of modified PC. One of the most useful properties of polycarbonate is its excellent optical property. Optical transmittance of the material is comparable to glasses and in the base PC resin, it is in the range of 86-88% [26]. Modification of PC for its enhanced mechanical properties generally has concomitant effects on its optical property. This effect is observed mainly because of difference in the refractive indices of polycarbonate and siloxane. The extent of optical transmittance and haze affected by siloxane also depends on the morphology, dispersion and concentration of siloxane. As shown in Fig. 6, the optical transmittance mildly decreases upto 1.5 wt% concentration of PDMSOH and then sharply decreases up to 3.0 wt%. This phenomenon can be understood by the fact that at lower concentrations, PDMSOH is finely dispersed in PC and its domain sizes are mostly less than 1-micron size as shown in SEM Fig 3(a). It therefore does not have much impact on the path of incident light and not much decrease in transmittance is found. However, at higher concentrations, when phase boundaries are bigger, as shown in Fig.3 (b), the material's optical property is substantially affected due to large aberration in the path of incident light and thus transmittance is reduced to 82% (Fig.6). Haze consistently yet mildly increased (Fig.6) as concentration was increased from 0.5 to 3.0 wt%. Effect of viscosity on both optical transmittance as well as haze was not observed and it was almost the same for all the viscosities of PDMSOH. Influence on optical properties of siloxane modification however calls for a detailed study so that the application of PC where both mechanical and optical properties are equally important, can be observed as per the requirement. There is a good scope of further research on the optical properties of PC simultaneously with modification of mechanical properties specially where higher concentrations of impact modifier are

needed. Siloxane itself has good transmittance and its incorporation in PC only mildly affects the optical property. Thus, modified PC maintains its usefulness for many optical applications of PC like snow goggles, bulletproof glass and visors.

CONCLUSIONS

- Low-temperature impact toughness of reactive blends of hydroxyl terminated siloxanes with polycarbonate is substantially enhanced from 124 to 655 J/m at -30°C and the method developed for impact modification is simple and cost-effective.
- This work also gives good insight about the concomitant effects on other properties, i.e. tensile strength, modulus, optical transmittance and haze while carrying out impact modification.
- Modification of impact toughness by the method reported here also has a good effect on tensile strength contrary to conventional blending with impact modifiers where impact strength is enhanced at the cost of reduction in tensile strength.
- Chemical linkage of siloxane by transesterification not only provides the advantage of copolymer of PC and PDMS but also acts as compatibilizer for additional amount of siloxane that may have to be added in the PC matrix for a particular application.
- Very useful and interesting results for tensile strength variation were also obtained which can be used to optimise the siloxane incorporation in order to achieve desired mechanical properties at both room temperature and sub-zero temperature.
- Optical properties of the modified PC do not change much and are well in the range of properties required for low-temperature optical application of PC, e.g. snow goggles, visors and bullet proof glasses, however there is ample scope of further detailed research on the optical properties of polycarbonate along with its impact modification.

Acknowledgement: *The authors are thankful to Dr. N. Eswara Prasad, Director DMSRDE, Kanpur, India for funding and constant support for this work. Contribution of the Chemical Engineering Department, HBTU, Kanpur for extending help in sample preparation and characterisation is also sincerely acknowledged. Authors sincerely acknowledge the contribution of Officers and staff of the Directorate of Personal Protection System & Engineering, DMSRDE, Kanpur and thank for their help in preparation of manuscript and experimentation.*

The paper has been presented in International Chemical Engineering Conference on "100 Glorious Years of Chemical Engineering & Technology" from

September 17 to 19, 2021, organized by Department of Chemical Engineering at Dr. B. R. Ambedkar NIT Jalandhar, Punjab, India (Organizing Chairman: Dr. Raj Kumar Arya & Organizing secretary: Dr. Anurag Kumar Tiwari).

REFERENCES

1. H. Brouwer, J. van den Bogerd, J. Hoover, *European Polymer Journal*, **71**, 558 (2015).
2. J. Wu, *Appl. Polym. Sci.*, **46**, 619 (1992).
3. D. G. LeGrand, *Polym. Lett.*, **7**, 579 (1969).
4. G. E. Niznek, D. G. LeGrand, *J. Polym. Sci. Polym. Sympos.*, **60**, 97 (1977).
5. R. P. Kambour, W. V. Ligon, R. R. Russell, *J. Polym. Sci. Polym. Lett.*, **16**, 327 (1978).
6. A. Nodera, T. Kanai, *J. Appl. Polym. Sci.*, **101**, 3862 (2006).
7. X. Chen, H. F. Lee, J.A. Gardella, *Macromolecules*, **26**, 4601 (1993).
8. D. Dhara, A. Purushotham, N. Rosenquist, W. D. Richards, *Polym. Eng. Sci.*, **49**, 1719 (2009).
9. D. G. LeGrand, J. T. Bendler, Handbook of polycarbonate science and technology, Chapter 5, Marcel Dekker, New York: 2000.
10. S.R. Kim, D.J. Kim, *J. Appl. Polym. Sci.*, **109**, 3439 (2008).
11. C.M. Hawkins, R. R. Gallucci, U.S. Pat. 4.994.532, 1991.
12. W. Zhou, J. Osby, *Polymer*, **51(9)**, 1990 (2010).
13. E. N. Peters, US Pat. 5,194,524, 1993.
14. A. Konig, W. Ebert, W. Kohler, US Pat. 6,066,700; 2000.
15. E. Parsons, M. C. Boyce, D. M. Parks, *Polymer*, **45**, 2665 (2004).
16. T. Ebeling, A. Hiltner, E. Baer, *Polymer*, **40**, 1525, 1999.
17. S. S. Pesetskii, B. Jurkowski, I. P. Storozcuk, V. N. Koval, *J. Appl. Polym. Sci.*, **73**, 1823 (1999).
18. R. Kumar, K. K. Kar, V. Kumar, *Mater. Res. Express*, **5**, 015306 (2018).
19. N. Bagotia, B. P. Singh, V. Choudhary, D. K. Sharma, *RSC Adv.*, **5**, 87589 (2015).
20. S. Kushwaha, K. K. Kar, P. Santhana, G. Krishnan, S. K. Sharma, *J. Reinf. Plast. Composite*, **30**, 1185 (2011).
21. W. S. DePolo, D. G. Baird, *Polymer Composites*, DOI 10.1002/pc.20554, 2009.
22. N. Bagotia, V. Choudhary, D. K. Sharma, *Composites, Part B: Engineering*, **124**,101 (2017).
23. N. Bagotia, V. Choudhary, D. K. Sharma, *Composites, Part B: Engineering*, **159**, 378, 2019.
24. Sh.-mei Zhang, H.-xian Zhang, W.-yi Zhang, Zh.-qiang Wu, F. Chen, Q. Fu, *Chinese J. Polym. Sci.*, **32(7)**, 823 (2014).
25. J. N. Srivastava, S. K. Gupta, *J. Appl. Polym. Sci.*, e51876, <https://doi.org/10.1002/app.51876>, (2021).
26. M. Aden, A. Roesner, A. Olowinsky, *J. Pol. Sci., Part B: Pol. Phys.*, **48**, 451 (2010).

Comparative study of castor oil and dehydrated castor oil as lubricants

J. Srivastava^{1,2*}, T. Nandi¹, R. K. Trivedi²

¹Defence Materials and Stores Research and Development Establishment, GT Road, Kanpur, India

²Harcourt Butler Technical University, Nawab Ganj, Kanpur, India

Received: October 13, 2021; Revised: January 01, 2022

Lubricants play a prime role not only in automobiles but also in mechanical systems used in various industries. Castor oil, one of the promising non-edible vegetable oils, can serve as base lubricating oil. It is abundantly available, non-edible oil. The viscosity, density, thermal conductivity, and pour point of castor oil are at par with conventional lubricants, however, the viscosity of castor oil is very high at 25° C that affects the efficiency of mechanical systems. Dehydrated castor oil, obtained after dehydration of castor oil, has much lower viscosity values than castor oil. It has been observed that dehydrated castor oil shows viscosity reduction up to 39-40% and a 17.5% increase in thermal conductivity as compared to castor oil. Under similar flow conditions, if the flow of dehydrated castor oil is in a turbulent region, castor oil flow is in the laminar region. Similarly, the value of the Prandtl number is higher in the case of dehydrated oil. The antiwear and antifricition performance of castor oil and dehydrated castor oil has also been studied and 14.5 % more reduction in coefficient of friction has been achieved with dehydrated castor oil, while wear reduction of 23 % more has been achieved with castor oil. In the present paper, the physicochemical, thermal, heat transfer and tribological properties of both castor oil (CO) and dehydrated castor oil (DCO) have been compared and discussed. Their advantages, disadvantages and performances as lubricants have also been explored.

Keywords: Castor oil; Vegetable oil; Dehydrated castor oil; Lubricant

INTRODUCTION

Lubricants are essentially required for mechanical parts of the systems. Conventionally, mineral oils have been used as lubricants for automotive, industrial and transport applications because of their good technical properties. These are petroleum-based hydrocarbons and their exposure to the environment generates pollution. In addition, several issues like depletion of petroleum reserves and increasing demand for lubricants due to industrialization promoted new alternatives of mineral oils. Vegetable oils are perceived to be a substitute to mineral oils due to certain inherent technical properties and their ability to be biodegradable. Vegetable oils have been used as lubricating oils from ancient days [1], till 19th century they have been used as an integral part of lubricating oil. Vegetable oils are triglycerides of fatty acids. Increasing crude oil prices and emphasis on the development of renewable, environmentally friendly industrial fluids have brought vegetable oils to a place of priority. As compared to mineral oil, vegetable oil has a high pour point, better viscosity index, low evaporation loss and works as a green lubricant [2]. The polar groups and long-chain fatty acids present in vegetable oil make it amphiphilic and provide a better film/force interconnection [3-5] that helps in minimizing friction and wear. Plant

oils biodegrade more easily than mineral oils because of their glyceride fatty acids. Vegetable oil-based lubricants are efficient in both boundary and hydrodynamic regimes [4,6,7]. The biggest benefit with these oils is the vegetable base origin and their abundant nature, while conventional lubricants depend upon petroleum resources. The usage of edible oils like soybean, sunflower, coconut, etc., as a lubricant is difficult as these have to fulfil the domestic requirements of a big population. Nonedible oils like castor oil can serve the purpose due to their abundance and excellent physical and chemical properties. Another advantage of castor is that its growing period is much shorter than that of *Jatropha* and *Pongamia* oilseeds. Being an annual crop it gives farmers the ability to shift away easily depending on market conditions. It is extracted from castor beans containing about 44-48 % of oil. Fig. 1. shows the castor tree, seeds and oil. Earlier, castor oil has not only been used in engines but also as gear and transmission oil, its application as a base stock for environmentally friendly lubricants in grinding [8], high-speed turning [9] and precision turning [10] has also been reported.



Fig. 1. Castor tree, seeds and oil

* To whom all correspondence should be sent:

E-mail: jyotisri69@rediffmail.com

Suhane et al. [11] investigated castor oil-based lubricant for automotive applications in comparison to available commercial servo gear oil.

Chemical composition of castor oil

Castor oil has 90% ricinoleic acid which is monounsaturated, 18-carbons fatty acid. Fig. 2 depicts the structure of this unique acid. In its structure, there is an acid group at the first carbon, a double bond between the ninth and tenth carbon followed by a hydroxyl functional group at the twelfth carbon [12].

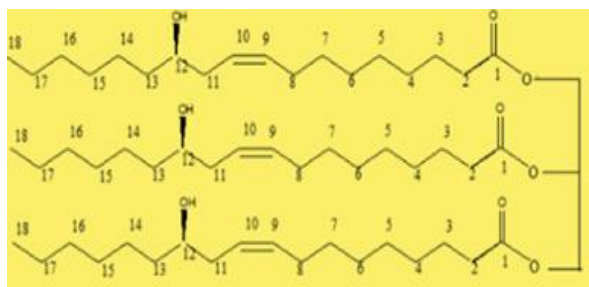


Fig. 2. Ricinoleic acid, the main fatty acid of castor oil

As a result, this unique functionality allows castor oil and its derivatives to find applications like lubricants, paints, inks & additives, textile and agricultural chemicals, rubber, plastic, food, cosmetics, paper, pharmaceutical and electronics & telecommunications sector. The ricinoleic acid comprises almost 90% of the total fatty acid composition. Other fatty acids are linoleic acid (4.0%), stearic acid (1.0%), palmitic acid (1.0%), dihydrostearic acid (0.6%), oleic acid (3.0%), linolenic (0.2%) and eicosanoic (0.2). Fig. 3. shows the pie chart distribution of castor oil constituents.

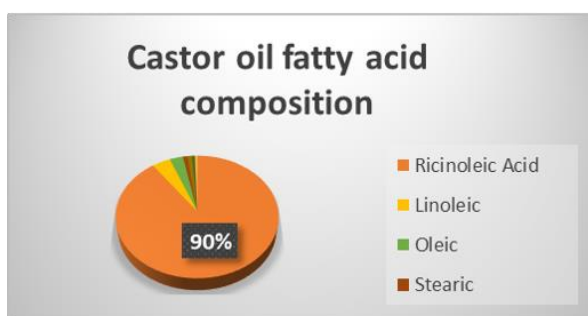


Fig. 3. Fatty acid composition of castor oil

It has been found that the viscosity of oil increases with increasing ricinoleic acid content of the oil, Viscosity performs a crucial part in mechanical system performance and reducing power losses. If the lubricant has a too high viscosity, it may make some part of the lubricant area deficient and increase drag that may lead to reduced efficiency.

The viscosity and other properties of castor oil are highly changed once it is dehydrated.

Dehydration of castor oil

When castor oil is heated in presence of certain catalysts, water is removed from the ricinoleic acid chain and dehydrated castor oil is formed, as shown in Fig. 4. Numerous catalysts have been notified for dehydration of castor oil like sulfuric acid, phosphoric acid, sodium bisulfate, and acid-activated clays [13,14]. The elimination of the hydroxyl group and an adjacent hydrogen atom leads to the generation of a new double bond in the fatty acid chain [15]. In this procedure, ricinoleic acid is reacted with an acid, takes away a hydroxyl group and a vinyl group is formed. The dehydrated castor oil is often used as a lubricant [16]. Dehydrated castor oil is now recognized with independent identity having its characteristics and benefits.

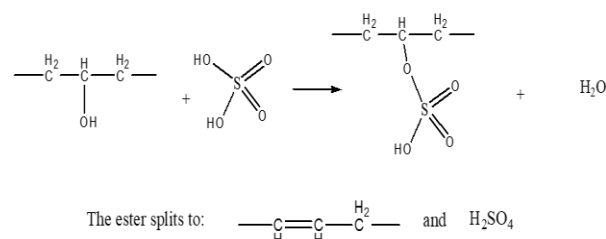


Fig. 4. Formation mechanism of dehydrated castor oil

MATERIALS AND METHOD

Castor oil and dehydrated castor oil have been obtained from Jayant Agro Organics limited (Mumbai, Maharashtra, India). FTIR spectra of both oils have been recorded by Perkin Elmer FTIR model Spectrum-2 in the mid higher range (4000-400 cm^{-1}). The thermal behavior of castor and dehydrated castor oil has been evaluated using a SDT Q600 thermal analyzer by TA Instruments. Thermal analyser measures the heat flow as a function of temperature under a controlled nitrogen atmosphere. The density of both oils has been measured in a pycnometer according to ASTM D287 method. Viscosity as an important property of lubricant can be evaluated using ASTM D-445 using Ostwald viscometer. Hydroxyl value is a measure of the content of hydroxyl groups in the oil that has been calculated for both oils by the ASTM D-1957 method. The thermal conductivity was evaluated by a thermal conductivity meter, Decagon Devices Inc., KD2Pro instrument. Flashpoint of castor and dehydrated castor oil was determined by ASTM D-92 using Cleveland open cup tester while pour point of castor and dehydrated castor oil was determined according to ASTM D-92 using pour point

instrument model NEWLAB 1300-SA supplied by Linetronic Technologies. Specific heat of both oils has been measured by the Nanofluid heat capacity apparatus supplied by Mittal enterprises New Delhi. Ducom four-ball tester model TR-30L-PNU-IAS has been used to evaluate the tribological properties of both oils. Evaluation of lubricant properties was conducted with speed of 1200 rpm, and load of 294 N at 75 °C. The test was conducted according to ASTM D4172. The frictional torque and coefficient of friction (COF) have been calculated using the following formula:

$$\mu = T\sqrt{6/3Wr}$$

where μ = coefficient of friction, T= frictional force Kg.mm, W= applied force in Kg and r= 3.67. Wear scar diameter was calculated by the image acquisition system. Morphology of worn surfaces was examined by FESEM, TESCAN, and MIRA-3.

RESULTS AND DISCUSSION

FTIR characterization of castor oil

For the identification of expected functional

groups and bands, especially hydroxyl groups, FTIR of both castor and dehydrated castor oil has been recorded. Fig. 5 shows the FTIR scan of both oils. The ester carbonyl (C=O) functional group shows the characteristic stretching band of triglyceride at 1743.25 cm^{-1} of both oils. It has been observed that the broad peak at 3435.48 cm^{-1} signifies the hydroxyl group (O-H) of the ricinoleic fatty acid present in castor oil but in the case of dehydrated castor oil the peak intensity becomes smaller because of the splitting of ricinoleic acid.

Physicochemical properties evaluation of castor oil and dehydrated castor oil

The important physicochemical characteristics of castor oil and dehydrated castor oil are shown in Table 1. Density plays a major role in lubricant functioning and performance in mechanical systems. It is also useful in calculating several physical factors of a fluid. From Table 1 it is evident that the castor oil has a density range that is advantageous in high bearing load and highly stable in severe conditions although pumpability is better with dehydrated castor oil due to lower density.

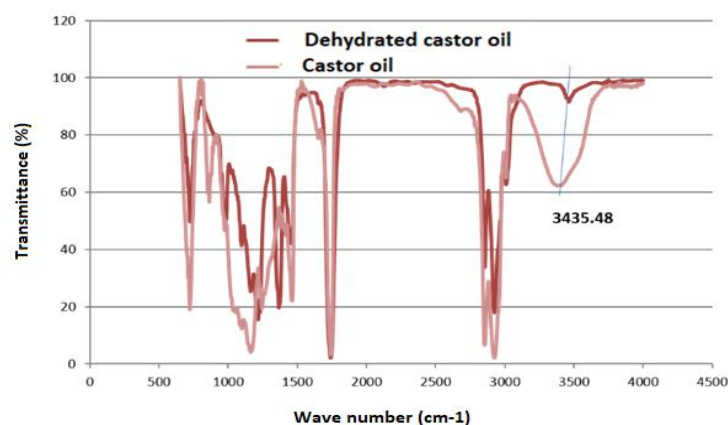


Fig. 5. FTIR comparison of castor oil and dehydrated castor oil

Table 1. Physicochemical characteristics of castor oil and dehydrated castor oil

Properties (Units)	Castor oil (CO)	Dehydrated Castor oil (DCO)
Density (Kg/m ³)	0.964-0.969	0.926-0.937
Kinematic viscosity (cst)		
@ 25 °C (cSt)	662.67-667.79	135.43-139.05
@100 °C (cSt)	19.72-20.32	18.29-19.32
Hydroxyl value (mg KOH g ⁻¹)	150-160	7.0-8.0
Thermal conductivity (W/m ² K) at 25°C	0.148±0.001	0.174±0.001
Flashpoint (°C)	245	211
Pour point (°C)	-27	-34

It has been observed that the viscosity of the castor is much higher as compared to dehydrated castor oil because of the increasing ricinoleic content

of the oil. A higher value of viscosity can cause churning losses to generate excessive heat generation due to molecular friction. In such cases,

dehydrated castor oil can serve as a potential lubricant in mechanical systems. Thermal conductivity is a necessary parameter in upgrading the heat transfer of base fluid. It is therefore beneficial for the fluid to own high thermal conductivity. Dehydrated castor oil shows an almost 17.5% increase in thermal conductivity as compared to castor oil. The hydroxyl value of dehydrated castor oil is less as compared with castor oil because during dehydration of castor oil, the hydroxy group-containing ricinoleic acid gets converted into 9,11 and 9,12 linoleic acid. Castor oil has a higher value of flash point. It means that the oil is less flammable, safer to handle or transport, beneficial in the high-temperature application as compared with dehydrated castor oil. It will be useful in the vehicle engine and as gearbox lubricant. Pour point of dehydrated castor oil is better than that of castor oil. Low pour point characteristics help easier handling and usage of lubricant in cold weather conditions.

Heat transfer evaluation in castor oil and dehydrated castor oil

Dimensionless numbers determine the fluid flow behavior in many aspects. Reynolds and Prandtl numbers help in assessing the flow behavior of both castor and dehydrated castor oil.

Reynolds number: The Reynolds number is the main dimensionless number in fluid mechanics anticipating the flow arrangements in different fluid flow conditions. It forms a basis to segregate the laminar and turbulent regimes. It can be evaluated using Equation 1:

$$N_{Re} = DV \rho / \mu \quad (1)$$

where D = diameter of the tube (m), V and ρ = velocity (m/s), density of liquid (Kg/m³), μ = dynamic viscosity (Pa-s) of liquid. The value of the Reynolds number for a laminar flow is always below 2100, whereas for turbulent flow its value is above 5000 [17].

In the case of dehydrated castor oil for a well-developed turbulent flow $N_{Re} = 5000$,

$$DV = 135.43 \times 5000 \times 10^{-6} = 0.67.$$

Putting this value of DV and kinematic viscosity in the case of castor oil in Equation 1, the Reynolds number becomes:

$$N_{Re} = 0.67 / 662.67 \times 10^{-6} = 1011.$$

For similar conditions of tube diameter and velocity, if the flow of dehydrated castor oil is in a turbulent region the flow of castor oil is in the laminar region. Thus, the heat transfer properties of

dehydrated castor oil are better than those of castor oil and it acts as a good lubricant.

Prandtl number: This dimensionless number expresses the relation between the viscosity of a fluid and the thermal conductivity. It, therefore, evaluates the relation between momentum and thermal transport competency of a fluid. It is defined as:

$$Pr = \text{Momentum Diffusivity} / \text{Heat Diffusivity} = (\mu / \rho) / (k / \rho C_p) = C_p \mu / k \quad (2)$$

where μ = dynamic viscosity (Pa-s), ρ = density (Kg/m³), k = thermal conductivity (in W.m⁻¹.K⁻¹) and C_p = specific heat of liquid (J.kg⁻¹.K⁻¹).

In the case of dehydrated castor oil (DCO):

dynamic viscosity = $135.43 \times 0.926 \times 10^{-3} = 125.40 \times 10^{-3}$, $C_p = 2.88$, $k = 0.174$. Putting all values in equation (2):

$$Pr(DCO) = 125.40 \times 10^{-3} \times 2.88 \times 10^3 / 0.174 = 2075.72$$

In the case of castor oil (CO):

dynamic viscosity = $662.67 \times 0.964 \times 10^{-3} = 638.81 \times 10^{-3}$, $C_p = 1.8$, $k = 0.148$. Putting all values in equation (2):

$$Pr(CO) = 638.81 \times 10^{-3} \times 1.8 \times 10^3 / 0.148 = 7769.$$

If the Prandtl number is less, thermal diffusion is predominant as compared to momentum diffusion. If the flow situations go on the same, for a higher heat transfer rate we have to choose a fluid with a lower Prandtl number, in this way dehydrated castor oil is much better than castor oil because of the lower value of Prandtl number. Oils with small values of Prandtl number are free-flowing liquids having a larger value of thermal conductivity.

Thermal properties evaluation of castor oil and dehydrated castor oil

The differential scanning calorimetry (DSC) thermal curves give a way of distinguishing between both oils. Fig. 6(a) depicts the DSC curve for castor oil, which shows sudden exothermic decomposition at elevated temperature. The decomposition initiates at 343.95°C with a peak value of 379.79°C. The value of enthalpy of decomposition is 157.4J/g. Fig. 6(b) shows the decomposition behavior of dehydrated castor oil which initiates at 347.61°C with a peak value at 389.69°C, the enthalpy value of decomposition is 340.3J/g. From both curves we may conclude that onset decomposition temperature of dehydrated castor oil is higher than that of castor oil so that it can be used up to higher temperatures.

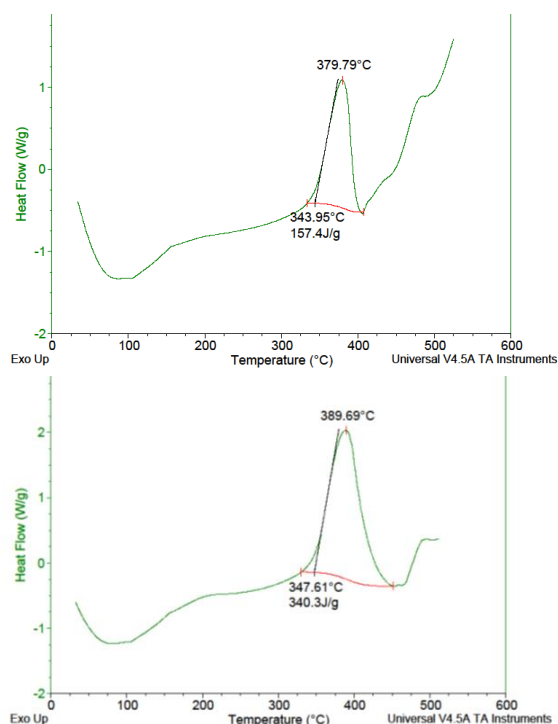


Fig. 6 (a, b). Differential scanning calorimetry of castor oil and dehydrated castor oil

Tribological properties evaluation of castor oil and dehydrated castor oil

Tribological tests were carried out according to the standard test methods for measurement of frictional and wear-preventive properties of castor oil and dehydrated castor oil in a Ducom four-ball tester, model TR-30L-PNU-IAS. The tests were carried out at atmospheric pressure of both castor oil and dehydrated castor oil at a load of 294N and 75°C temperature with a constant speed of 1200 rpm. After 30 minutes of run, the three bottom balls have been taken off, cleaned with acetone. The scars marked on the bottom of the three balls were observed under an optical microscope to access the wear characteristics of the lubricants. The wear characteristics were analysed by observing the pattern of wear created over the balls called wear scar diameter. The wear scar diameter was measured along the minor and major axis and was found the same on both axes. The frictional behaviour, i.e.

frictional torque, coefficient of friction (COF) of castor oil and dehydrated castor oil is shown in Fig. 7 (a). The value of COF of dehydrated castor oil and castor oil were 0.0482 and 0.0552, respectively. The reduction in friction characteristics was found to be 12.6%. The thin lubricating film formation ability on the surfaces of contacting mechanical components, determines the friction reduction efficiency which is better with dehydrated castor oil. Due to the better film-forming ability and lubricity of dehydrated castor oil compared to castor oil the frictional force got reduced rendering a reduction in the coefficient of friction. The frictional force and the wear scar images of castor and dehydrated castor oil are shown in Figs. 7 (b) and 7 (c), respectively. In the case of castor oil, a smaller wear scar diameter was present as compared with dehydrated castor oil. The worn surface analysis of bottom balls in both oils has been examined using FESEM at a magnification of 250×. Figs. 7 (d, e) show the morphology of scars present in both oils. The worn surface of castor oil shows a circular, smoother and flatter scar, with 445 µm diameter in balls while dehydrated castor oil shows a rough surface with scratches and grooves having a scar of 550 µm diameter in balls. The viscosity of lubricants plays a very important role in the lubricating and tribological properties of the lubricants. In the case of dehydrated castor oil the viscosity is much lower. Due to the lower viscosity of the dehydrated castor oil its wear-preventive property is comparatively lower than that of the castor oil. Owing to lower viscosity, there is more wear in the case of dehydrated castor oil. Due to higher wear there is more formation of wear particles. The broken particles present on the scar image as shown in Fig.7(e) will act like abrasive particles and will cause abrasive and erosive wear when the oil is used as a lubricant in an engine or any other mechanical system. The anti-wear property of castor oil is better compared to dehydrated castor oil. The reduction in wear characteristic accessed through measuring wear scar diameter of castor oil compared to dehydrated castor oil was found to be 23%.

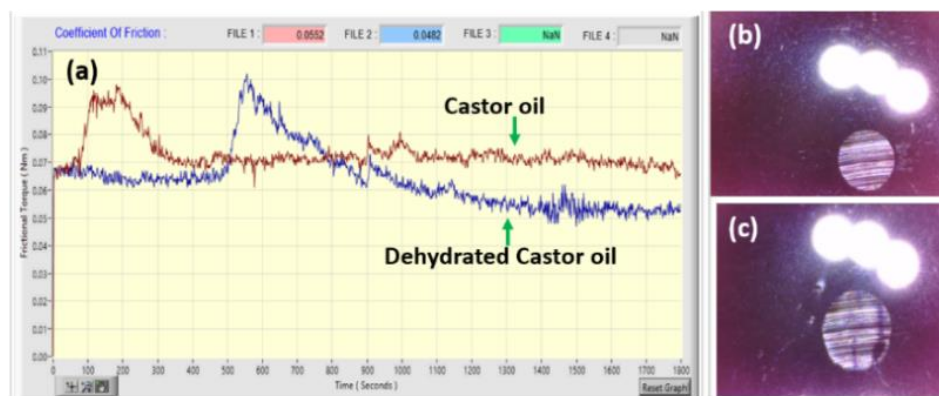


Fig. 7 (a) COF of castor oil and dehydrated castor oil (b, c) Wear scar image

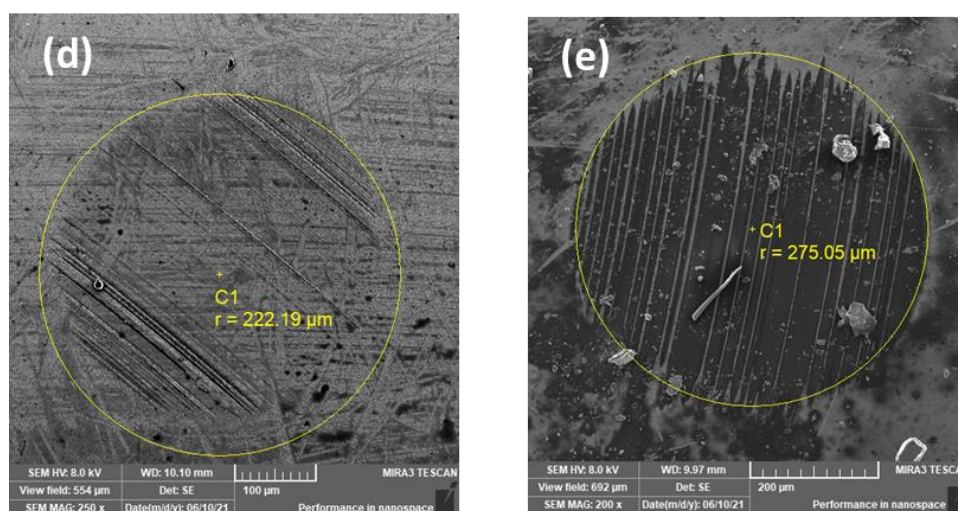


Fig. 7 (d, e). FESEM of castor oil and dehydrated castor oil

CONCLUSIONS

- Castor oil itself is a good alternative for lubrication, because of its good physiochemical, heat transfer and tribological properties necessary for lubricants.

- Dehydrated castor oil shows viscosity reduction up to 39-40% as compared with castor oil.

- The thermal conductivity of dehydrated castor oil is by 17.5 % higher than of castor oil.

- Under similar conditions of tube diameter and velocity, if the flow of dehydrated castor oil is in a turbulent region, castor oil flows in the laminar region. Thus, the heat transfer properties of dehydrated castor oil are better than of castor oil and it acts as a good lubricant.

- The value of Prandtl number for dehydrated castor oil is 2075.72 while that for castor oil is 7769. Therefore, dehydrated castor oil is a good option for heat-conducting liquids.

- It was observed that dehydrated castor oil yields a response to friction test by 14.5% more reduction in COF as compared with castor oil.

- The anti-wear behaviour of castor oil was better and 23 % more reduction in wear scar diameter has been obtained as compared to dehydrated castor oil.

- The dehydrated castor oil can serve as a potential alternative as a lubricant. Its viscosity at 25°C is much lower than that of base castor oil. Lower viscosity-oils can reduce frictional losses between moving mechanical parts of the engine and lower pumping and cranking losses, thus improving fuel economy and efficiency of engines.

Acknowledgement: J. S. would like to express his special thanks to Dr. N. Eswara Prasad, OS & Director, DMSRDE, for his constant motivation and encouragement to conduct this work.

REFERENCES

1. D. Dowson, History of Tribology, Professional Engineering Publication Limited, Bury St. Edmunds, Suffolk, UK, 1998.
2. Y. Singh, R. Garg, S. Kumar, *Green*, **5**, 59 (2015).
3. L. A. Quinchia, M. A. Delgado, T. Reddyhoff, C. Gallegos, H. A. Spikes, *Tribology International*, **69**, 110 (2014).
4. A. Nakarmi, A. Joshi, *Nepal Journal of Science and Technology*, **15**, 45 (2014).
5. D. S. Chinchkar, S. T. Satpute, N. R. Kumbhar, *International Journal of Engineering Research & Technology*, **5**, 2278 (2012).
6. S. Boyde, *Green Chem.*, **4**, 293 (2002).
7. X. Wu, G. Zhao, X. Wang, X. Liu et al., *Tribology Letters*, **65**(2) (2017).
8. S. Guo, L. Changhe, Y. Zhang, Y. Wang et al., *Journal of Cleaner Production*, **140**(3), 1060 (2017).
9. H. J. Pei, W. J., Zheng, G. C., Wang, H. Q. Wang et al., *Advanced Materials Research*, **381**, 20 (2012).
10. H. J. Pei, Y. J. Sheng, C. G. Shen, G. C. Wang et al., *Applied Mechanics and Materials*, **130-134**, 3830 (2012).
11. A. Suhane, R. M. Sarviya, A. Rehman, H. K. Khaira, *Int. Journal of Engineering Research and Applications*, **4**, 104 (2014).
12. E. B. Mubofu, *Sustain. Chem. Process.*, **4**, 1 (2016).
13. D. N. Bhowmick, S. A. N. Sarma, *Industrial & Engineering Chemistry Product Research and Development*, **16**(1), 107 (1977).
14. A. O. Mamudu, E. A. Charles, F. Elehinafe, O. Odunlami et al., *International Journal of Mechanical Engineering and Technology*, **10**(3), 506 (2019).
15. V.R. Patel, G. G. Dumancas, L. C. K. Viswanath, R. Maples, B. J. J. Subong, *Lipid Insights*, **9** 1 (2016).
16. N. P. Chauke, H. E. Mukaya, D. B. Nkazi, *Science Progress*, **102**, 199 (2019).
17. W. L. McCabe, J. C. Smith, P. Harriot (eds.), Unit Operations of Chemical Engineering, McGraw Hill, New York, 1985, p. 37.

Investigation on cypress wood membrane for water filtration

M. Hanief*, K. Zaman, S. Ul Bashir, J. Showkat, M. Zubair

Mechanical Engineering Department, National Institute of Technology, Srinagar, J&K (India)

Received: October 14, 2021; Revised: January 16, 2022

An efficient yet inexpensive, biodegradable, and readily available filtration system is needed for countering the threats of unsafe water. This research aims at studying gymnosperm xylem tissue as a potential alternative to the polymeric membranes that involve a huge cost and energy for their manufacturing and are also not environmentally friendly. The xylem conductive tissue of tree trunk was investigated in the present study to act as a membrane for water filtration. This is attributed to the presence of pores in pit membranes which makes them permeable to liquids. The size of these pores fits well for the application of microfiltration. Kashmiri Cypress (*Cupressus cashmeriana*) was used in this study. A pressure-driven filtration process was used to determine the efficacy of the filter. Particle size analysis was done on the filtrate. The results demonstrated the feasibility of the setup for use in domestic applications. A gymnosperm xylem filter used in this study was able to effectively filter out particles > 300 nm. A flow rate of 4 liters per day was obtained under a pressure of 0.295 bar, with filter diameter of 1cm and 0.75mm thickness. Fourier Transform Infrared Spectroscopy test was conducted on the filtrate to determine the constituents of the filtrate. The test revealed that the chemical composition remained unchanged after filtration.

Keywords: Xylem filtration; Pit membranes; Microfiltration; Particle size analysis; FTIR

INTRODUCTION

The dearth of safe and clean drinking water is a major reason of mortality in the underdeveloped countries. Potable or drinking water is one having acceptable quality with respect to physical, chemical, and bacteriological parameters so that it can safely be used for drinking and cooking purposes [1]. The most deadly water pollutants are of biological origin. The most recurrent and global health hazards associated with drinking water are infectious diseases caused by pathogens such as bacteria, viruses, protozoa, or parasites [1,2]. Among these, widespread waterborne pathogens are bacteria (e.g. *Escherichia coli*, *Salmonella typhi*, *Vibrio cholerae*), viruses (e.g. adenoviruses, enteroviruses, hepatitis, rotavirus), and protozoa (e.g. *giardia*) [1]. These pathogens lead to child mortality and also give rise to malnutrition and retarded growth of infants. The WHO has reported that around 1.6 million humans lose their life every year due to the diarrheal diseases attributed to non-availability of safe drinking water and proper sanitation [3]. The children under the age of 5 years constitute 90% of these mortalities, mostly prevalent in developing countries. Therefore, to prevent the spread of waterborne diseases multiple barriers including prevention of contamination, sanitation, and disinfection are necessary [1]. However, if only one barrier is possible, it has to be disinfection unless evidence exists that chemical contaminants are more harmful than the risk from

ingestion of microbial pathogens [1]. Additionally, water quality control at the place of use is most effective due to the issues of regrowth of microbes, by-products of disinfectants, corrosion of pipelines and contamination in the distribution system [2,4]. Chlorination, filtration, UV-disinfection, pasteurization/boiling, and ozone treatment are some common techniques for water disinfection [1,2,5]. Though at large scale chlorine treatment is effective, it is expensive for smaller places like towns and villages. Also, boiling is an effective method for water disinfection; but the cost of fuel required to disinfect water is expensive [1]. Disinfection with UV radiation is a promising point-of-use technology available today [1]. Again it requires electricity and maintenance of a UV lamp, or enough sunlight. Under these circumstances small and cheap filtration equipment can satisfactorily solve the problem of point-of-use disinfection. Unfortunately, there does not exist an ideal technology for this purpose. The carbon-based filters are inexpensive, but are not effective in expunging pathogens [1]. Sand filters offer an excellent substitute that can remove pathogens but they require a sizeable area and maintenance knowledge [1]. The membrane filtration processes capable of removing pathogens [2,4] have high cost, undergo membrane fouling, and require power for pumping water on account of low flow rates [6], hence, are difficult to have their wide implementation in developing countries.

* To whom all correspondence should be sent:
E-mail:hanief@nitsri.net

In this regard, novel processes are urgently needed which outperform current technologies. To be precise, membrane materials that are cheap, readily available, effective at pathogen removal and finally disposable, could considerably impact our capability to provide clean drinking water. A hope for this purpose comes from the nature itself. A potential solution exists in the form of plant xylem which is a porous material that conducts fluid in plants [7]. Plants have specialized xylem tissues to transport sap from their roots to the shoots. Xylem tissues have developed under competing pressures, offering minimal resistance to the ascent of sap while maintaining the structure of small nanoscale pores to prevent cavitation. The size of these pores typically varies from few nanometers to around 500 nm, depending on the species of plants [8]. The plant xylem happens to be an ideal material for filtering out pathogens. This presents an opportunity to researchers to investigate whether plant xylem can be adopted as an inexpensive water filtration device.

The xylem tissue has tiny ducts working in parallel (Fig. 1(a)). The elements of conduction in xylem tissue vary in angiosperms and gymnosperms (Fig 1(b)). In gymnosperms, these ducts are present as unicellular dead elements called tracheids. Tracheids can have a diameter and length up to 80 μm and 10 mm, respectively. Vessels are the elements of water conduction in angiosperms. The vessels may have a diameter up to 0.5 mm, while their length ranges from a few millimeters to a few meters [9]. Pits connect these conducting elements with their adjacent ones. The pit membranes have pore size ranging from a few nanometers to a maximum of around 500 nm, depending on the plant species. Pores in the pit membranes were the basic filtration unit in this research. The angiosperms have longer vessels and, therefore, to force water through the pit membrane, a large thickness of the xylem is required. In angiosperms, xylem tissue makes up a smaller fraction of the cross-sectional area of the trunks and branches and hence was not used. The shorter tracheids in the xylem tissue of gymnosperms are ideal for the purpose. Correa and Sens [10] investigated the pine, virola, and cedar wood membrane for filtration. The study investigated the removal of color and turbidity with the flow in the perpendicular direction of fibers. There was a small difference in respect to the efficiency of membranes with a thickness between 1.0 and 2.0 cm. The membranes were in the range of 30–35% efficiency for color and turbidity. The membrane with a thickness of 3.0 cm had enhanced performance with 50% average efficiency for color and turbidity. It has been found that the anisotropy

of wood poses challenges when deformation occurs with loss or gain of humidity leading to cracks during the drying process. The use of wood membrane filters intended for the separation proved to be effective. Several processes are in the initial phase of development, in which the main determining factor is the relationship between filtration and the pore size of the filtered material. Due to the geometric conformation of membranes, the filtration performed in a conventional manner passes in the cross-flow direction. The reason being that the flow observed certain turbulence on its surface which results in the dragging of particles that cause incrustation. With cross-flow filtration, it is advisable to apply some pressure to “push” fluid through the pores of the membrane for collection on the other side. The applied pressure must comply with the manufacturer’s recommendations to avoid surface damage. The wood is mainly composed of lignin (ranging from 18 to 35%), hemicelluloses, and cellulose (ranging from 65 to 75%) polymeric materials which are considered complex, particularly polymeric substances. A study of filter elements with varying degrees of thickness to establish a relationship between wall thickness and efficiency was performed by Correa and Sens [10]. In order to understand the water transport through wood, familiarity with its chemical composition is important. These compositions vary according to several factors, such as geographic location, climate, and soil type. Therefore, the chemical composition is not accurately defined for a wood species or even for a specific wood. There are other components that are present mainly in the form of extractable organic and inorganic substances, such as oils, resins, sugars, starches, tannins, nitrogenous substances, organic acids, and organic salts (ranging from 4–10%). These extracts contribute to the organoleptic properties of wood, such as smell, color, taste, and its resistance to fungi and insects. The elements that make up the wood, in general, are carbon (50%), oxygen (44%), hydrogen (5.5%), and traces of many metal ions [2]. Sens *et al.* [11] studied dead-end filtration and helical cross-flow in wood. The three species of wood studied were: caixeta (*Tabebuia cassinoides*), garapuvu (*Schizolobium parahyba*), and pine (*Pinus elliottii*). They concluded that the filtration obtained was microfiltration, and filtration in the perpendicular direction was found to be infeasible. Boutilier *et al.* [12] conducted experiments on wood from white pine (*pinus strobus*). They used deionized water for the experiments. Red pigment (Higgins Ink), 20 nm fluorescent polystyrene nano-spheres, and

inactivated fluorescent dye-labeled *Escherichia coli* were also used.

Studies revealed that the sap flow rate in plants in the range of several liters per hour may be feasible with less than 10 cm-sized filters, using only hydrostatic pressure to drive the flow [7]. The investigation first of its kind on the pine, *pinus strobus*, which grows in USA was used by Boutilier et al. [12]. Nile-red coated 20-nm fluorescent polystyrene nano-spheres and Alexa 488 fluorescent dye-labeled *Escherichia coli* were used in this study. The present study aims to investigate the filtration characteristics of the *Cupressus cashmeriana* so as to find if it can be used as a filtration material. Since the safety of drinking water is a critical issue in this part of the world the Kashmiri cypress was chosen because of its availability.

In this context, new approaches that can improve upon current technologies on the grounds of expenditure, biodegradability, availability are urgently needed. A potential solution exists in the form of plant xylem – a porous material that conducts fluid in plants. Plants have evolved specialized xylem tissues to conduct sap from their roots to their shoots through the process of transpiration. Under competing pressures, the xylem has evolved into a robust conductive tissue that efficiently allows the flow of sap while also preventing the cavitation and development of bubbles that could halt the process.

Various experiments were performed on this tissue to reveal about its permeability and various factors affecting it, necessary for development of a cost-efficient filtration system to serve the purpose.

In angiosperms, xylem tissue constitutes a smaller fraction of the cross-sectional area of the trunks and branches and hence was not used. The observed conductivities were in the range of $5\text{-}6 \times 10^{-10} \text{m}^2 \text{Pa}^{-1} \text{s}^{-1}$. Their pigment filtration experiments revealed a size cutoff of about 100 nm and most of the filtration occurred within the first 2-3 mm of the xylem filter. The xylem filter had a bacterial rejection rate exceeding 99.9%. Ericson et al. [6] conducted permeability experiments on wood and analyzed the factors affecting the rate of flow. The fluids used were zinc chloride, water, and benzene.

The present study aimed to investigate the filtration capability of Kashmiri cypress scientifically known as *Cupressus cashmeriana*. The experiments were performed to study the permeability and filtration capability necessary for developing a cost-efficient filtration system to serve the purpose. Post the experimentation, particle size

analysis (PSA) was performed for determining the size range of the particles in the unfiltered and filtered samples.

To evaluate the chemical composition of both the filtered and unfiltered samples, Fourier Transform Infrared Spectroscopy (FTIR) was used.

EXPERIMENTAL SETUP

Materials and methods

The setup comprised an air compressor (Fig. 2), of 1.5 hp capacity, to generate the required pressure gradient. A transparent pliable plastic tube of ample length and diameter was used to hold the specimen membrane by steel clips. The other end of the tube was connected to the compressor. A measuring cylinder of 10ml capacity was used for measuring the flow rate. An adjustable stand was used to hold the setup upright. For sealing the filters, epoxy resin was used. The filter elements were secured using pipe clips. Branches from cypress (*Cupressus cashmeriana*) were cut with a manual hack saw. The branches were cut into small pieces of desired size by an electric saw. 1.5 cm thick sections with a cross section of approximately 2.5 cm^2 were cut from the branch. The sections were inspected for the presence of any nodes. The bark was peeled off and the sections were soaked in distilled water. The ends were cleaned with ethanol using a brush. Then the sections were inserted into the end of the plastic tube and sealed using epoxy resin. The ends were secured using pipe clips.

Filtration and flow rate measurement

The compressor tank was prefilled until a specific pressure was reached. The pressure used for the study was 0.295 bar (gauge pressure) equivalent to 3 m head of water, for our filtration experiments. The contaminated water was introduced into the tube which was subjected to high pressure from one end, the other end was sealed with the wood membrane. Then the same end was connected to the compressor tank and the pressure was applied. The filtrate was collected in a measuring cylinder and the flow rate was measured using stopwatch. Three readings were taken and the flow rate was averaged. The samples were pre-treated with alum before the filtration process. The filtrate samples were collected and sealed in the test tubes to avoid any contamination from the atmosphere (Fig. 3). In order to determine the particle size of the contaminants before and after the filtration Anton Paar LiteSizer 500 was used.

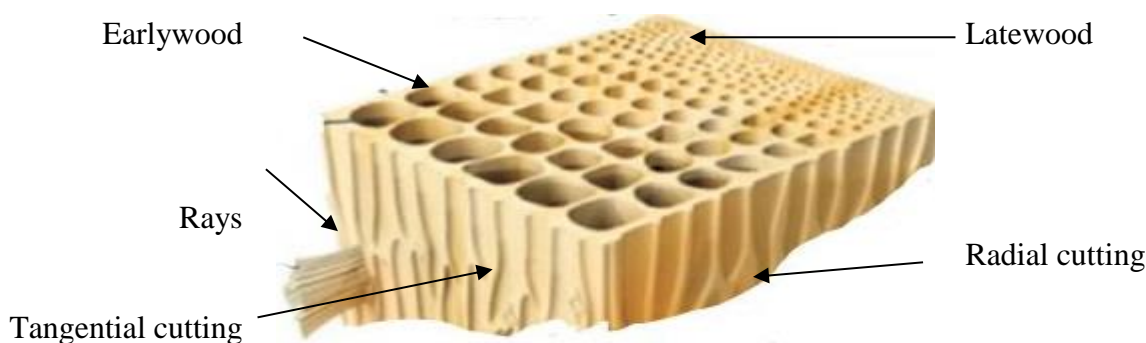


Fig. 1. (a) Anatomy of wood depicting its porosity [1]

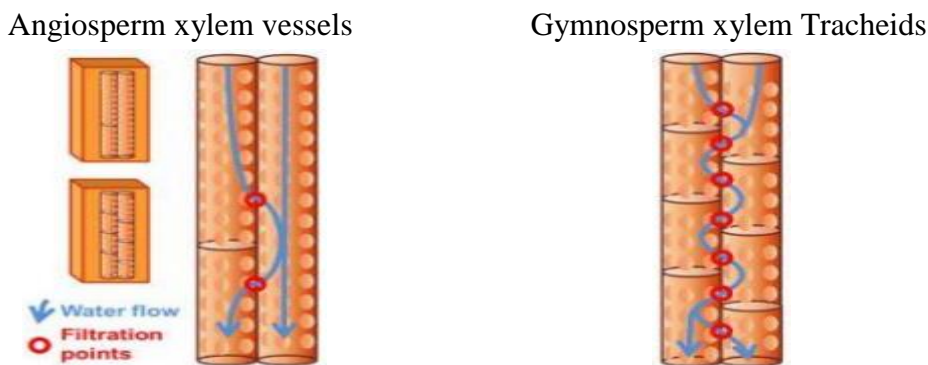


Fig. 1. (b) Flow through xylem conductive tissue [2]

RESULTS AND DISCUSSION

In the preliminary testing phase, the efficacy of the filter was tested visually by filtering a suspension of clay and sand in water. It was compared with the unfiltered water sample. The filtrate was clear, indicating that the filter was capable of removing turbidity caused by suspended and colloidal impurities. The flow rate measurements revealed that the filter with a thickness of about 0.65 cm and cross-sectional area of 100 cm² had a flow rate of 4 liters per day under a gauge pressure of 0.295 bar (3 m of water) which is enough to meet the daily drinking water needs of one person. The flow rate was directly proportional to the applied pressure and the filter cross-sectional area and inversely proportional to the membrane thickness. The hydrodynamic conductivity was calculated using Eq. (1):

$$Q = kA\Delta P/l \quad (1)$$

where Q is the volumetric flow rate (m³s⁻¹), ΔP is the pressure difference across the filter (Pa), A and l are the cross-sectional area (m²) and the thickness of the filter (m), respectively. The value of hydrodynamic conductivity was in the range of 8 to 10 × 10⁻¹³ m²Pa⁻¹s⁻¹.

Particle size analysis (Fig. 4) was performed on the collected samples to determine the effectiveness of the membrane to eliminate the suspended matter. The tests revealed that the size of the contaminants ranged from ~90 nm to ~10 μm. Then the filtrate was analyzed. The size of the contaminants in the filtrate ranged from ~90 nm to ~300 nm. The filtrate particle size distribution peaked at ~100 nm. The filter was effectively able to reject particles larger than ~300 nm. The rejection rate was greater than 99.8%. Most pathogenic bacteria larger than this size are therefore removed. For example, *Vibrio cholera*, the bacteria that causes the water-borne disease cholera is 1-3 μm in length and 0.5-0.8 μm in diameter and the typhoid-causing bacterium *Salmonella typhi*, is 2 – 5 μm in length and 0.5 - 1.5 μm in diameter. This implies that the filter is capable of filtering out most fungal spores and bacteria from polluted water. Fourier Transform Infrared Spectroscopy (FTIR) test was done using Perkin Elmer Spectrum IR on the unfiltered and filtered samples. FTIR plots the transmittance, which is percentage amount of radiation absorbed by the sample *versus* wave number (cm⁻¹), which is defined as the reciprocal of wave length. The results were identical for the unfiltered and filtered samples. It was concluded that no change in the chemical

composition took place. According to preliminary tests, the filter successfully eliminated the turbidity.

The size of the pores in the pit membranes ranges in nanometers, and hence, it is effective in removing suspended and colloidal impurities. Flow rate experiments indicated that flow rate is directly proportional to cross section area and pressure difference and inversely proportional to filter thickness.

A thicker filter offers more resistance to the flow of water through it. However, a thicker filter increases the rejection rate up to a certain limit (Fig. 5). In a separate experiment the filtered samples were pre-treated with alum. It was observed that the treatment with alum prior to filtration increased the flow rate and the filter life for turbid water. No change in chemical composition was detected using FTIR analysis. The profiles in Fig. 6 and Fig. 7 were

similar, implying that the unfiltered and filtered samples had the same broad chemical composition. This was to be expected as the given study lacks chemical treatment procedures. Chemical contaminants can be adsorbed using adsorbents such as activated carbon. The experimental results of the study are presented in Table 1 for a cross sectional area of 100 cm^2 and $P=0.295 \text{ bar}$. After conducting experiments on fresh wood, an additional investigation was performed on the dried wood. It was found that dried wood is not effective for filtration. The idea was thus discarded as the flow rate was by two orders of magnitude slower. Also to compensate for the decrease in flow rate, thinner sections were cut, but no appreciable filtration effect was observed in this case. The thinner sections were also prone to cracking on application of pressure.

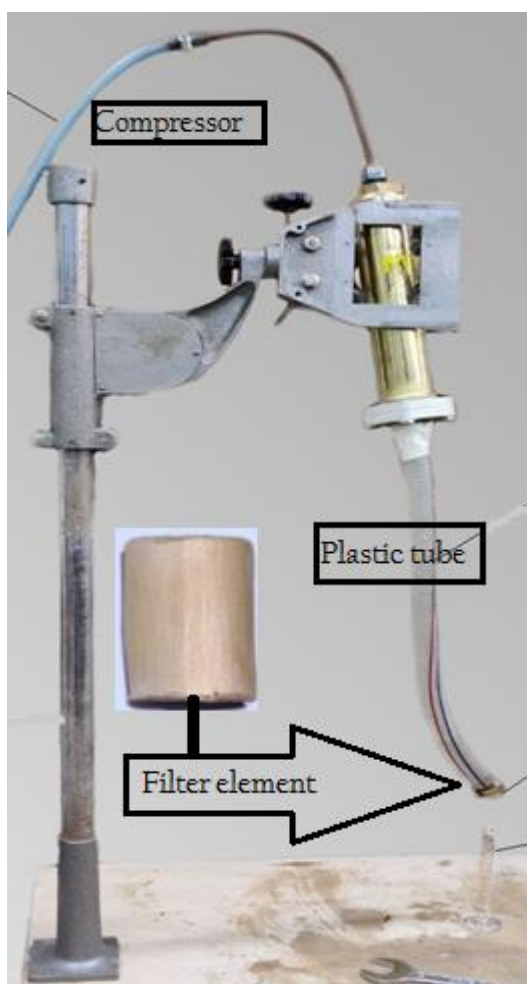


Fig. 2. Set-up used for experiments



Fig. 3. Test results

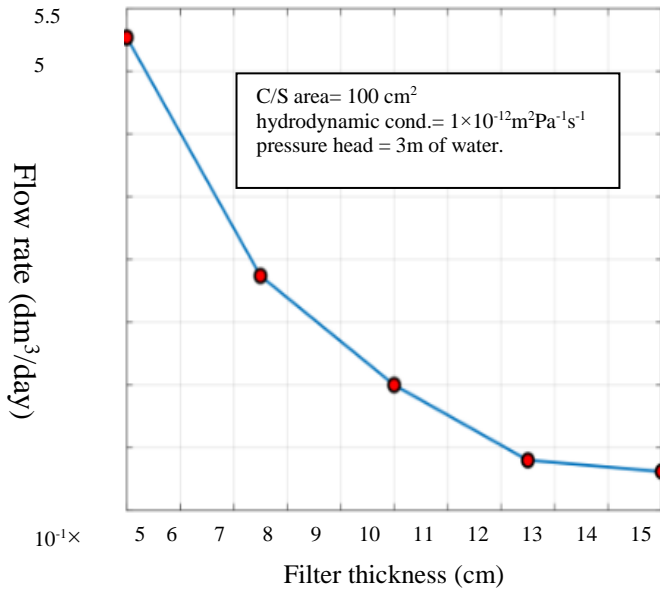


Fig. 4. Particle size distribution in the sample before filtration and after filtration

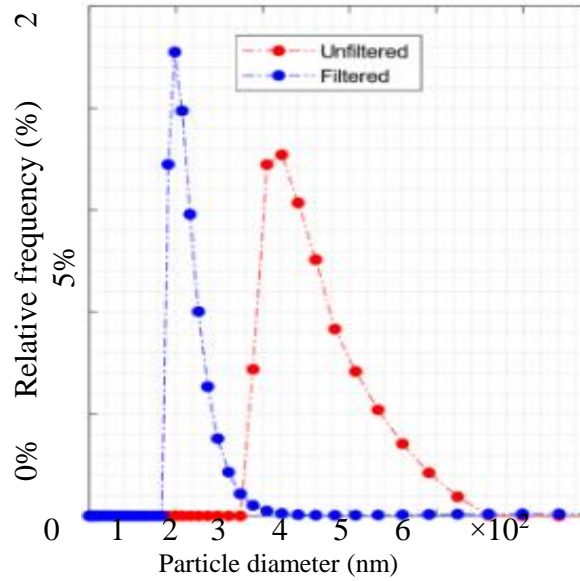


Fig. 5. Variation of the flow rate with filter thickness

Table 1. Experimental results

Thickness of filter element (cm)	Time taken	Flow rate (ml/s)	Flow per day (dm ³ /day)
0.50	164	0.061	5.27
0.75	257	0.039	3.37
1.00	345	0.029	2.50
1.25	454	0.022	1.90
1.50	476	0.021	1.81

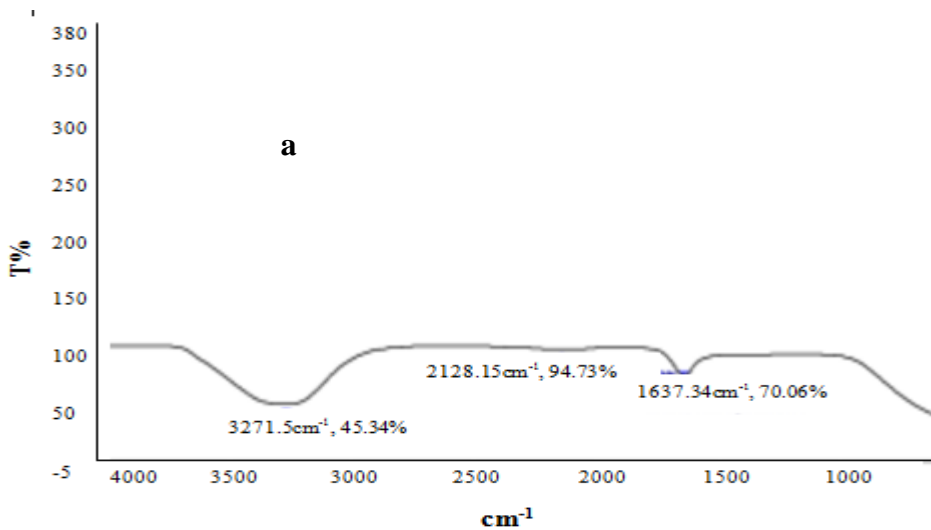


Fig. 6. FTIR spectrograph of unfiltered sample

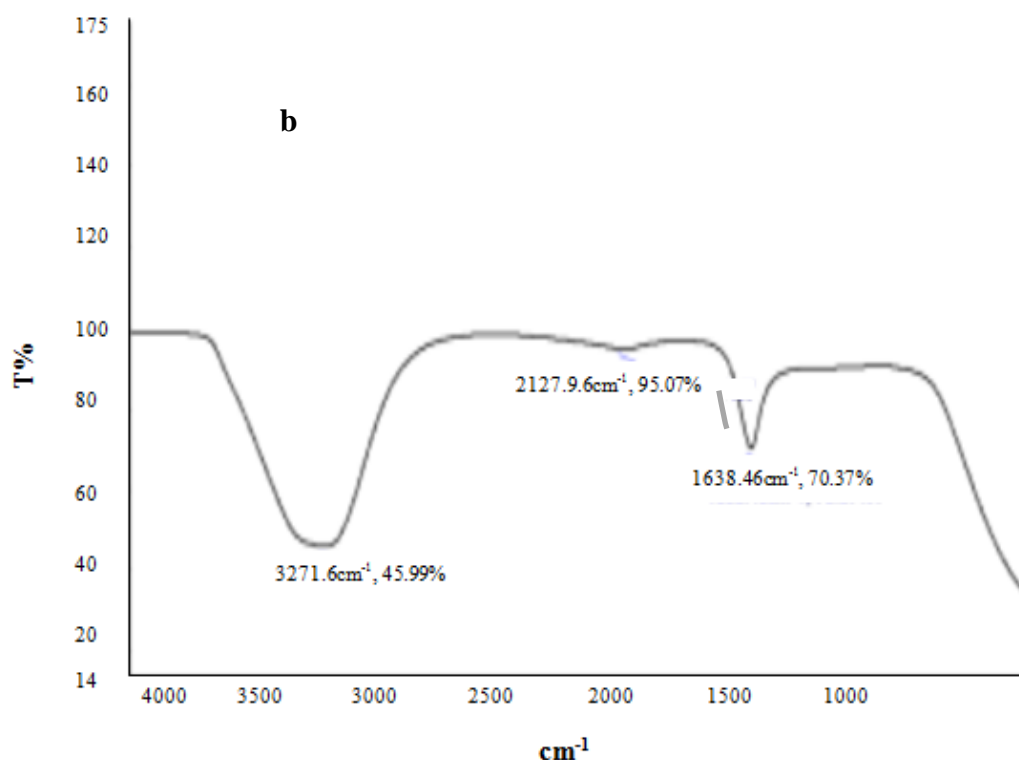


Fig. 7. FTIR spectrograph of filtered sample

CONCLUSIONS

Plant xylem can be used effectively for filtration of water. A gymnosperm xylem filter was prepared using *Cupressus cashmeriana*, which was able to effectively filter out particles larger than 300 nm. The particle rejection rate was 99.8%. A flow rate of 4 liters per day was obtained through a filter element of cross-sectional area 100 cm² under a gauge pressure of 0.295 bar. The chemical composition was found to remain unchanged after filtration.

Cheap conventional treatment methods like treatment with alum before filtration can increase the filter life significantly. There is a bright scope for investigating other gymnosperm species which have much smaller pit membranes for filtration of viruses and other pathogens. Wood seasoning and its effect on filtration need further study. Ion exchange methods can be used in conjunction with the xylem filter to develop a much more effective filtration system.

Acknowledgements: To be presented in International Chemical Engineering Conference on “100 Glorious Years of Chemical Engineering & Technology” from September 17 to 19, 2021, organized by Department of Chemical Engineering at Dr B R Ambedkar NIT Jalandhar, Punjab, India (Organizing Chairman: Dr. Raj Kumar Arya & Organizing secretary: Dr. Anurag Kumar Tiwari).

REFERENCES

1. A. Gadgil, *Annual Review of Energy and the Environment*, **23**, 253 (1998).
2. M. Peter- Varbanets, C. Zurbrugg, C. Swartz, W. Wouter Pronk, *Water Research*, **43**, 245(2009).
3. World Health Organization, http://www.who.int/water_sanitation_health/mdg1/en/.
4. S. S. Madaeni, *Water Research*, **33**, 301(1999).
5. M. D. Sobsey, C. E. Stauber, L. M. Casanova, J. M. Brown, M. A. Elliott, *Environmental Science and Technology*, **42**, 4261 (2008).
6. S. L. Loo, A. G. Fane, W. B. Krantz, T. T. Lim, *Water Research*, **46**, 3125 (2012).
7. J. S. Sperry, *International Journal of Plant Sciences*, **164**, S115 (2012).
8. B. Choat, A. R. Cobb, S. Jansen, *New Phytologist*, **177**, 608 (2008).
9. S. Jansen, B. Choat, A. Pletsers, *American Journal of Botany*, **96**, 409 (2009).
10. E. Correa, M. L. Sens, Filtrac, UFSC, Florianopolis, SC, 23(2002).
11. M. L. Sens, M. L. Emmendoerfer, L. C. Muller, *Desalination and Water Treatment*, **53**(1), 15 (2015).
12. M. S. H. Boutilier, J. Lee, V. Chambers, V. Venkatesh, R. Karnik, *PLoS One*, **9**(2), e89934. (2014).

Substance flow analysis of lead and chromium through wastewater management system in a region

M. Gupta, A. Kumar*, S. Kumar, M. K. Jat

Malaviya National Institute of Technology Jaipur, Jaipur-302017, India

Received: November 23; Revised: January 14, 2022

Inappropriate waste management practices have resulted into pollution of the environment in urban and rural areas in India. The pollution from heavy metals requires attention owing to the toxicity of these metals for human beings. The study analyses the management of wastewater in Hanumangarh district, a region in the state of Rajasthan, India and the consequent flow of two heavy metals, lead and chromium. For this purpose, the *status quo* for the management of wastewater has been compared with two alternative scenarios. The analysis has been performed using the techniques of material flow analysis (MFA). The results indicate the major flows of Pb and Cr in the system and, the points of action for achieving the waste management goals more closely than the current system.
[copyright information to be updated in production process]

Keywords: Wastewater management; material flow analysis; heavy metals; scenario analysis; urban pollution.

INTRODUCTION

Wastewater management in India has become one of the major problems for Indian cities. The mismanagement of municipal wastewater in Indian cities has led to the accumulation of hazardous substances into the environment [1, 2]. The heavy metals in Indian cities are one of the important classes of hazardous substances in the anthroposphere [3].

Lead and chromium are both heavy metals that have been linked to cancer in humans. Individuals exposed to extremely high levels of lead and chromium suffer from anaemia, weakness, kidney and brain damage. Lead exposure at exceptionally high levels can be lethal. Because lead can pass through the placenta, pregnant women who are exposed to it risk harming their unborn child. Lead is harmful to an infant's nervous system as it develops. Exposure to chromium damages the liver, produces pulmonary congestion and edema, upper abdomen discomfort, nasal irritation, and tooth discoloration [4, 5]. As a result, it becomes important to understand the flow of these substances, i.e., Pb and Cr in a region. The techniques of MFA have been used to study the mass flows of Pb and Cr through a wastewater management system [6]. Scenario analysis has been used to better comprehend the long-term environmental consequences of alternative waste management systems [7].

MFA is based on the conservation of matter and permits the identification and measurement of a substance's sources in system, its temporal accumulation within the system, and its transfer to natural or manmade sinks. Substance-bearing items

or materials are transformed, transported, or stored in intermediate stages. Coefficients of transfer are used to characterize the flow of such process inputs to outputs. The MFA methodology is advantageous for identifying the primary sources and sinks of emissions, as well as for planning reduction targets and long-term retention or disposal [8].

The objectives of the study are: (i) to quantify the flow of lead and chromium through a wastewater management system; (ii) to postulate alternative scenarios and quantify the flow of lead and chromium *via* various stages of a wastewater management system in all the scenarios; (iii) to compare the three scenarios in terms of the quantities of wastewater, Pb and Cr being discharged into the environment. The scope of the study is limited to the ULBs of Hanumangarh District in the state of Rajasthan.

MATERIALS AND METHODS

Study Area

The district of Hanumangarh is located at 29° 5' to 30° 6' north and 74° 3' to 75° 3' east. The district covers a total land area of 9,703 square kilometers. Prior to this, the city was known as "BHATNER". In year 1805, emperor Soorat Singh of Bikaner captured BHATNER after defeating Bhatias and as the day of his victory was Tuesday (known as the day of god "Hanuman"), he named BHATNER as "HANUMANGARH". There are total six ULBs in the Hanumangarh district, namely, Bhadra, Nohar, Pilibanga, Rawatsar, Sangaria, and Nagar Parishad Hanumangarh.

* To whom all correspondence should be sent:
E-mail: amitrathi.ucf@gmail.com

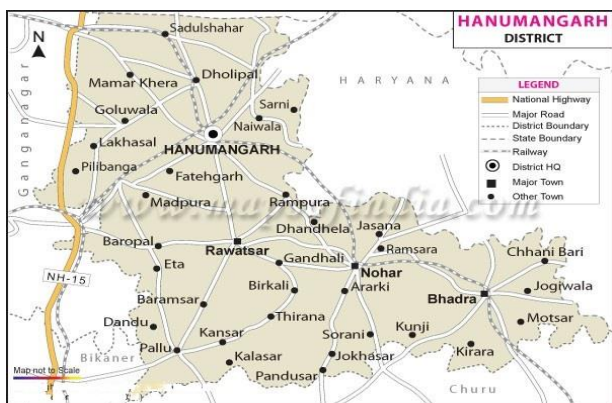


Figure 1. Map of Hanumangarh (Source: [9])

Data Collection

Data have been collected through personal interviews, telephonic conversation with representatives from the various governmental departments in Hanumangarh district. Data were also gathered from the official websites of the city, state and, municipal agencies such as the Department of Industries, CPCB, CPHEEO and RSPCB. An extensive literature search was conducted to determine the lead and chromium concentrations in treated & untreated wastewater, fecal sludge, and sewage sludge.

Scenarios for analysis

The current study looked at three different municipal wastewater management scenarios. The first scenario depicts the current state of wastewater management in Hanumangarh. In scenario 2, the emphasis is on increasing the reach of sewer connections for the households and the wastewater reaching the wastewater treatment plants (WWTPs). The scenario 3 involves increasing wastewater reaching WWTPs and the provision of an engineered landfill for disposal of sewage sludge. Table 1 presents a summary of all the three scenarios.

Scenario 1 illustrates the current state of wastewater management in the area. According to statistics provided by the Hanumangarh administration, the total quantity of wastewater reaching the wastewater treatment facilities for treatment in the is about 2062 million litre (ML)/annum. As all the households in the district are yet to be connected to a sewage system, this wastewater quantity represents a fraction of the volume of wastewater being generated in the district. Majority of the households that are not connected to the sewerage system, are using on-site treatment of wastewater by employing septic tanks. These septic tanks are cleaned every 2-3 years. The fecal sludge from the septic tank is illegally disposed of outside the city limits. The effluent from the septic tank is

discharged into the storm water drains and it is assumed that it ultimately makes its way into the agriculture soil.

Table 1. Scenarios for WW management in Hanumangarh urban area

Scenario	WW fraction for treatment	Treated WW Utilization	Disposal of sludge
Present Scenario (Scenario 1)	24% of wastewater reaching the STPs	Application to agriculture fields	Uncontrolled dumping
Enhanced Treatment Scenario (Scenario 2)	90% of wastewater reaching the STPs	Application to agriculture fields	Uncontrolled dumping
Alternate Scenario (Scenario 3)	90% of wastewater reaching the STPs	Application to agriculture fields	Engineered Landfill

Scenario2 is being postulated with the objective of increasing the connectivity of the households to the sewerage system and subsequently the amount of wastewater treated in the district. Fecal sludge (settled sludge) produced by a septic tank is assumed to be disposed off in the forest soil, whereas wastewater treatment plant sludge is discarded in the agricultural soil.

The alternate scenario, referred to as 3, is defined by the incorporation of engineered landfill into the first two scenarios. Production and collection of wastewater are the same as in scenario 2, with the exception that the sludge generated in septic tanks and WWTPs is disposed off in an engineered landfill.

Estimations for MFA

Material flow analysis is being used to examine the wastewater management of the system under consideration. For computational considerations, a one-year timeframe was chosen in accordance with the static MFA method. The following processes are included in the study: collection, sewage system, wastewater treatment plant, septic tank, engineered landfill, and soil (categorized into agriculture soil and other soil).

To calculate uncertainty in the data obtained from literature, the Monte Carlo Simulation (MCS) is employed. The statistical distributions of the input variables are assumed as normal distribution in this study. The confidence interval was selected as 95 percent [10]. The concentrations of lead and chromium in the influent and effluent wastewater, and sludge were taken from literature reviews [11–15] and calculated for this study using Monte Carlo simulation.

The entire quantity of WW generated inside the system boundary is taken into consideration in the first two stages, namely the urban household and the generating process, respectively. The input and output flows for wastewater have been assumed to be the same in all three scenarios.

The total amount of wastewater generated was estimated by taking into account the water supply as specified in [9]. The fraction of grey water in the wastewater generated is taken from [16].

In the sewer system process, the total number of households that are linked to the sewage system is taken into consideration in order to determine the total flow of wastewater. In scenario 1, only a fraction of households is linked to the sewage system (as provided by the Hanumangarh officials), which amounts to 24 percent of the total amount of wastewater flowing through the system. In scenarios 2 & 3, the total amount of wastewater that enters the sewage system is assumed to equal 90 percent of the total.

Septic tank is the method by which black water generated is treated at the household level, and it is taken into consideration in all three scenarios discussed here. In scenarios 1, 2, & 3, the wastewater from all the households without connectivity to sewer network, is discharged into the septic system. The effluent from the septic tank is assumed to go into the other soil.

WWTPs are the facilities that treat wastewater. According to scenario 1, only 24 percent of the entire wastewater is treated; however, according to scenarios 2 & 3, 90 percent of the entire wastewater is assumed to be treated. In all three cases, the flow from the sewage system is received by this mechanism.

Each of the three scenarios involves the use of treated wastewater on agricultural soil. The sludge from wastewater treatment plant is being disposed of in agricultural land and, has been assumed the same in scenarios 1 & 2. The sludge settled in the septic tank is emptied every 2-3 years and is discarded illegally outside the city limits. The sludge from septic tanks has been assumed to be disposed on forest soil in scenario 1 and scenario 2.

Scenario 3 assumes an engineered landfill, and that all of the sludge (from the WWTPs and settled sludge from the septic tanks) is disposed of there. The data regarding the concentrations of lead and chromium in settled sludge and overflow wastewater from septic tank are derived from [17].

The processes, agriculture soil, and forest soil have all been taken into consideration in order to illustrate the movement of pollutants into the soil. Due to the fact that some waste processing products,

such as treated wastewater, are used in agriculture soil particularly, the soil has been divided into two categories.

RESULTS AND DISCUSSION

The results from the material flow regarding the overall wastewater quantities, and quantities of lead, and chromium for all the scenarios are discussed in this section.

In scenario 1, the maximum flow is 8,232 ML to agricultural soil, of which only 2,062 ML is treated wastewater, the remaining is untreated wastewater and sludge from WWTPs (Figure 2). In contrast to scenario 1, scenario 2 has more houses connected to the sewer system, resulting in 7429 ML of treated wastewater being discharged in agricultural land (with only 536 ML of untreated wastewater and 74 ML of sludge being discharged) as shown in Figure 3. In scenario 3, the same quantities of treated and untreated wastewater (as in scenario 2) are applied to agricultural soil, however, all of the sludge produced is discarded in the engineered landfill (Figure 4). According to scenario 1, the agricultural soil getting the maximum deposition of Cr is amounting to 4.8 tons (Figure 5). According to scenario 2, the same quantity, i.e. 4.8 tons of Cr are disposed on the agricultural soil, indicating the *status quo* in terms of Cr loadings to the environment. (Figure 6). On the other hand, just 2 tons of Cr are disposed of in the agricultural soil each year, as per scenario 3. Furthermore, by disposing off the 2.7 tons of Cr in the engineered landfill, the harmful effects of Cr may be contained by the landfill (Figure 7).

For the lead fluxes, the highest quantity of lead, i.e. 0.87 tons, is being applied to the agricultural soil in scenario 1 (Figure 8). However, despite the fact that scenario 2 has a larger number of households connected to a sewer system, it discharges higher amounts of lead into the agricultural soil, approximately 1.1 tons per year (Figure 9). The increase in Pb loadings to the agriculture soil is due to change in WW management system in scenario 2 from septic tank to the sewer system and the consequent change in final disposal from forest soil to agriculture soil. In scenario 3, the bulk of the lead is removed from the environment by confining it in an engineered landfill (Figure 10).

Upon examining all the scenarios, it becomes clear that just expanding the treatment system of wastewater will not be sufficient to address the present issue of heavy metal contamination. The bulk of heavy metals still winds up in agricultural soil as shown in scenario 2 (with greater volumes of wastewater being treated in WWTPs).

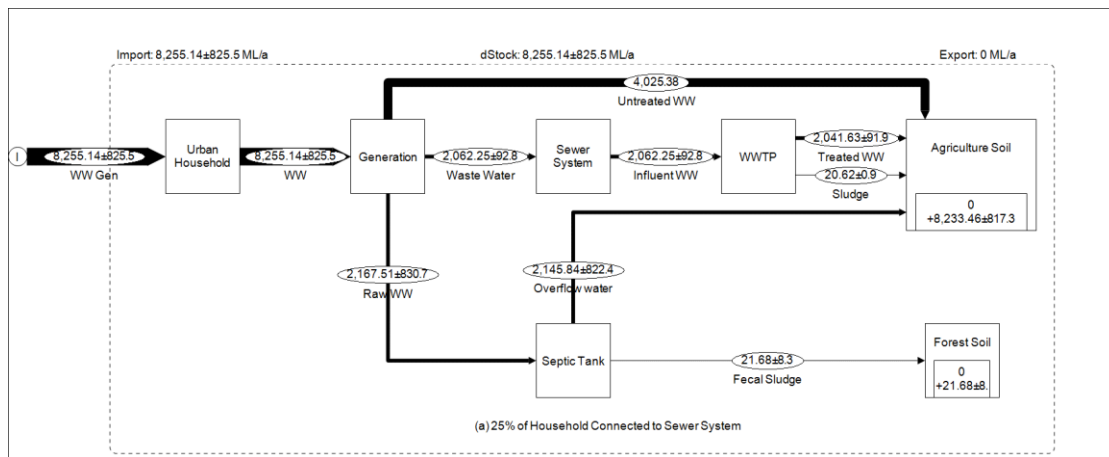


Figure 2. WW flow through Hanumangarh in scenario 1

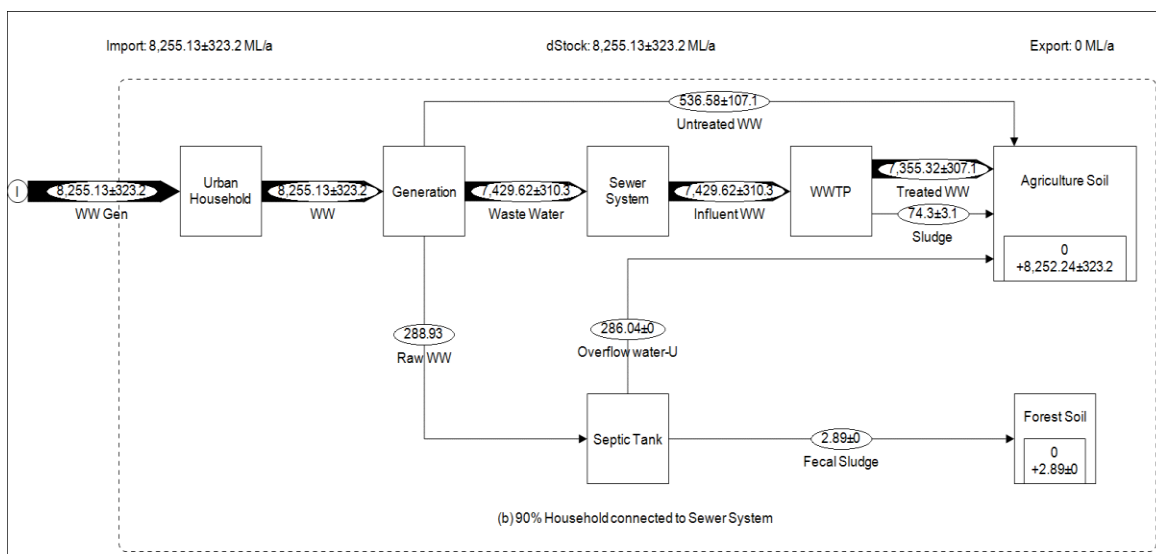


Figure 3. WW flow through Hanumangarh in scenario 2

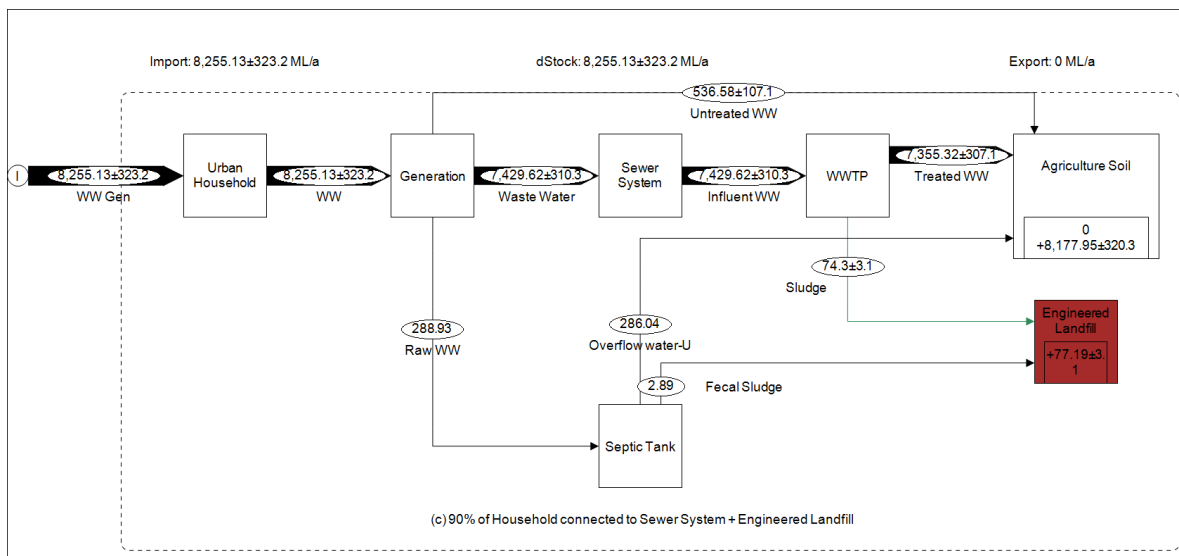


Figure 4. WW flow through Hanumangarh in scenario 3

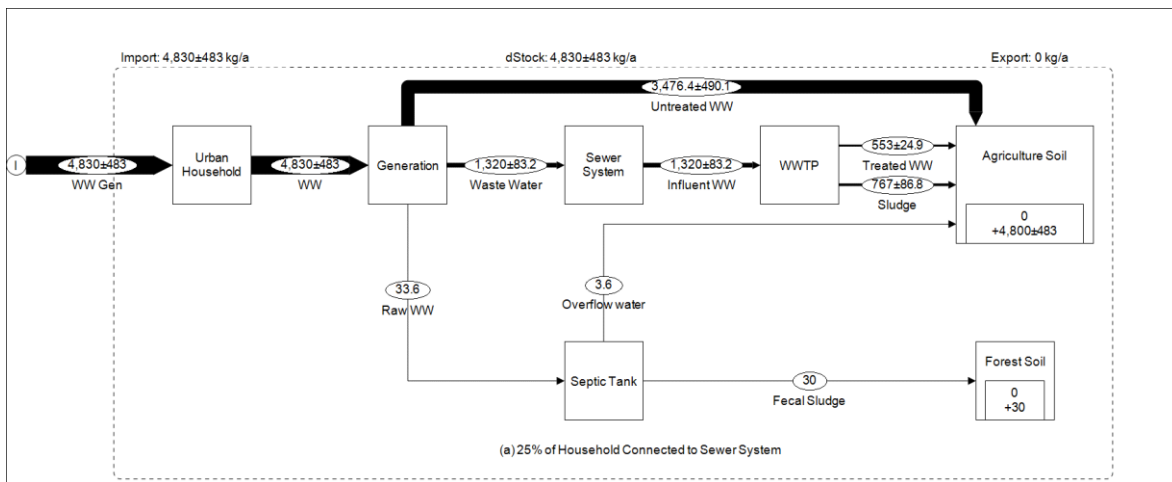


Figure 5. Flow of Cr through WW management system of Hanumangarh in scenario 1

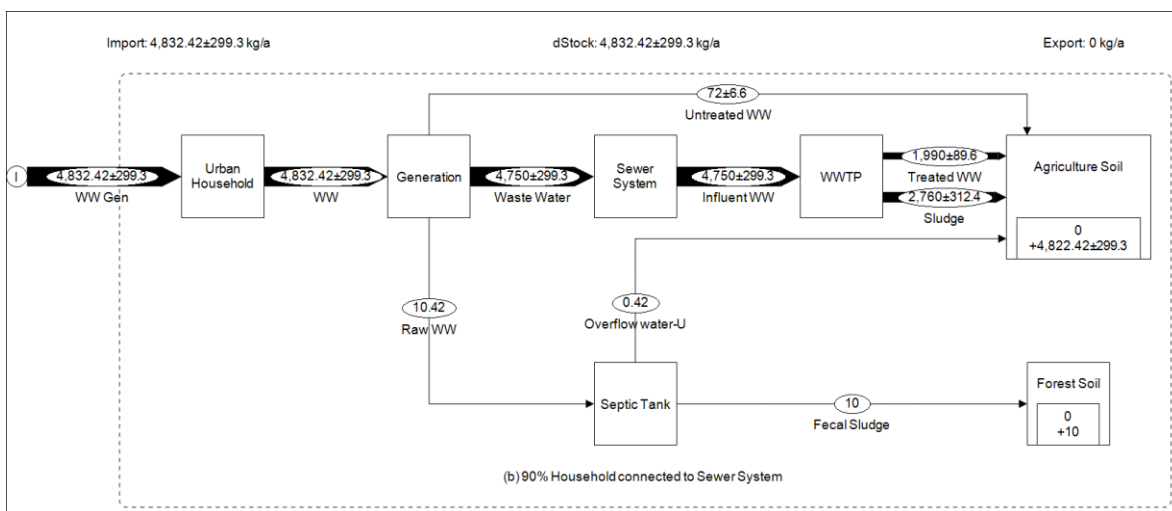


Figure 6. Flow of Cr through WW management system of Hanumangarh in scenario 2

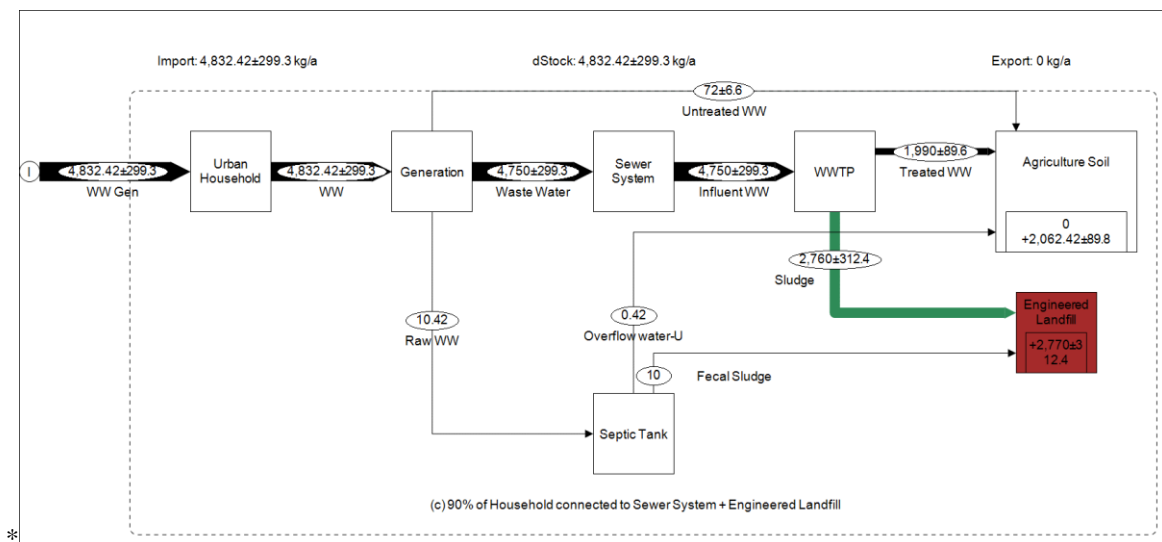


Figure 7. Flow of Cr through WW management system of Hanumangarh in scenario 3

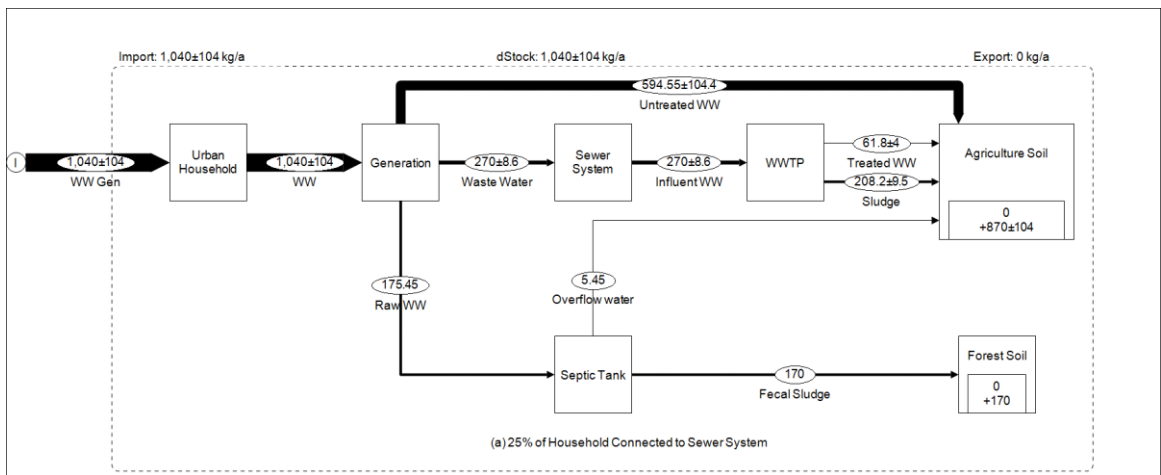


Figure 8. Flow of Pb through WW management system of Hanumangarh in scenario 1

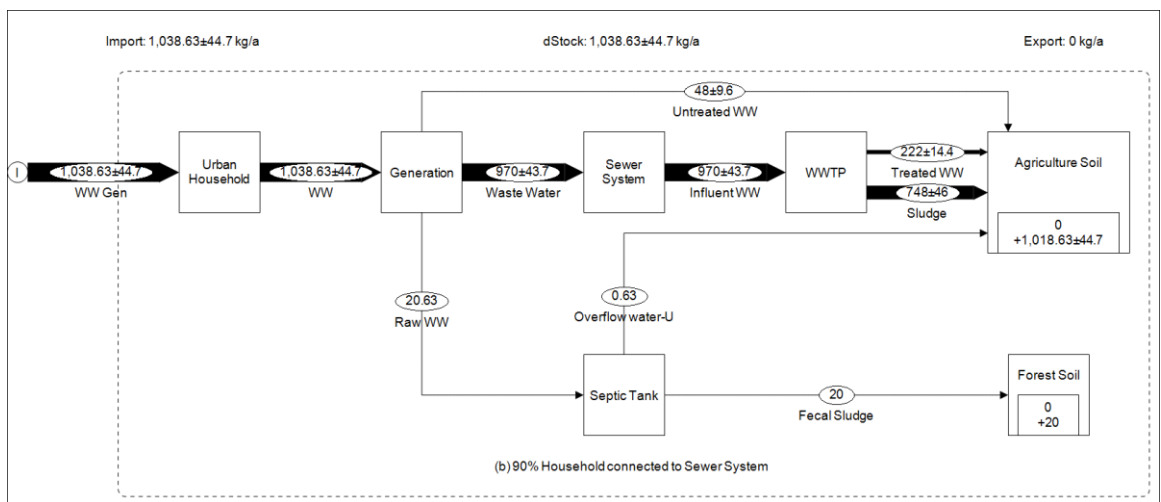


Figure 9. Flow of Pb through WW management system of Hanumangarh in scenario 2

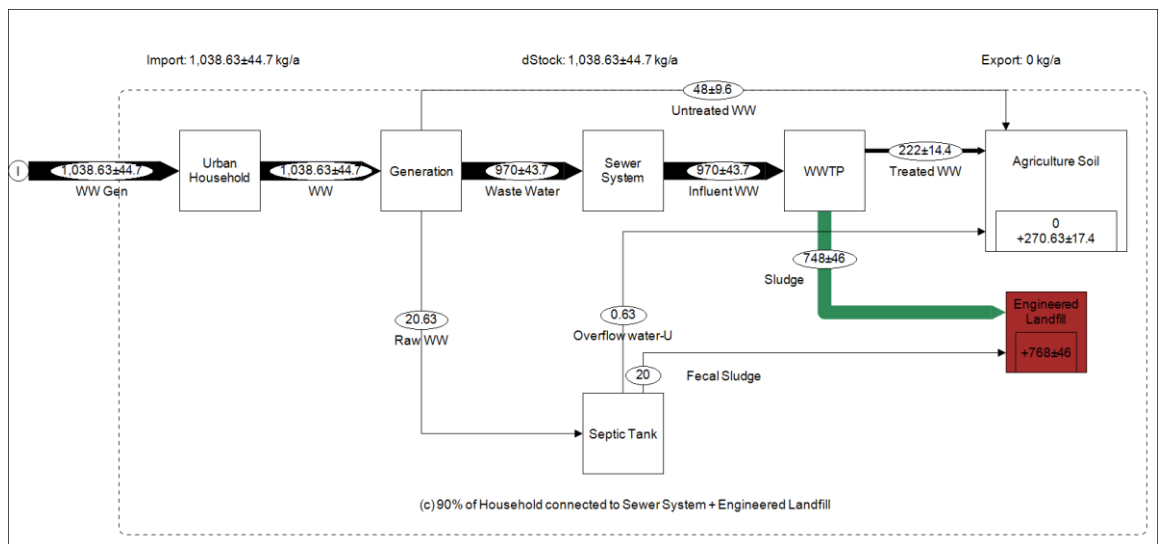


Figure 10. Flow of Pb through WW management system of Hanumangarh in scenario 3

Table 2 compares the amounts of lead and chromium released into the environment from the wastewater management system in Hanumangarh district.

Table 2. The flows of Pb and Cr in three scenarios

	S-1	S-2	S-3
Mass of Pb releasing into the environment (tons/years)	1.04 ±0.104	1.04 ±0.04	0.27 ±0.01
Mass of Cr releasing into the environment (tons/years)	4.830 ±0.483	4.830 ±0.299	2 ±0.09

In scenario 3, on the other hand, the use of an engineered landfill site results in the containment of lead and chromium from the surrounding environment. The present study indicates that the wastewater management system in an urban area can be a significant source of heavy metal pollution in the urban environment. These may enter the wastewater from the materials and activities in an urban area, e.g. runoff from roofs, food, or activities such as car washes [17]. In addition to deposition of pollutants from the atmosphere, application of insecticides and pesticides, as well as recycling of these toxins in the form of compost or sludge, among other also causes soil contamination [18].

Considering that modifying agricultural practices is a time-consuming process, the suggested option for the next several years (10-15) is an engineered landfill with enhanced capacity of the wastewater treatment system, as stated in scenario 3.

As per findings of this study, Hanumangarh emits around 3.46 g of lead per capita per year through wastewater management. For another study [4] in the same region (i.e. the state of Rajasthan) for wastewater management in a smaller system, the per capita use for lead metal comes out through be 6.9 g/capita/year. The results from this are also comparable to the study done at country level in China [19], where the per capita usage was calculated as 2.97 g/year. However, for a study done at city level in China [20], per capita consumption for lead is estimated to be 1.75 kg/year. These differences among the studies may be the result of considering a wide range of sectors in MFA studies for Pb flow [21].

CONCLUSION

Upon examining all the scenarios, it becomes clear that just expanding the collection and treatment of wastewater will not be sufficient to address the present issue of heavy metal contamination in

Hanumangarh district. The bulk of heavy metals still winds up in agricultural soil. The material flow analysis shows the importance of engineered landfill and enhanced treatment of wastewater for the better management of wastewater. The use of engineered landfill for the disposal of sludge ensures the isolation of heavy metals from the environment.

Acknowledgements: The authors would like to express their gratitude to Hanumangarh officials for investing their valuable time and supplying the study with the necessary data.

REFERENCES

1. R. S. Lokhande, P. U. Singare, D. S. Pimple, *Resour. Environ.*, **1**(1), 13 (2011), doi: 10.5923/j.re.20110101.02.
2. L. Sörme, R. Lagerkvist, *Sci. Total Environ.*, **98**(1–), 131 (2002), doi: 10.1016/S0048-9697(02)00197-3.
3. N. Lester, *Sci. Total Environ.*, **30**(1), 1 (1983), doi: 10.1016/0048-9697(83)90002-5.
4. A. Agarwal, A. Kumar, S. Dangayach, in: *Advances in Energy and Environment. Lecture Notes in Civil Engineering*, **142**, R. Al Khaddar, N. D. Kaushik, S. Singh, R. K. Tomar (eds.) Springer, Singapore, 2021.
5. J. Johnson, L. Schewel, T. E. Graedel, *Environ. Sci. Technol.*, **40**(22), 7060 (2006), doi: 10.1021/es060061i.
6. P. H. Brunner, H. Rechberger, *Practical handbook of material flow analysis*, Boca Raton, FL, USA, Lewis Publishers, 2016.
7. T. J. B. M. Postma, F. Liebl, *Technol. Forecast. Soc. Change*, **72**(2), 161 (2005), doi: 10.1016/j.techfore.2003.11.005.
8. L. Burger Chakraborty, A. Qureshi, C. Vadenbo, S. Hellweg, *Environ. Sci. Technol.*, **47**(15), 8105 (2013), doi: 10.1021/es401006k.
9. District Industries Centre Hanumangarh, "Industrial Potential Survey of District Hanumangarh (2019-2020)," 2020.
10. M. Aucott, A. Namboodiripad, A. Caldarelli, K. Frank, H. Gross, *Water. Air. Soil Pollut.*, **206**(1–4), 349 (2010), doi: 10.1007/s11270-009-0111-z.
11. E. Chirila, C. Draghici, A. Puhacel, *Environ. Eng. Manag. J.*, **13**(9), 2211 (2014), doi: 10.30638/eemj.2014.246.
12. K. M. Gani, M. Ali, A. Rajpal, H. Jaiswal, A. A. Kazmi, *J. Water Sanit. Hyg. Dev.*, **6**(1), 115 (2016), doi: 10.2166/washdev.2016.134.
13. F. Busetti, S. Badoer, M. Cuomo, B. Rubino, P. Traverso, *Occurrence and Removal of Potentially Toxic Metals and Heavy Metals in the Wastewater Treatment Plant of Fusina (Venice, Italy)*, 9264 (2005).
14. K. B. Chipasa, *Accumulation and fate of selected heavy metals in a biological wastewater treatment system*, **23**, 135 (2003).
15. M. J. Brown, J. N. Lester, *The role of bacterial extracellular polymers*, **13**, 1979.
16. E. Tilley, C. Lüthi, A. Morel, C. Zurbrügg, R.

- Schertenleib, *Development*, 158 (2008).
17. B. Vinnerås, H. Palmquist, P. Balmér, H. Jönsson, *Urban Water J.*, **3**(1), 3 (2006), doi: 10.1080/15730620600578629.
 18. O. Yuksel, *Environ. Monit. Assess.*, **187**(6) (2015), doi: 10.1007/s10661-015-4562-y.
 19. W. Liu, Z. Cui, J. Tian, L. Chen, *J. Clean. Prod.*, **205**, 86 (2018), doi: 10.1016/j.jclepro.2018.09.088.
 20. M. Oguchi, H. Sakanakura, A. Terazono, H. Takigami, *Waste Manag.*, **32**(1), 96 (2012), doi: 10.1016/j.wasman.2011.09.012.
 21. R. B. Chowdhury, G. A. Moore, A. J. Weatherley, M. Arora, *Resour. Conserv. Recycl.*, **83**, 213 (2014), doi: 10.1016/j.resconrec.2013.10.014.

Comparison of particle size distribution estimated by Rosin-Rammler equation vs Malvern particle size analyzer for different brands of PPC cement

S. Mahaboob Subhani¹, S. Altaf Hussain², P. Dinesh Sankar Reddy^{1,3*}

¹ Department of Chemical Engineering, Jawaharlal Nehru Technological University Anantapur, Ananthapuramu, 515002, India

² Department of Chemical Engineering, Lords Institute of Engineering & Technology, Hyderabad, 500091, India

³ Department of Chemical Engineering, National Institute of Technology Andhra Pradesh, Tadepalligudem, 534101, India

Received: November 17, 2021; Revised: February 05, 2022

In modern science precision and accuracy play a vital role towards accomplishing good quality final products. Precision and accuracy are very much inevitable either for raw materials, intermediates or semifinal / final products. In current scientific scenario, lot of instruments, gadgets and equipments are being developed, imbibing high technologies, which were considered to be expensive. Equipment by name Malvern is also considered as an expensive gadget to measure particle size distribution of μm size particles. This paper deals with the established particle size distribution by a simple and manual method using an empirical equation called Rosin-Rammler equation. Cements of different brands and different grades were procured from local market and tested for particle size distribution. The results obtained were compared with the results of Malvern particle size analyzer and the deviation is found to be 10% as maximum. The results depict that manual analysis by using the empirical Rosin-Rammler equation is very much matching with the standard particle size analyzer. Therefore, manual analysis of particle size distribution using Rosin-Rammler equation can be adopted in experimental analysis/research.

Keywords: Cement, Particle size distribution, Rosin-Rammler equation, Malvern particle size analyzer

INTRODUCTION

Cement is a binding substance usually inorganic in nature used for construction purpose, which sets when dries and hardens to adhere to other materials, by way of fixing with them together. Generally, cement is used on its own, but rather found to be binding with sand and gravel. Cement is used with fine sand and gravel mixture in aggregate for making mortar for masonry use like bricklaying and stuccos to produce concrete [1]. Cement used in construction is inorganic in nature as it contains lime and calcium silicate which shows the characteristic features of hydraulic or non-hydraulic ability which depends on the cement to set in the presence of water. The cement which sets when it dries reacting with carbon dioxide in the air is very resistant to attack by chemicals after setting; the cement which will not set in wet conditions or under water is set to be non-hydraulic cement [2]. The particle size distribution of cement is very important to understand the response of its physical and chemical nature, since it is a matter which is important in understanding its physical and chemical properties, since it directly affects the strength and load bearing properties. It also affects the nature of reactions and needs to be closely monitored in production operations. Particle size distribution may be represented as the "range"

analysis, where the amount of each size range is listed in a particular order. It may also be represented in "cumulative" form, in which the total mixture of all sizes "retained" or "passed" by a single notional "sieve" is represented for a range of sizes [3]. Range analysis will fetch, when a particular size is desired. The particle size affects the properties of powder in multiple ways. It affects i) the setting time of cement, ii) the hiding power of pigments present in it, iii) the activity of chemical catalysts, iv) the taste of food, v) the potency of drug and sintering shrinkage of powders. Therefore, for quality control of the final product, it is very much essential to maintain particle size distribution of any powder [4].

In the process of cement production, the fine product is analyzed and characterized by 95% below the 90 μm mesh usually recommended or based on the Blaine value. Particle size is a critical property and is used to characterize powders. It is possible to get high strength with lower Blaine (surface area) number. This is possible only when attempt is made to analyze the size distribution of the powder. As far as particle size distribution is concerned, the maximum usage of particle size distributions data may be generated if the data were represented by a mathematical expression. Such

* To whom all correspondence should be sent:

E-mail: pdsreddy@nitandhra.ac.in

mathematical function permits ready graphical/analytical representation and produces maximum opportunities for interpretations, extrapolations, and comparative analysis of different particle size distributions [5]. Different measurement techniques are in place to produce different results while measuring non-spherical particles. The techniques or instruments used for particle size analysis need to generate data in a form relevant to the process, reliable to the method and simple to understand. Laser diffraction is commonly used for particle size measurement and it is said to be a standard method which many industries follow for characterization and control. In this method a laser beam is scattered directly related to their size by particle size analyzer [6]. When the particle size decreases the scattering increases logarithmically observed in laser diffraction [7], intensity of beam is subjected to particle size, decrease is subjected to particle volume. Laser diffraction ranges from 0.2 to 2000 μm [8].

Dynamic light scattering is known as an accurate, reliable and repeatable technique which measures the size of molecules in the sub μm region and it gives results in particle hydrodynamic diameter [9]. This method is non-invasive and is also called photon correlation spectroscopy. Sedimentation is a traditional method which gives large errors for particles of large aspect ratio [10]. This equipment is used in paint and ceramic industries and is simple to use, as well as complex to determine as particles function setting of viscosity [11,12], in which density of material is needed, this method is not good for emulsions where the material settles too quickly. Ultrasound is used instead of light to collect information of the particles in the fluid disperse [13]. Sound waves similar to light absorb the particles disperse and scattered in a fluid system and measure the particle size distribution at very high concentration in this acoustic spectroscopy [14]. The distribution of particle size using Rosin-Rammler distribution parameters has been used to explain the particle size distribution of powders of different types and sizes [15-17]. These distribution parameters are in general suited to representing powders made by crushing, grinding and milling operations [18-20].

MATERIALS AND METHODS

Standard sieves of BIS had been used to assess particle size distribution [21] of 90, 75, 63 and 45 μm in size. Power sieve shaker is used to vibrate the powder for half an hour and particle size distribution has been estimated. Based on the values obtained in manual sieving, further distribution was carried out

by using Rosin-Rammler equation [15-17]. Furthermore, the values of particle size distribution are generated in Rosin-Rammler equation have been compared with standard Malvern particle size analyzer results.

Empirical equation for the particle size distribution is given by:

$$Q_3(x) = 1 - e^{-\left[\frac{x}{x_d}\right]^n} \quad (1)$$

where x = particle size (μm), x_d = constant related particle size, n = constant indicating the width of the distribution, $Q_3(x)$ = cumulative percentage undersize (%).

Estimation of parameters of different samples in Rosin-Rammler equation

Five different brands of Pozzolona Portland Cement (PPC) cement were procured from the local market, then subjected to sieving with sieves of 90, 75, 63 and 45 μm in size used in screening and from the retained weight of each sieve from the weighing balance, with the obtained data of mesh size to particles retained, a graph between $Q_3(x)$ and x is plotted. From the graph, using the values of slope and intercept ' x_d ' and ' n ' were evaluated. These values were embedded in Rosin-Rammler equation (1) to produce the entire particle size distribution.

RESULTS AND DISCUSSION

Manual Sieving

Standard sieves of 90, 75, 63 and 45 μm were taken to analyze cement particle size distribution by using a vibrator [21]. Coarser size, i.e. 90 μm was kept on the top and finer size, i.e. 45 μm was kept in bottom, below which the last container pan was kept to collect very fine particles. Particles retained on each sieve were weighed and accordingly cumulative mass weight was estimated.

Generation of X_d and n values of Rosin-Rammler equation

Based on the values of Table 1, a graph was plotted between $\ln(\text{particle size})$ vs $\ln[-\ln(1 - \text{cumulative undersize}/100)]$, and the slope line was drawn, from which ' x_d ' and ' n ' values were estimated based on which, ' n ' and ' c ' values were obtained from the equation $y = 1.372x - 4.786$. ' x_d ' was obtained by $\exp.(c/n)$ where ' c ' value is directly taken from the equation. Rosin-Rammler constants x_d , and n , i.e. $x_d = 32.73$ and $n = 1.3$, were incorporated in the equation from Fig. 1.

Table 1. Particle size distribution of cement obtained by manual sieving.

Sieve size (µm)	Powder retained weight (g)	Cumulative powder mass weight (g)	Cumulative undersize (%)
90	1.24	1.24	98.76
75	3.68	4.92	95.08
63	6.49	11.41	88.59
45	7.39	18.80	81.20

Values of x_d and n were incorporated in Rosin-Rammler equation, and the particle size distribution was generated for five samples, i.e S1, S2, S3, S4 and S5, similarly particle size distribution was estimated in Malvern Analyzer. The distribution of both methods is projected in graphs. RS1, RS2, RS3, RS4, RS5 depict particle size distribution values of samples 1-5 using Rosin-Rammler equation, while MS1, MS2, MS3, MS4, MS5 depict particle size distribution of samples 1-5 using Malvern analyzer.

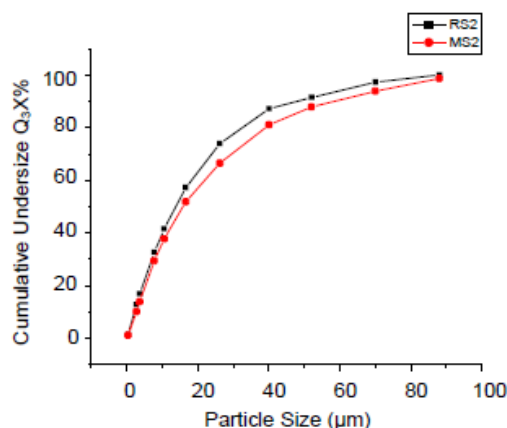


Fig. 3. Particle size distribution of sample 2 by Malvern and Rosin Rammler

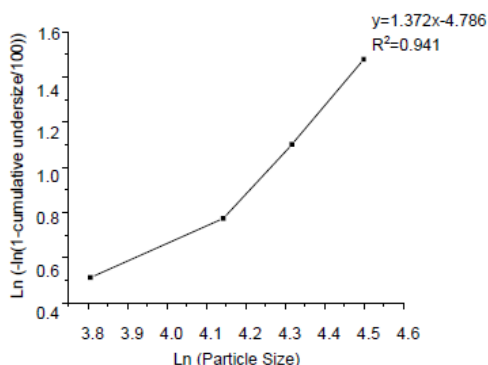


Fig. 1. Graph depicts Ln (particle size) vs Ln (-ln (1-cumulative undersize/100))

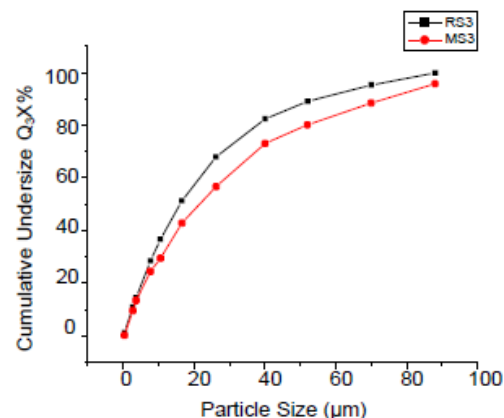


Fig. 4. Particle size distribution of sample 3 by Malvern and Rosin-Rammler

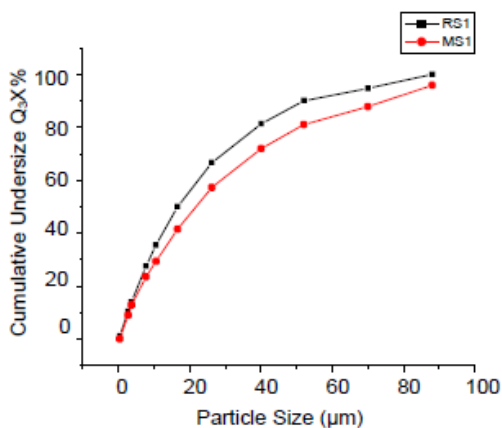


Fig. 2. Particle size distribution of sample 1 by Malvern and Rosin-Rammler

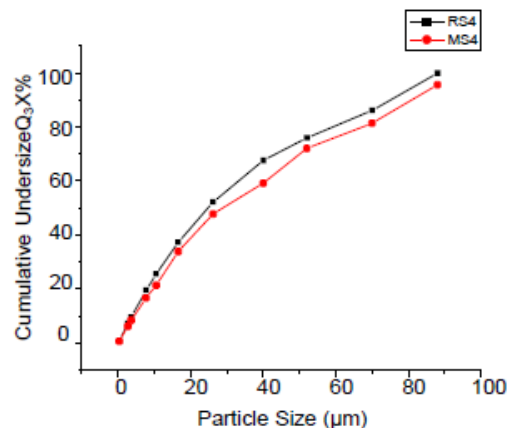


Fig. 5. Particle size distribution of sample 4 by Malvern and Rosin-Rammler

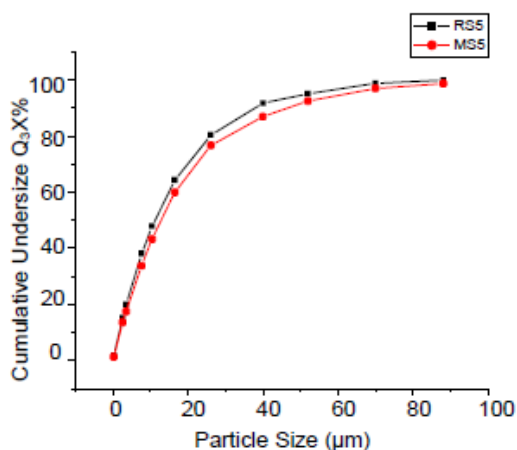


Fig. 6. Particle size distribution of sample 5 by Malvern and Rosin-Rammler

Figs. 2 to 6 show a comparison of particle size distribution of sample 1 to 5 by Malvern analyzer and Rosin Rammler distribution method. It can be clearly seen that percentage deviation between two methods, i.e. Rosin-Rammler distribution and Malvern analyzer is almost negligible, for all five samples.

CONCLUSION

With the series of cement analysis/particle size distribution by using Rosin-Rammler equation, it was observed that the results are very much close to those of Malvern particle size analyzer. Different brands of cement / grades were used to estimate the particle size distribution. A deviation of approximately 10% was noticed which is in a well - accepted range. The size of the cement particles according to Rosin Rammler equation estimation is in the range of 1 µm to 100 µm, which is very much matching with the established Malvern Particle analyzer. Therefore, it can be concluded that particle size distribution measurement using Rosin Rammler equation is almost accurate in line with conventional Malvern particle size distribution for analyzing PPC cement samples.

Acknowledgements: To be presented in International Chemical Engineering Conference on “100 Glorious Years of Chemical Engineering & Technology” from September 17 to 19, 2021, organized by Department of Chemical Engineering at Dr. B. R. Ambedkar NIT Jalandhar, Punjab, India (Organizing Chairman: Dr. Raj Kumar Arya & Organizing secretary: Dr. Anurag Kumar Tiwari).

The authors express deep sense of gratitude to the management of Anjani Powder Research Centre,

where part of research has been done. The authors also express thanks to National Academy of Construction, Gachibowli, Hyderabad. The authors are also thankful to Prof. Pitchumani Balakrishnan for his constant cooperation and help. The authors are thankful to the management of Lords Institute of Engineering & Technology, Hyderabad for their encouragement and support.

REFERENCES

1. H. F. W. Taylor, Cement chemistry, 2nd edn., Thomas Telford Publishing Company Ltd., United Kingdom, 1997.
2. P. C. Hewlett, Lea's chemistry of cement and concrete, London. Arnold, 1998.
3. R. Sugraney, J. I. Alvarez, M. Cruz-Yusta et al. *Constr. and Build. Mater.*, **41**, 139 (2013).
4. E. J. Hukkanen, R. D. Braatz, *Sen and Acta B.*, **96**(1), 451(2003).
5. B. A. Wills, Particle size analysis, in: Mineral Processing Technology, Pergamon Press, Oxford, England, 1992.
6. C. F. Bohren, D. R. Huffman, Absorption and Scattering of Light by Small Particles, John Wiley & Sons, New York, 1998.
7. M. Cyr, A. Tagnit-Hamou, *Mat. and Struct.*, **34**, 342 (2001).
8. ISO13320-1:1999(E), Particle size analysis - Laser diffraction methods—Part1: General principles.
9. B. J. Berne, R. Pecora, Dynamic Light Scattering, Courier Dover Publications, Mineola, 2000.
10. R. A. Bagnold, O. Barndorff-Nielsen. *Sediment.*, **27** (2), 199 (1980).
11. N. R. J. Fieller, D. D. Gilbertson, W. Olbricht. *Nat.*, **311**, 648 (1984).
12. ISO 13317-1:2001, Determination of particle size distribution by gravitational liquid sedimentation methods, Part1: General principles and guidelines.
13. Lord Rayleigh, The Theory of Sound, Macmillan and Co, New York, 1878.
14. A. S. Dukhin, Ph. J. Goetz, Characterization of Liquids, Dispersions, Emulsions, and Porous Materials Using Ultrasound, Elsevier, 2017.
15. K. M. Djamarani, I. M. Clark, *Pow. Technol.*, **93**(2), 101 (1997).
16. Ph. K. Gbor, Ch. Q. Jia, *Chem. Eng. Sci.*, **99**, 1979 (2004).
17. Y. S. Cheong, G. K. Reynolds, A. D. Salman, M. J. Hounslow, *Int. J. Min. Proc.*, **74**(S), S227 (2004).
18. P. E. Rosin-Rammler. *J. Inst. of Fuel.*, **7**, 29 (1933).
19. F.T. Olorunsogo, *Cem. and Concr. Research*, **28**(6), 907 (1998).
20. S. Grzeszczyk, G. Lipowski, *Cem. and Concr. Research*, **27**(6), 907 (1997).
21. British Standard Specification for test sieves BS 410:1986.

Application of *Cocos nucifera*'s husk to remove Malachite green dye and response surface modelling

Arpita Ghosh*

Centre for Sustainability & Environmental Management, Indian Institute of Management Sirmaur, Rampur Ghat Rd, Paonta Sahib, Himachal Pradesh 173025, India

Received: November 15, 2021; Revised: January 02, 2022

Toxic compounds are present in a vast variety of chemicals found in the environment. The study was performed to provide a remedy by using coconut husk (a waste matter) as a biosorbent to remove textile dye (i.e. malachite green dye) from synthetic solutions. The coconut husk was dried and crushed into powder form and was used for the experiment. Different parameters affecting color removal were analyzed in conventional batch mode and response surface optimization was performed. The optimum conditions of parameters (pH: 3-7, biosorbent dose: 20-50 g/L, and time: 80-300 minutes) for removal of color were found applying RSM. The model predicted the maximum removal of color to be 92.81% at pH 6.94, time 278.15 minutes, and dosage 41.10 g/L. Sustainability and circular economy can be reached with the objective of effluent treatment using biological waste matter.

Keywords: Biosorption; Coconut husk; Malachite green dye; Optimization; Sustainability; Response surface methodology (RSM).

INTRODUCTION

The United States Environmental Protection Agency (USEPA) listed the toxic organic and inorganic contaminants in 1978 [1]. Due to rapid increase in population and growth of industrialization in the country, the quality of both surface and groundwater changes day by day [2]. Maximum Industrial effluent consists of various contaminants which cause toxic consequences on human beings and environment. A large number of chemicals are found in the environment containing toxic substances. Different dissolved minerals from soil layers mix with the groundwater. The surface water is contaminated with the discharges of agricultural fields containing pesticides, fertilizers, and waste chemicals from industries and domestic waste [3-6].

Adsorption offers a distinct advantage over other methods to remove pollutants from wastewater. Adsorption can be operated in maximum chemical, physical, and biological systems. It is commonly used in industrial processes due to its sludge-free clean operation, simplicity of design, high reduction capacity, and ease of operation at a continuous scale. Biosorption is a physicochemical process where inactive biological materials accumulate pollutants, causing their removal from liquid, solid, or air medium on its surface functional groups. Worldwide evaluation of waste-biomass as adsorbents (wheat shell, rice husk, sawdust, pine bark, cereal chaff, etc.) is becoming popular as it is environmental-

friendly, renewable, abundant, (diverse materials that could be used for this purpose) and cost-effective. It is a potential alternative to traditional techniques for the removal of pollutants from the contaminated effluent even from a diluted solution. As a result, research into the use of biomaterials as biosorbents of organic and inorganic contaminants has grown in popularity in recent years. The biosorbent is a potent adsorbent, less expensive than other manufactured- adsorbents. The search for new biosorbents is essential for the development of wastewater treatment rather than the use of the conventional adsorbent activated carbon [7]. Different scientists have studied MG removal using different biosorbents (Table 1) such as modified sphagnum peat moss, fish scales, cattail leaves, chemically modified biomasses of pine, oak, hornbeam and fir sawdust, eucalyptus bark, *Yarrowia lipolytica* isf7, *Zea mays* L. (maize) husk leaves, brown marine algae *Turbinaria conoides*, *Coriolus versicolor*, chlorella-based biomass, *Carica papaya* wood. The coconut's (*Cocos nucifera*) husk is widely available and not easily biodegradable due to high lignin content. Generally, this voluminous husk either ends up its life at landfill or is used to burn which simultaneously increases the air pollution and causes different lung diseases. Also many devotees in India use the coconut husk for burning purpose during puja. That also causes the emission of toxic green house gases like NO_x, CO₂ at home, and CO.

* To whom all correspondence should be sent:

E-mail: arpi.335@gmail.com;

arpita.ghosh@iimsirmaur.ac.in

Table 1. Literature data on removal of Malachite green dye using different biosorbents

Biosorbent used	Experimental conditions	Findings	References
Modified sphagnum peat moss	a) Dye concentration: 60 mg/L b) pH: 6.5 c) Adsorbent concentration: 0.6g/L d) Contact time: 90 min e) Stirring speed: 160 rpm	Maximum adsorption capacity 121.95 mg/g at 20 °C	[8]
Fish (<i>Labeo rohita</i>) scales	a) Dye concentration: 50 mg/L b) pH: 8 c) Adsorbent concentration: 2g/L d) Contact time: 3 h e) Stirring speed: 150 rpm	Maximum adsorption capacity 38.46 mg/g at 40 °C	[9]
Cattail (<i>Typha angustifolia</i>) leaves	a) Dye concentration: 50 mg/L b) pH: 4 c) Adsorbent concentration: 0.25g/L d) Contact time: NA e) Stirring speed: 400 rpm	Maximum adsorption capacity 18.84 mg/g at 45 °C	[10]
Cetyltrimethylammonium bromide (CTAB) modified multi-component biosorbent composed of pine, oak, hornbeam and fir sawdust biomasses	a) Dye concentration: 30 mg/L b) pH: 8 c) Adsorbent concentration: 11 mg d) Contact time: 120 min e) Stirring speed: 400 rpm	Maximum adsorption capacity 52.610 mg/g	[11]
Eucalyptus bark	a) Dye concentration: 50 mg/L b) pH: 5 c) Adsorbent concentration: 0.4g d) Contact time: 270 min e) Stirring speed: 400 rpm	Maximum adsorption capacity 59.88 mg/g at 20 °C	[12]
<i>Yarrowia lipolytica</i> isf7	a) Dye concentration: 35 mg/L b) pH: 7 c) Adsorbent concentration: 5mg d) Contact time: 48 h e) Stirring speed: NA	Maximum adsorption capacity 155.098 mg/g	[13]
<i>Coriolus versicolor</i>	a) Dye concentration: 0.39 mg/L b) pH: NA c) Adsorbent concentration: 0.05g d) Contact time: 24.81 min e) Stirring speed: NA	Maximum adsorption capacity 18.84 mg/g at 45 °C	[14]
<i>Zea mays</i> L. (maize) husk leaves	a) Dye concentration: 200 mg/L b) pH: 6 c) Adsorbent concentration: 2.5g/L d) Contact time: 30 min e) Stirring speed: NA	Maximum adsorption capacity 81.5 mg/g at 50 °C	[15]
Brown marine algae <i>Turbinaria conoides</i>	a) Dye concentration: 100 mg/L b) pH: 8 c) Adsorbent concentration: 0.55 g d) Contact time: 150 min e) Stirring speed: 200 rpm	Maximum adsorption capacity 66.6 mg/g at 30 °C	[16]

Chlorella-based biomass	a) Dye concentration: 10 mg/L b) pH: 7 c) Adsorbent concentration: 2 g d) Contact time: 60 min e) Stirring speed: 400 rpm	Maximum adsorption capacity 9.775 mg/g	[17]
<i>Carica papaya</i> wood	a) Dye concentration: 10 mg/L b) pH: 10 c) Adsorbent concentration: 0.1 g d) Contact time: 24 h e) Stirring speed: 120 rpm	Maximum adsorption capacity 52.62 mg/g at 30°C	[18]

Table 2. Experimental range and levels of independent process variables

Independent variables	Range and levels (coded)				
	- α	-1	0	+1	+ α
pH (A)	1.63	3	5	7	8.36
Dose (B)	9.773	20	35	50	60.22
Time, minutes (C)	5	80	190	300	374.99

Table 3. 2³ Factorial experimental setup and percentage color removal as response

Run	pH (A)	Dose, g/L (B)	Time, minutes (C)	Experimental results (% color removal)
1	7.00	20	80	62±0.01
2	5	35	190	60±0.03
3	5	9.77	190	15±0.01
4	3	50	300	58±0.01
5	3	20	300	1.1±0.01
6	1.64	35	190	10.5±0.02
7	3	50	80	2.3±0.01
8	8.36	35	190	92±0.01
9	5	35	190	60±0.01
10	5	35	190	61±0.01
11	5	35	190	62±0.01
12	7	50	300	88.3±0.01
13	5	35	190	60±0.02
14	5	35	5	12±0.03
15	7	20	300	76±0.02
16	3	20	80	0.7±0.01
17	7	50	80	21±0.01
18	5	35	190	60±0.01
19	5	35	375	74±0.03
20	5	60.23	190	29±0.02

Table 4. Analysis of variance for the response surface quadratic model for color removal

Source	Sum of squares	Degree of freedom (df)	Mean square	F value	Probability value (P value)
Model	17493.24	9	1943.69	1040.17	<0.0001
Residual	18.69	10	1.87		
Lack of fit	15.19	5	3.04	4.34	0.0665
Pure error	3.50	5	0.70		
Cor total	17511.93	19			

$R^2 = 0.9989$; adjusted $R^2 = 0.9980$; predicted $R^2 = 99.31$

Table 5. Regression analysis by using central composite design

Model Term	Coefficient estimate	Standard error	F value	P value	Remarks
A	23.60	0.37	4069.64	< 0.0001	Significant
B	3.91	0.37	111.51	< 0.0001	Significant
C	17.70	0.37	2288.63	< 0.0001	Significant
AB	-10.90	0.48	508.65	< 0.0001	Significant
AC	3.15	0.48	42.48	< 0.0001	Significant
BC	13.58	0.48	788.95	< 0.0001	Significant
A ²	-3.01	0.36	69.77	< 0.0001	Significant
B ²	-3.01	0.36	1374.33	< 0.0001	Significant
C ²	-5.92	0.36	270.71	< 0.0001	Significant

Circular material management needs to be practiced following 5Rs principles (reduce, reuse, recycle, repurpose, regenerate) to recover the resources from being wasted and to recover their value as well. Segregated organic waste can be used for composting and bio gasification, which has economic value and is environmental friendly as well. Similarly, segregated non-organic dry waste can go for recycling purpose. In developing countries like India there are too many landfills for all the unsegregated mixed waste. In developed countries there are 5Rs practices which save the material from being wasted and recover its economic value as well. To achieve SDG goal 12, i.e. responsible production and consumption and circular economy of the waste generated from coconut, the present study was performed. Coconut husk was used to remove textile dye (Malachite green dye) from synthetic wastewater. The effect of pH, adsorbent dose and time on percentage removal of color was studied in conventional batch mode and in statistical optimization experiment.

MATERIALS AND METHODS

Malachite green (MG) dye

Malachite green [(C₂₃H₂₅ClN₂) molecular weight: 365, color index: 42000] dye is extensively applied in various textile industries. It is found to be hazardous and known for its cytotoxic, genotoxic and carcinogenic potential. It was procured from Thermoelectrons LLS India PVT LTD Mumbai. The maximum absorbance of MG dye is at 621 nm. Dilute solutions of NaOH (1M) and HCl (1M) were used to adjust the pH of synthetic dye solution using a digital pH meter (Fisher Scientific) measured with standard buffer solutions.

Coconut husk

Coconut water is very popular for its mineral

value in summer time. In India coconut oil also is commonly used as cooking oil and hair oil purposes. The raw coconut husk (supplementary picture) was collected from a local shop at Delhi NCR, India for the present study.

Biosorbent preparation

The coconut husk was cleaned using distilled water to separate the external dirt and dried at 60-65°C in a hot-air oven for 48 hours. Then the dried coconut husk was crushed in small particles using a motor pestle and kept under sunray for 7 days to further remove the moisture content. The coconut husk-biosorbent was kept in an air-tight bottle.

Experimental procedure for batch biosorption

Diluting the appropriate amount of stock solution in a 250 ml flask yielded 100 ml of synthetic solution (100 mg/L concentration) of Malachite green dye. Predetermined amount of biosorbent dose was added in the conical flask by agitating with a shaker (Biosphere Corporation) at 30°C temperature. The liquid sample was withdrawn at different times (60, 120, 180, 240, 300 minutes) to determine the effect of time on percentage removal of color. The pH of dye solution was varied from 3.0 to 9.0 to analyze the consequence of varying pH on percentage removal of color. The biosorbent dose was varied from 10-50 g/L to analyse the effect of biosorbent dose on percentage removal of color. After centrifugation (Bench Top Centrifuge by REMI Motors Limited) at 5000 rpm of the sample for 15 minutes, the supernatant was analysed using a colorimeter at 621 nm. The color removal of supernatant was tested by a Delux Photo Colorimeter manufactured by Labrotionics, India. All glassware was cleaned with distilled water and air-dried in a hot-air oven. The dye solution was analysed using a colorimeter before and after adsorption experiments.

The amount of dye adsorbed is calculated in percentage (%) by equation (1):

$$\% \text{Removal} = \frac{(C_0 - C_e)}{C_0} \times 100\% \quad (1)$$

where, C_0 is the initial concentration (mgL^{-1}) of dye, C_e is the final concentration of dye after biosorption.

Optimization of experimental parameters

Statistically based central composite design (CCD) of RSM was performed to check the optimum conditions of experimental parameters (independent parameters: pH, dose, time) for maximum color removal (dependent variable: response) of MG dye solution (dye concentration: 100 mg/L). The software Design Expert Version 7.0.0 (Stat Ease, USA) was applied in this investigation. The maximum and minimum levels of experimental parameters are tabulated in supplementary Table 2. The optimal location is determined using the following formula, equation (2):

$$Y = \beta_0 + \sum_{i=1}^K \beta_i X_i + \sum_{i=1}^K \beta_{ii} X_i^2 + \sum_{i=1}^K \sum_{j=i+1}^K \beta_{ij} X_i X_j + \epsilon \quad (2)$$

where, Y is the predicted response, X_i and X_j indicate the independent variables, β_0 , β_i , β_{ii} , β_{ij} , are the statistical errors and denote regression coefficients. The trials (number 20) were carried out at factorial points (coded 1 notation), axial points (0), and centre points (0) in duplicate.

RESULTS AND DISCUSSION

Effect of pH, biosorbent dose and time on % removal of color in conventional batch mode

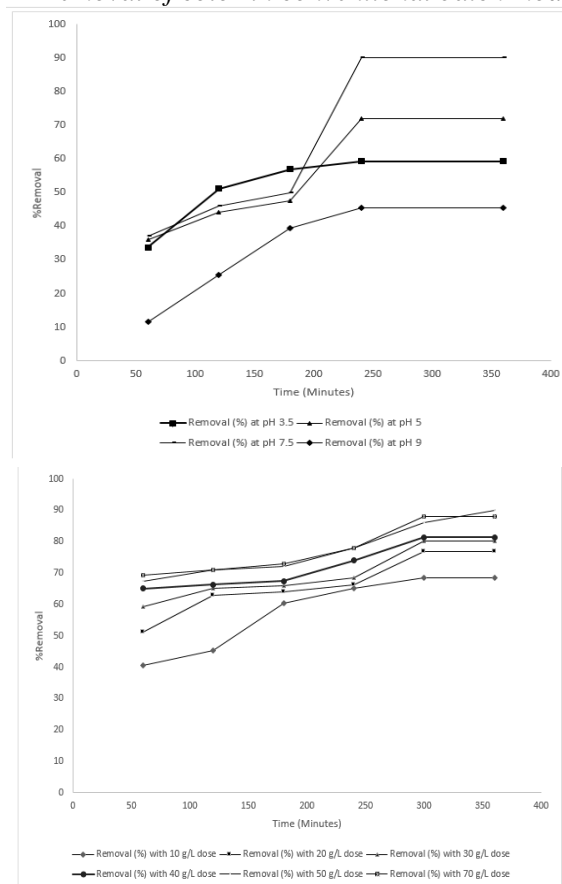


Figure 1. Effect of a) pH b) biosorbent dose on color removal at different times in conventional batch mode.

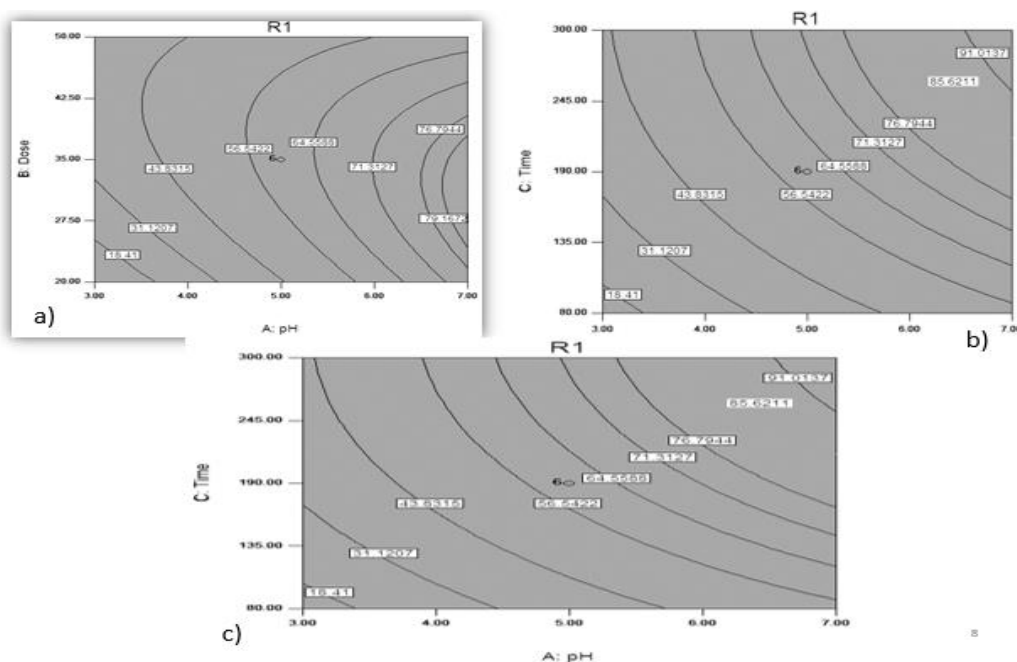


Figure 2. RSM contour plots for the consolidated effect of a) pH and biosorbent dose b) pH and time c) biosorbent dose and time on the % removal of MG dye.

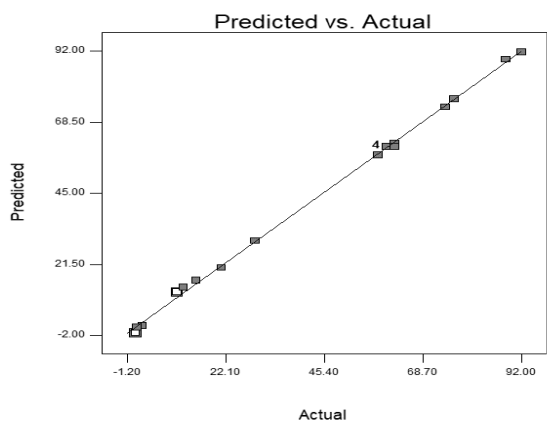


Figure 3. Comparison of the actual experimental data with predicted data by RSM model.

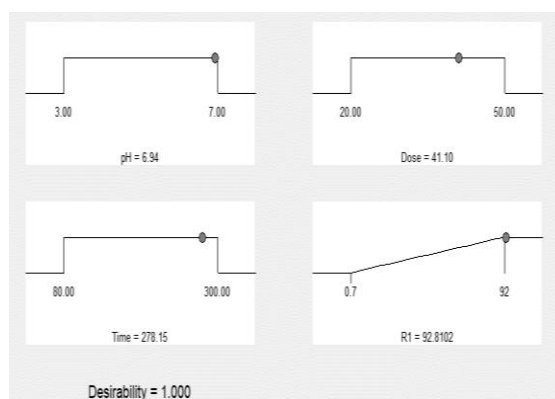


Figure 4. The RSM optimization ramp of desirability (1.000).

Figure 1 shows the biosorption of the MG dye at different pH values of the solution with time. Color removal was obtained to be in the range of 59%-90% at 360 minutes on varying the pH from 3.5 to 9 (Figure 1a). The color removal (90 %) was noticed to be maximum at pH 7.5 till 240 minutes from 100 mg/L concentration of MG dye solution. The color removal of MG dye was studied by varying the quantity of biosorbent dose (10, 20, 30, 40, 50 g/L) in the synthetic solution at different time intervals while keeping fixed other parameters (i.e., dye concentration: 100 mg/L, pH: 7, temperature: 30°C, shaking speed: 120 rpm). Percent MG removal was obtained in the range of 68% - 90% at 360 minutes, varying the dosage from 10-70 g/L (Figure 1b). The percent adsorption was increased when the biosorbent dosage is increase. The percentage color removal (90%) reaches maximum using 50 g/L biosorbent dose at pH 7.5. Initially with increasing pH and dose the removal was improved. Major color removal was noticed at pH 7.5 in conventional batch mode. Above 50 g/L dose the removal was observed to decrease. After optimum points of pH (7.5) and dose (50 g/L) the removal became stagnant or slightly reduced.

Combined effect of experimental parameters on % removal of color in response surface optimization

The integrated effect of two parameters on % removal of color is shown in the 2-D contour plots (Figures 2a,b,c). It was validated that pH, dose and time have a vigorous effect on % color removal (Table 3). Maximum color removal was predicted by the model to be 92.81% at pH 6.94 and time 278.15 minutes, dosage 41.10 g/L. The primary dye concentration at 100 mg/L and shaking speed of 120 rpm were kept settled during the experiments. In terms of actual factors, the quadratic equation 3 expresses the link between the theoretical removal and the independent process parameters:

$$\begin{aligned} \%Color\ removal = & -142.63689 + 29.31439A + \\ & 4.66698B - 0.012611C - 0.36333AB + \\ & 0.014318AC + 0.0082272 BC - 0.75194A^2 - \\ & 0.059330B^2 - 0.000489636C^2 \end{aligned} \quad (3)$$

where A is pH, B is biosorbent dose (g/L) and C is time in minutes. The removal (92%) was calculated using the optimum points and the above CCD equation. The statistical importance of the model was estimated by ANOVA (Table 4). The low probability of F-value and non-significant lack of fit, entails high significance of this statistical model. The value of determination coefficient R^2 (0.9989) indicates goodness of fit [19, 20]. The outcomes proposed that equation was preferable for the CCD model. In the recent study, A, B, C, AB, AC, BC, A^2 , B^2 and C^2 are significant experimental parameters (Table 5). Figures 3 and 4 distinguish between actual experimental data and those predicted by the RSM model and the optimization ramp of desirability (1.000), respectively. The RSM optimization validated that there was prominent effect of pH, dose and time on the color removal.

Recommendation & Conclusion

The coconut husk is flabby and voluminous. The transport cost of the material is associated with it and also the chance of material loss due to overflow from the vehicle. The value chain can be disturbed in this way. Effective transportation will require more cost, and that can be an obstacle in using the husk (imagining the cost of carrying the raw materials increases) [21]. Also, another issue is regarding the preservation of the raw materials intact that are away from getting rotten. Any place, which has the problem of flood and water stagnancy (as an outcome of climate change) will stand as a problem. Effective transportation and storage are the requirements to solve these.

The waste biomass of coconut husk was examined as biosorbent to remove a textile dye;

Malachite green from synthetic solutions prepared at laboratory. The MG removal process was influenced by varying pH, time, and coconut husk-dose. The optimum color removal predicted by the model was observed to be 92.81% at pH 6.94 and time 278.15 minutes, dosage 41.10 g/L, initial dye concentration being kept fixed at 100 mg/L during the experiments. This study shows that coconut husk can be applied as an efficient biosorbent to reduce textile dyes in the effluent of a treatment plant. Further, the coconut husk is not easily biodegradable and causes a huge amount of solid waste generation.

Textile industry can collect the coconut husk from the local coconut seller through strong supply chain management. The adsorbent can be prepared easily at their R&D lab or it can be procured from relevant technical institutes *via* collaboration. The adsorbent can be used in continuous mode to treat the dye contaminated effluent in a simple agitated reactor. Also, there is scope of recovery of adsorbent and dye through desorption. In this way, waste to wealth can be aimed by focusing the circular economy & sustainability goals for effluent treatment using waste matter.

REFERENCES

1. M. R. Greenberg, Impact of Industrial Activity on Water Quality, in: Sourcebook on the Environment: A Guide to the Literature, 1978, 205.
2. Z. Aksu, I. A. Isoglu, *J. Hazard. Mater.*, **137** (1), 418 (2006).
3. A. M. B. Ben Hamissa, F. Brouers, B. Mahjoub, M. Seffen, *Adsorpt. Sci. Technol.*, **25** (5), 311 (2007).
4. A. Ghosh, P. Das, *Indian Chem. Eng.*, **56** (1), 29 (2014).
5. A. Ghosh, M. G. Dastidar, T. R. Sreekrishnan, P. Patra, *Asian Journal of Atmospheric Environment*, **13**(4), 276 (2019).
6. A. Ghosh, M. G. Dastidar, T. R. Sreekrishnan, *Chem. Eng. Technol.*, **39** (9), 1636 (2016).
7. V. Basavarao, S. Rammohanrao, *Chem. Eng. J.*, **116** (1), 77 (2006).
8. F. Hemmati, R. Norouzbeigi, F. Sarbisheh, H. Shayesteh, *J. Taiwan Inst. Chem. Eng.*, **58**, 482 (2016).
9. S. Chowdhury, P. Das Saha, U. Ghosh, *Biorem. J.*, **16** (4), 235 (2012).
10. E. K. Guechi, O. Hamdaoui, *Desalin. Water Treat.*, **51** (16–18), 3371 (2013).
11. F. Deniz, R. A. Kepekci, *Microchem. J.*, **132**, 172 (2017).
12. S. Boutemedjet, O. Hamdaoui, *Desalin. Water Treat.*, **8** (1–3), 201 (2009).
13. A. Asfaram, M. Ghaedi, G. R. Ghezalbash, E. A. Dil, I. Tyagi, S. Agarwal, V. K. Gupta, *J. Mol. Liq.*, **214**, 249 (2016).
14. N. C. Yildirim, M. Tanyol, N. Yildirim, O. Serdar, S. Tatar, *Ecotoxicol. Environ. Saf.*, **156**, 41 (2018).
15. A. A. Jalil, S. Triwahyono, M. R. Yaakob, Z. Z. A. Azmi, N. Sapawe, N. H. N. Kamarudin, H. D. Setiabudi, N. F. Jaafar, S. M. Sidik, S. H. Adam, B. H. Hameed, *Bioresour. Technol.*, **120**, 218 (2012).
16. R. R. Rajesh Kannan, M. Rajasimman, N. Rajamohan, B. Sivaprakash, *Front. Environ. Sci. Eng. China*, **4** (1), 116 (2010).
17. W. T. Tsai, H. R. Chen, *J. Hazard. Mater.*, **175** (1–3), 844 (2010).
18. S. Rangabhashiyam, S. Lata, P. Balasubramanian, *Surfaces and Interfaces*, **10**, 197 (2018).
19. F. Ghorbani, H. Younesi, S. M. Ghasempouri, A. A. Zinatizadeh, M. Amini, A. Daneshi, *Chem. Eng. J.*, **145** (2), 267 (2008).
20. K. Somnuk, P. Smithmaitrie, G. Prateepchaikul, *Energy Convers. Manag.*, **68**, 193 (2013).
21. T. Ilame, A. Ghosh, *Management of Environmental Quality: An International Journal*, 2021, Dec 3.



Supplementary picture: Collected Coconut husk

A statistical analysis and optimization of Indian coal grinding in a laboratory ball mill: dry & wet method

S. Gautam*, A. Gautam, M. Patel, H. Parmar, K. Patel

Department of Chemical Engineering, Shroff S. R. Rotary Institute of Chemical Technology, Vataria, Ankleshwar, 393135, Gujarat, India

Received: October 19, 2021; Revised: January 02, 2022

This study explores the different product particle size of coal while applying dry and wet grinding and optimization of parameters affecting the grinding process with both methods. Grinding of coal up to μm size is indispensable to achieve its maximum calorific value and better combustion. A systematic experiment, as well as modeling of grinding of Indian coal of size $-3.5 +1$ mm was done by response surface methodology. There were five different parameters chosen, which were found to be affecting the grinding process, namely: amount of feed (100-150-200 g), ball mill rotational speed (20-30-40 rpm), time of grinding (4-7-10 min), and number of balls (10-15-20); in case of wet grinding amount of water (10%-20%-30% of feed by weight) was added. Effect of parameters and their interaction on the fineness was evaluated by Box-Behnken design and ANOVA. Moreover, wet grinding shows better results of fineness of coal. Grindability of the coal was tested by standard Bond grindability test and calculated from breakage rate by Mohs' hardness. Experimental results are in good agreement with model equation and regression coefficient (R^2) was obtained to be 0.97 and 0.98 for dry and wet grinding, respectively.

Keywords: Grinding of coal, Surface response methodology, Dry and wet grinding, Ball mill, Box-Behnken design.

INTRODUCTION

India is the third-largest country after USA and China in energy consumption. The demand is increased by 7.9 % in 2018, and its global share is 5.8 %. The total primary energy consumption from coal is 452.2 metric tons which is 55.88 % of total energy required in the calendar year 2018. As per consumption and population, India is largely dependent on coal imports to fulfill its energy demands by 2030; India's dependence on energy imports is expected to exceed 53% of the country's total energy consumption. Nonetheless, the requirement of energy to grind coal up to 100 μm is huge, but the efficiency of combustion increases with decreased particle size [1].

Preheating coal in an oven has been shown to reduce grind strength, although it is unlikely that this would be an economically possible method, at least not through associated energy requirements [2]. Fine particles of coal have several applications like coal water slurry [3, 4], micro size coal in cement clinker production, coal beneficiation of air-fluidized bed, reduction of sulfur, ash and other impurities in micro size coal particles [5, 6]. Mineralogical characteristics of materials and operating variables noticeably affect the fineness of coarse particles [7, 8]. These parameters include the mill speed, ball size, filling rate, feed size distribution, pulp density and material hardness. According to [9], pulp density has the most significant effect on the fineness of

particles. Most fine particles were obtained at 45 vol. % solid concentration of copper ore, quartz and coal.

In a previous study [10], dry grinding of coal in a laboratory ball mill showed that grinding is most influenced by the amount of feed and time of grinding. In another reference, ball charge has been found to have a significant effect on the product fineness for same specific energy consumption and increases power draws of the mill linearly [11]. In a study, the charge ratio, Bond work index and the ball diameter of Turkish coal and ore grinding were taken as the variables in the experiments, however, time of grinding is also an important parameter to decide the fineness in the grinding experiments [12, 13]. The ash content was quite low compared to the Indian coal. The ball size should be large enough and weight of balls must be sufficient to grind the charge efficiently. The current work uses constant ball size, and these are considered to be efficient for the grinding media.

Fine grinding being of importance for liberation of coal and attaining maximum calorific value, further enhancement in the performance of ball mill can be obtained by evaluating the effects of operating parameters on mill efficiency. The number of balls, feed size, time of grinding, rotational speed and grinding aid as water for wet grinding were considered to be controlling factors. The grinding and breakage of particles may depend on different parameters as discussed earlier. The effect of optimum parameters on fine grinding with dry and

* To whom all correspondence should be sent:
E-mail: shinaiitd@gmail.com

wet methods was found using Box-Behnken design and ANOVA. MATLAB code and Microsoft Excel were used to regress from the model.

Standard Bond grindability test for coal

The Bond grindability test is a closed loop grinding and screening process, which is continued until steady state conditions is achieved. Applying the Bond test it is assumed that all particles break similarly then only equilibrium or steady state is achieved. The test was executed by packing the coal and grinding media with 2000 cm³ volume. This volumetric weight was used for the grinding tests. From the beginning of the cycle the ball mill was operated at 25 rpm for 30 min, arbitrarily chosen below the critical speed. At the end of each grinding cycle, the product was poured from the mill and screened on the test sieve (P_i). The oversize material was sent back to the mill along with fresh feed to maintain 2000 cm³ volume. The weight of product per unit of mill revolution is named as ore grindability of the cycle, it was used to calculate and estimate the number of revolutions required in second cycle, it was equivalent to 250 % of the circulating grinding media and feed. This process was continued until equilibrium was attained for the grindability which arises in 6-12 cycles. After achieving equilibrium, the last three values were considered as the average standard Bond grindability. The products of the final three cycles were combined to form the equilibrium rest product. Sieve analysis was done for 80% passing size of the product.

After crushing the samples in a jaw crusher and roll mill, standard grindability tests were performed. The Bond work index (W_i) was calculated as Equation 1:

$$W_i = 1.1 \times \frac{44.5}{P_i^{0.23} G_b^{0.82} \left[\left(\frac{10}{\sqrt{P_{80}}} \right) - \left(\frac{10}{\sqrt{F_{80}}} \right) \right]} \quad (1)$$

where W_i is the work index in kWh/t; P_i , test sieve size at which test had been performed; G_b , Bond's ball mill grindability, net weight of ball mill product passing 80 % of test sieve per cycle (g/cycle); P_{80} , sieve opening of 80 passing; F_{80} , sieve opening 80 % of feed passing. For each coal sample all the parameters mentioned were calculated and W_i is reported in Table 1.

MATERIALS & METHODS

Coking coal which was collected from the overflow stream (washed coal) of a dense medium cyclone at Gujarat Mineral Development Corporation, Gujarat, was used as the raw material. A jaw crusher and a roll mill were used to prepare

particles for grinding in a ball mill. The particle size initially present was of 4-5 mm. The d_{80} size of coal particles for ball mill feed was -3.5 +1 mm. Grinding tests were performed in a cylindrical laboratory-scale ball mill and specifications of the ball mill and balls are mentioned in Table 2. The rotation speed of the ball mill was kept below the critical speed.

Table 1. The values of F_{80} , P_{80} , G_b and W_i of different dry and wet coal samples.

Coal	F_{80} (μm)	P_{80} (μm)	G_b (g/cycle)	W_i (kWh/t)
Dry coal	385	2.15	7562	16.23
Coal with 10% water of feed	372	2.02	7845	14.25
Coal with 20% water of feed	387	1.84	7926	14.21
Coal with 30% water of feed	385	1.75	7985	14.23

Table 2. Specification of sample and ball mill

Mill	Inner diameter (D), cm	21
	Length, cm	25
	Operational speed (N, rpm)	20, 30, 40
	Critical speed (N_c , rpm)	121-133
Media charge	Materials	Alloy steel
	Mass of a ball, gm	67
	Ball diameter, (d) cm	2.4
Material	Ball density, g/cm ³	7.6
	Sample	coal
	Moisture, %	5.35
	Volatile compounds, %	18.65
	Fixed carbon, %	35.6
	Ash content, %	40.04
	Calorific value	4766 Cal/g
Critical speed ^a calculation	$N_c = \frac{30}{\pi} \sqrt{\frac{2g}{(D-d) \sin \beta \sqrt{1}}}$	

^a In critical speed, it is to be noted that ϕ is the filling ratio of grinding media and charge volume to the mill volume which is 0.19-0.23, it is kept below 0.6 in a ball mill. β is the material angle of repose for balls, 29°.

Response surface methodology

Conventional method takes much longer time to find the optimum parameters and does not provide any information regarding interaction of parameters to each other and parameters combined effect is not perceivable on the response. The minimum number of experiments to be performed according to the Box-Behnken design can be found by the following equation:

$$N = 2N_f(N_f - 1) + C_p \quad (2)$$

where N_f is the number of parameters used to fit the model, and C_p is the number of the central points. A design matrix accordingly was prepared for dry and wet grinding in Tables 3 and 4, respectively.

A Box-Behnken design with three levels was employed to evaluate the effect of different independent parameters on coal grinding. To find the optimum conditions, a quadratic model was used to relate the grinding of coal to independent parameters:

$$y = \alpha_0 + \sum_{j=1}^n \alpha_j x_j + \sum_{j=1}^n \alpha_{jj} x_j^2 + \sum_{j=1}^{n-1} \sum_{k=2}^n \alpha_{jk} x_j x_k + \delta \quad (3)$$

The set of a regression coefficient α 's is unknown and estimated by the least square method. In a vector matrix, the equation for the least square fit can be represented by:

$$Y = X\alpha + \delta \quad (4)$$

where Y is defined as the measured value and X to be a matrix of independent variables.

Regression coefficient α can be found by the non-singular regression matrix transpose X' .

$$\beta = (X'X)^{-1}X'Y \quad (5)$$

where X' is the transpose of the matrix X and $(X'X)^{-1}$ is the inverse of the matrix $X'X$.

So these first four independent parameters for dry grinding and five independent parameters for wet grinding were coded at three levels with the same step size; that are +1, 0, and -1, where +1 represents the maximum value, 0 represents the centre, and -1 represents the minimum value of each parameter which was considered for analysis. Within the present research framework, the discussion was focused on the effect of the number of balls (A), amount of feed charged (B), grinding time (C), rotational speed (D) for dry grinding. An additional parameter the amount of water (E) was also included in wet grinding on the fineness of coal using a Box-Behnken design.

RESULTS AND DISCUSSION

Statistical analysis with Box-Behnken design

The independent parameters and their levels are presented in Table 2. If the total number of variables along with full factorial is considered $(3)^4$, 81 experiments will be required. Instead of doing that many experiments, the Box-Behnken design required 27 experiments as per the design. Eq. (2) represents the model equation which correlates the response which is a fineness (d_{80}) and different independent parameters for dry grinding. In wet grinding an independent parameter amount of water is also considered. Due to increase in the number of parameters, the number of experiments as per Box-Behnken design is also changed to 47 experiments. The model equations for both conditions are given below.

dry grinding:

$$d_{80} = 5.319 - 0.077A - 0.017B - 0.021C - 0.0218D + 0.00023AB - 0.0026AC - 0.0009AD + 0.00015BC - 0.00004BD - 0.0027CD + 0.0024A^2 + 0.00005B^2 + 0.006C^2 + 0.0008D^2 \quad (6)$$

wet grinding:

$$Y_{d80} = 9.922 - 0.303A - 0.013B - 0.4206C - 0.4206C - 0.0681D - 0.077E - 0.00027AB + 0.016AC + 0.001AD + 0.0016AE + 0.00019BC - 0.00047BD - 0.00015BE - 0.002CD + 0.0017CE + 0.003DE + 0.004A^2 + 0.00012B^2 + 0.005C^2 + 0.00009D^2 - 0.00022E^2 \quad (7)$$

where A is the number of balls; B is the amount of feed; C is the time of grinding; D is the revolutions per minute of the ball mill and E is the % amount of water added for wet grinding as defined in Table 4. The design matrix considering minimum, maximum and central value defined in Tables 4 and 5 for dry and wet grinding, respectively, was evaluated as per model. The experimental values were obtained by performing experiments, and the predicted values were calculated using Eqs. 6 and 7.

The experimental results were subjected to variance analysis (ANOVA) for both grinding methods. The results of ANOVA are shown in Table 5. The F -value of dry and wet grinding was 32.81 and 162.21, respectively. It was higher than 95% confidence level (P -value is less than 0.05). The values of P -values were acceptable for both models; it indicated that both models were convincing. Model terms or variables having P -values less than 0.05 are significant terms, on the other hand, variables having a P -value greater than 0.1 are not much significant for the model. Lack of fit in both cases was < 0.05 , 0.012 for dry grinding and 0.04 for wet grinding, respectively. It is not significant in

both cases. The values of regression coefficients are predicted values using Eqs. (6) and (7) and shown in Figure 1 for dry and wet grinding; the experimental values are in good agreement.

Table 3. Design matrix with coded & actual design parameters for dry grinding

Run No.	Coded				Uncoded				d_{80} exp	d_{80} pre
	A	B (g)	C (min)	D (rpm)	A	B (g)	C (min)	D (rpm)		
1	-1	-1	0	0	10	100	7	30	2.90	2.96
2	-1	1	0	0	10	200	7	30	2.94	2.89
3	1	-1	0	0	20	100	7	30	2.64	2.70
4	1	1	0	0	20	200	7	30	2.89	2.84
5	0	0	-1	-1	15	150	4	20	2.97	2.93
6	0	0	-1	1	15	150	4	40	2.90	2.91
7	0	0	1	-1	15	150	10	20	2.89	2.89
8	0	0	1	1	15	150	10	40	2.50	2.54
9	-1	0	0	-1	10	150	7	20	2.95	2.93
10	-1	0	0	1	10	150	7	40	2.82	2.84
11	1	0	0	-1	20	150	7	20	2.95	2.87
12	1	0	0	1	20	150	7	40	2.62	2.59
13	0	-1	-1	0	15	100	4	30	2.94	2.96
14	0	-1	1	0	15	100	10	30	2.79	2.71
15	0	1	-1	0	15	200	4	30	2.94	2.96
16	0	1	1	0	15	200	10	30	2.87	2.79
17	-1	0	-1	0	10	150	4	30	2.96	2.93
18	-1	0	1	0	10	150	10	30	2.77	2.80
19	1	0	-1	0	20	150	4	30	2.84	2.86
20	1	0	1	0	20	150	10	30	2.48	2.57
21	0	-1	0	-1	15	100	7	20	2.92	2.94
22	0	-1	0	1	15	100	7	40	2.85	2.78
23	0	1	0	-1	15	200	7	20	2.87	3.00
24	0	1	0	1	15	200	7	40	2.75	2.79
25	0	0	0	0	15	150	7	30	2.67	2.67
26	0	0	0	0	15	150	7	30	2.67	2.67
27	0	0	0	0	15	150	7	30	2.67	2.67

Table 4. Design matrix with coded & actual design parameters for wet grinding

Run No.	Coded					Uncoded					d_{80} exp	d_{80} pre
	A	B (g)	C (min)	D (rpm)	E (ml)	A	B (g)	C (min)	D (rpm)	E (ml)		
1	-1	-1	0	0	0	10	100	7	30	20	2.56	2.56
2	-1	1	0	0	0	10	200	7	30	40	2.85	2.83
3	1	-1	0	0	0	20	100	7	30	20	2.41	2.39
4	1	1	0	0	0	20	200	7	30	40	2.75	2.79
5	0	0	-1	-1	0	15	150	4	20	30	2.98	2.95
6	0	0	-1	1	0	15	150	4	40	30	2.32	2.35

7	0	0	1	-1	0	15	150	10	20	30	2.62	2.60
8	0	0	1	1	0	15	150	10	40	30	1.71	1.70
9	0	-1	0	0	-1	15	100	7	30	10	2.05	2.05
10	0	-1	0	0	1	15	100	7	30	30	2.63	2.65
11	0	1	0	0	-1	15	200	7	30	20	2.51	2.49
12	0	1	0	0	1	15	200	7	30	60	2.72	2.74
13	-1	0	-1	0	0	10	150	4	30	30	3.02	3.05
14	-1	0	1	0	0	10	150	10	30	30	2	2.01
15	1	0	-1	0	0	20	150	4	30	30	2.43	2.41
16	1	0	1	0	0	20	150	10	30	30	2.42	2.45
17	0	0	0	-1	-1	15	150	7	20	15	2.84	2.89
18	0	0	0	-1	1	15	150	7	20	45	2.42	2.46
19	0	0	0	1	-1	15	150	7	40	15	1.14	1.16
20	0	0	0	1	1	15	150	7	40	45	2.61	2.68
21	0	-1	-1	0	0	15	100	4	30	20	2.62	2.67
22	0	-1	1	0	0	15	100	10	30	20	2.11	2.18
23	0	1	-1	0	0	15	200	4	30	40	2.83	3.01
24	0	1	1	0	0	15	200	10	30	40	2.65	2.51
25	-1	0	0	-1	0	10	150	7	20	30	2.88	2.95
26	-1	0	0	1	0	10	150	7	40	30	2.06	2.05
27	1	0	0	-1	0	20	150	7	20	30	2.78	2.70
28	1	0	0	1	0	20	150	7	40	30	2.16	2.10
29	0	0	-1	0	-1	15	150	4	30	15	2.43	2.39
30	0	0	-1	0	1	15	150	4	30	45	2.75	2.76
31	0	0	1	0	-1	15	150	10	30	15	1.78	1.72
32	0	0	1	0	1	15	150	10	30	45	2.42	2.44
33	-1	0	0	0	-1	10	150	7	30	15	2.3	2.28
34	-1	0	0	0	1	10	150	7	30	45	2.62	2.58
35	1	0	0	0	-1	20	150	7	30	15	1.95	1.93
36	1	0	0	0	1	20	150	7	30	45	2.75	2.72
37	0	-1	0	-1	0	15	100	7	20	20	2.81	2.86
38	0	-1	0	1	0	15	100	7	40	20	1.92	1.93
39	0	1	0	-1	0	15	200	7	20	40	2.98	3.02
40	0	1	0	1	0	15	200	7	40	40	2.42	2.44
41	0	0	0	0	0	15	150	7	30	30	2.33	2.33
42	0	0	0	0	0	15	150	7	30	30	2.33	2.33
43	0	0	0	0	0	15	150	7	30	30	2.33	2.33
44	0	0	0	0	0	15	150	7	30	30	2.33	2.33
45	0	0	0	0	0	15	150	7	30	30	2.33	2.33
46	0	0	0	0	0	15	150	7	30	30	2.33	2.33

Table 5 ANOVA analysis of dry and wet grinding

Dry grinding					
Source	The sum of square distances (SS)	Mean squares	F-value	P-value	$P_A = (SS/SS_{total}) \%$
Model	0.4736	0.0338	32.81	0.000	-
A	0.0118	0.0118	11.52	0.005	2.68
B	0.0608	0.0608	59.04	0.000	13.79
C	0.00035	0.00035	0.34	0.57	0.08
D	0.00375	0.0037	3.64	0.081	0.85
Square	0.0924	0.023	22.4	0.000	20.96
A*A	0.0202	0.0202	19.67	0.001	4.58
B*B	0.0805	0.0805	78.14	0.000	18.26
C*C	0.0163	0.0163	15.88	0.002	3.70
D*D	0.0377	0.0377	36.64	0.000	8.55
Interaction	0.0585	0.0097	9.47	0.001	13.27
A*B	0.0132	0.0132	12.82	0.004	2.99
A*C	0.0064	0.0064	6.21	0.028	1.45
A*D	0.0081	0.0081	7.85	0.016	1.84
B*C	0.002	0.0025	1.96	0.186	0.45
B*D	0.0016	0.0016	1.55	0.237	0.36
C*D	0.0272	0.027	26.4	0.000	6.17
Lack-of-fit	0.0123	0.0012			
Pure Error	0	0			
Total	0.4408				
Wet grinding					
Source	Adj SS	Adj MS	F	P	$P_A = (SS/SS_{total}) \%$
Model	6.344	0.3172	162.21	0.000	-
A	0.229	0.2299	117.56	0.000	5.05
B	0.033	0.0339	17.37	0.000	0.73
C	0.171	0.1713	87.62	0.000	3.77
D	0.0463	0.0463	23.68	0.000	1.02
E	0.161	0.161	82.33	0.000	3.55
Square	0.6127	0.1225	62.66	0.000	13.51
A*A	0.1199	0.1199	61.35	0.000	2.64
B*B	0.3206	0.3205	163.92	0.000	7.07
C*C	0.0186	0.0186	9.54	0.005	0.41
D*D	0.00078	0.00078	0.4	0.533	0.02
E*E	0.0256	0.0256	13.12	0.001	0.56
Interaction	1.3432	0.1343	68.68	0.000	29.62
A*B	0.0126	0.0126	6.45	0.018	0.28
A*C	0.255	0.255	130.39	0.000	5.62
A*D	0.01	0.01	5.11	0.033	0.22
A*E	0.0576	0.0576	29.45	0.000	1.27
B*C	0.0023	0.00235	1.2	0.283	0.05

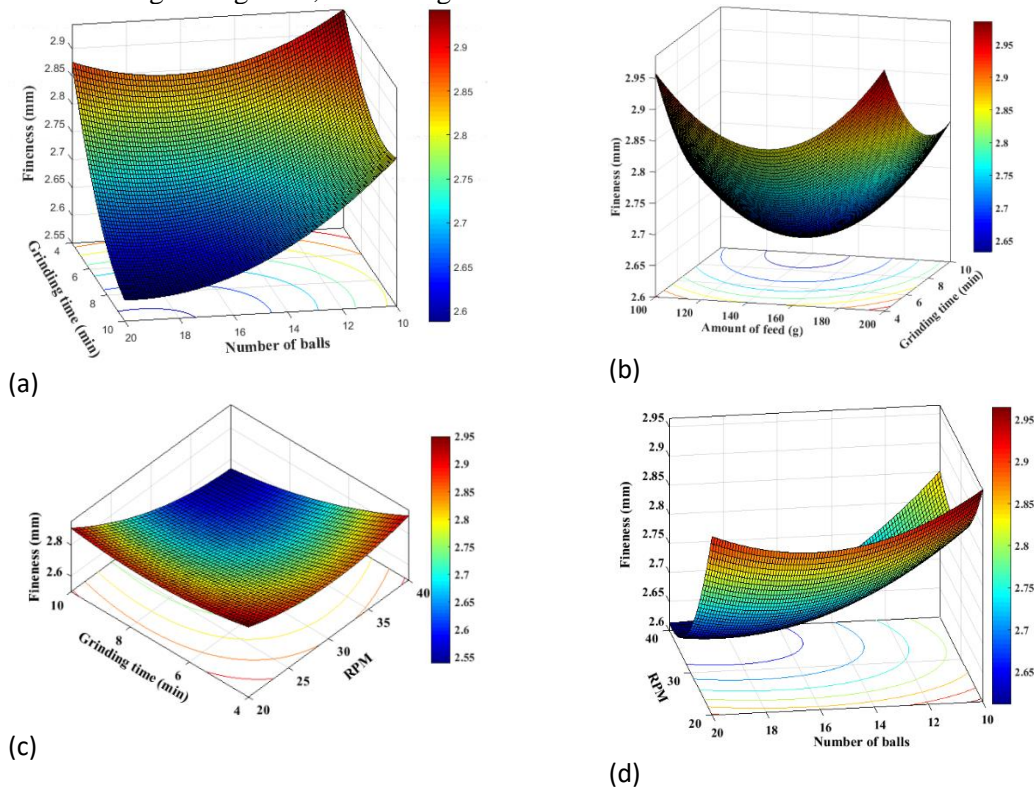
B*D	0.1496	0.1496	76.54	0.000	3.30
B*E	0.0313	0.0313	16.03	0.000	0.69
C*D	0.0156	0.0156	7.99	0.009	0.34
C*E	0.0256	0.0256	13.09	0.001	0.56
D*E	0.893	0.893	456.61	0.000	19.69
Lack-of-fit	0.0488	0.0024			
Pure Error	0	0			
Total	4.53				

Effect of variables on fineness for dry grinding

In order to understand the interaction effect of operating parameters on the d_{80} the results are shown as 3D surface plots in Figures 1 (a - f). Since the model has four independent parameters, one factor was kept constant at the centre level for each plot.

Figure 1 (a) shows the effect of grinding time and number of balls on fineness of coal particles. At constant grinding time, decreasing number of balls has a reversed trend on fineness; similar effect has also observed for the decreasing grinding time for constant number of balls. Figure 1 (b) indicates the effect of grinding time and amount of feed on fineness. For constant grinding time, increasing or

decreasing amount of feed exhibits coarser particle size and a minimum particle size at the centre value. It implies that too low or too high loading of feed will not result in fine particles. It can be explained by the feed to ball ratio in the ball mill. Bu *et al.* [6] have used this ratio in the range of 0.88 - 0.9 and observed an optimum fineness and breakage of particles. In the present experiments, 0.86 had been used as the feed to ball ratio. It is reported that the breakage rate of quartz and chlorite both were observed increasing with increase in feed size up to 0.5 mm and reduced when further increasing the size.



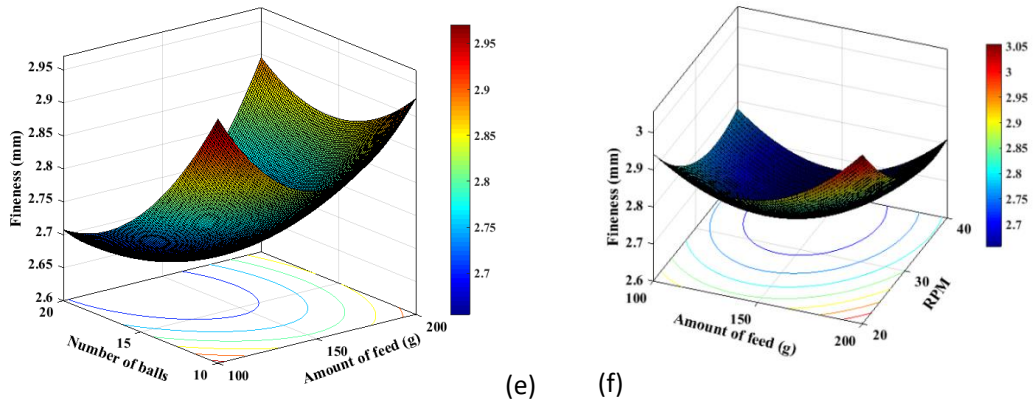
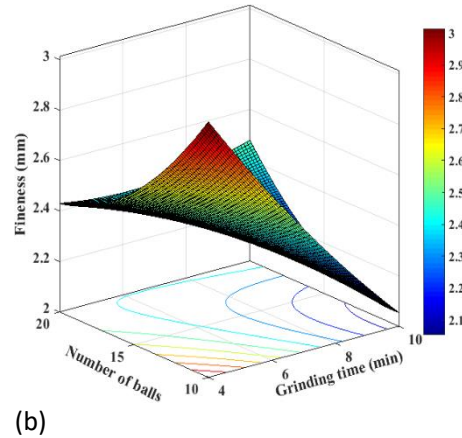
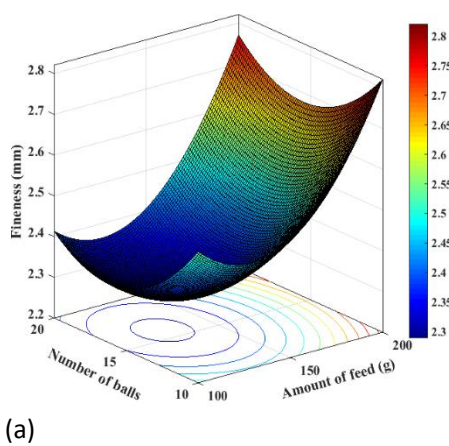


Figure 1 (a-f) 3D plots of all four parameters combination effect on response as fineness of coal.

Figure 1 (c) shows the effect of grinding time and revolutions per minute (rpm) of the ball mill on the fineness of coal particles. Grinding time does not affect much at a constant speed of revolution of the ball mill. On the other side, increasing speed of the ball mill at constant grinding time does not facilitate producing fine particles. Figure 1 (d) shows the effect of rpm of mill speed and number of balls with fineness. In this plot, it can be seen that the increasing ball mill speed at a constant number of balls, the particle size decreases. Effect of number of balls on fineness is similar to Figure 1 (a) and fineness increases with increasing number of balls. Coal is used in stirred for variable ball mill speed and it is observed that increasing speed from 360 to 1440 rpm reduced the particles from mm to μm . However, energy consumption was high at 1440 rpm speed, therefore it was expected to use an optimum speed of the ball mill.

Figure 1 (e) shows the effect of the amount of feed and number of balls on the fineness or d_{80} of particles. Feed amount shows the similar effect as in Figure 1 (b) that at a constant number of balls, too low or too high feed will yield less breakage of particles and fewer fine particles. At the same instance, with constant feed amount, fine particles increased at the centre and decreased at minimum and maximum number of balls. Figure 1 (f) shows the effect of the amount of feed and rpm of the ball mill on fineness. The ball mill speed at higher and lower values yields coarser particle size. However, at the centre is the minimum particle size. The effect of ball mill speed is opposite to that in Figure 1 (d), this may be due to the interaction of the different parameters in both cases. However, the amount of feed has a similar effect on fineness as in Figures 1 (b and e).



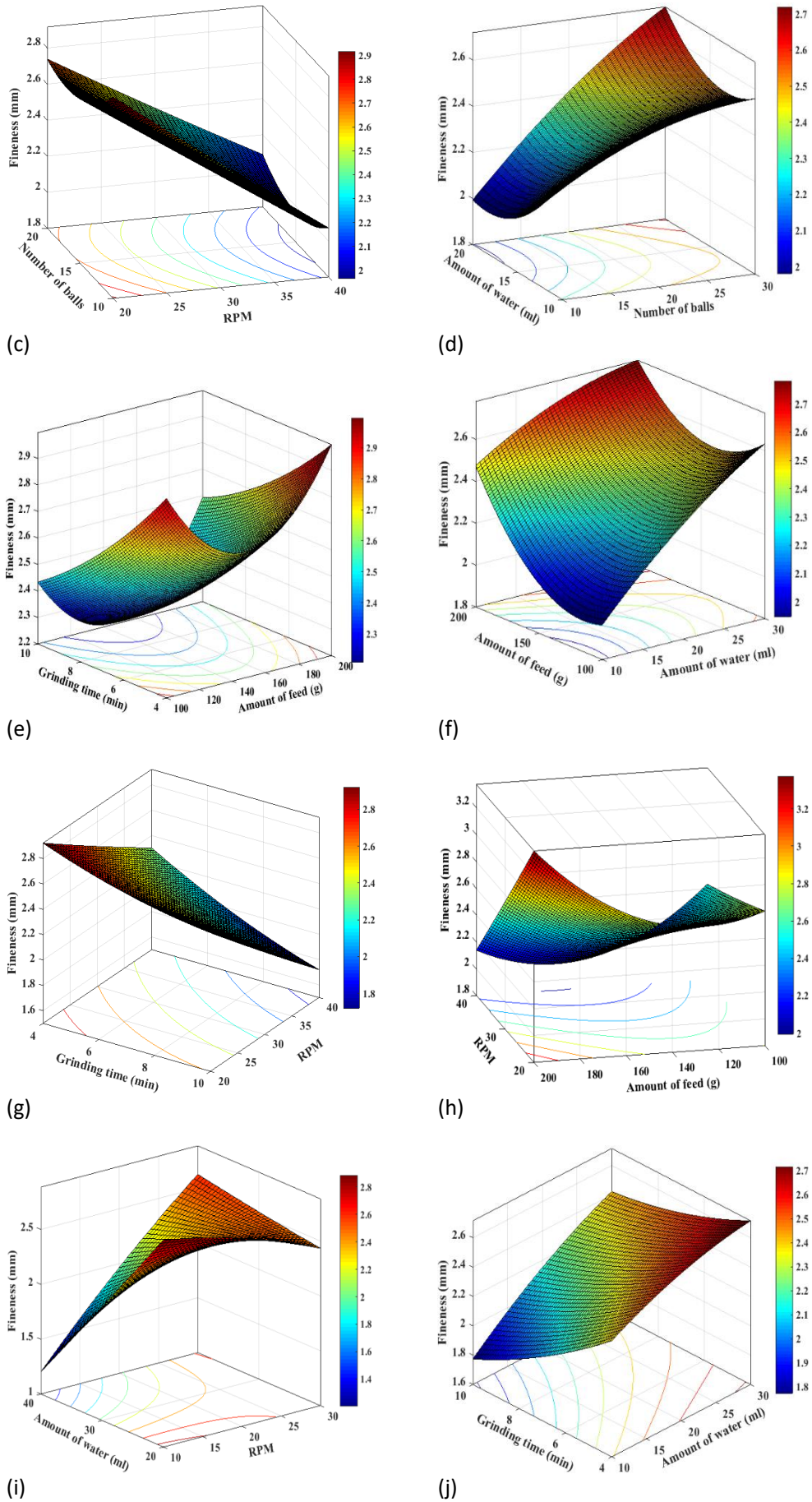


Figure 2 (a - j) 3D plots of wet grinding independent parameters with their response as fineness of coal.

Effect of variables on fineness for wet grinding

In these experiments, five independent parameters were taken to model the system as in Eq. (7). Water as the fifth parameter was added to increase the pulp density. Accordingly, a matrix as in Table 6 was prepared. Figure 2 (a) shows the effect of the number of balls and amount of feed on the fineness of coal particles. It can be seen that at a constant number of balls, the particle size increases with increasing amount of feed. It is known from the literature that slurry density has a major effect on grinding and fineness. It can be seen that at a number of balls for a constant feed, a minimum particle size was observed at the centre and increasing or decreasing the number of balls reduces the fineness of the particles. The similar behaviour was observed in the dry grinding.

Figure 2 (b) shows the effect of a number of balls with grinding time on fineness. Number of balls has a similar effect as in Figure 2 (a), however, for a constant number of balls an increase in grinding time is almost ineffective to fineness of particles. Figures 2 (c) and 2 (d) depict the effect of the number of balls with ball mill speed and amount of water added, respectively. Effect of number of balls with constant ball speed has not much significance on fineness. However, on increasing the rpm of the ball mill at a constant number of balls, fineness increases. On the other side of the constant number of balls the increasing amount of water will produce minimum particle size at the centre value than the highest and lowest values.

Figures 2 (e) and 2 (f) show the effect of the amount of feed in grinding time, and of the amount

of water on fineness, respectively. Amount of feed shows a similar effect on fineness, which is a minimum at the centre and increasing size while reaching a high and low value of feed with constant grinding time and amount of water in both plots. However, grinding time and amount of water at constant feed reveals that increasing both parameters results in fine particles.

Figures 2 (g), 2 (h) and 2 (i) illustrate the interaction of rpm of the ball mill with grinding time, amount of feed and amount of water. Increasing rpm of the mill decreases the particle size for constant grinding time and amount of feed, however, reverse trends were observed on fineness for mill speed with a constant amount of water. Figures 2 (g) and 2 (j) show that increasing grinding time will result in finer particles. Increasing amount of water with constant grinding time and mill speed in Figure 2 (i) and (j) result in coarse particles.

Optimum conditions for dry and wet grinding

Table 6 shows the optimized conditions by the model equation, three experiments were performed and the error was calculated. The error was observed ± 5 %. The fineness can also be compared in the table, the same size of feed was taken in both types of grinding and 0.526 mm and 2.411 mm of product size were predicted for wet and dry grinding, respectively; eventually, experiments confirmed the prediction. It is to be noted that for the same experiment dry grinding requires 20 balls and wet grinding needed only 13 balls and much smaller particles were yielded with wet grinding.

Table 6. Validation of experiments for dry and wet grinding for predicted model equations developed

Dry Grinding							
Run no	A (numbers)	B (g)	C (min)	D (rpm)	d_{80} predicted (mm)	d_{80} experimental (mm)	
1	20	133.06	10	40	2.411	2.36	
2	20	133.06	10	40	2.411	2.32	
3	20	133.06	10	40	2.411	2.35	
Wet Grinding							
Run no	A (numbers)	B (g)	C (min)	D (rpm)	E (ml)	d_{80} predicted (mm)	d_{80} experimental (mm)
1	12.9 \approx 13	152.525	10	40	10% of feed = 15.2	0.526	0.510
2	12.9 \approx 13	152.525	10	40	10% of feed = 15.2	0.526	0.535
3	12.9 \approx 13	152.525	10	40	10% of feed = 15.2	0.526	0.515

CONCLUSIONS

In the present work, the three-level factorial Box–Behnken experimental design models were investigated for wet and dry grinding of coal for five variables, namely: grinding time, ball charge, amount of feed, amount of water, and rotational speed used for dry and wet grinding. These were all possible parameters which influenced the fineness of coal particles.

It can be concluded from the results that all parameters have a significant effect on fine particles production by grinding. The model equation with RSM and the P -value and F -value indicated a good agreement between predicted and experimental values. The correlation coefficient (R^2) for dry grinding was 0.97 and for wet grinding was 0.98.

REFERENCES

1. C. L. Prasher, *Crushing and Grinding Process Handbook*, Wiley, Chichester, 1987.
2. P. C. Harrison, N. Rowson, in: *Proceedings of the 1997 Jubilee Research Event*, Institution of Chemical Engineers, Nottingham, UK, 1997.
3. F. Boylu, H. Dinçer, G. Ateşok, *Fuel Processing Technology*, **85** (4), 241 (2017).
4. X. Bu, G. Xie, Y. Chen, C. Ni, *International Journal of Coal Preparation & Utilization*, **37** (3), (2004).
5. K. Sato, K. Shoji, K. Okiura, I. Akiyama, A. Baba, *Powder Technology*, **54** (2), (1988).
6. X. Bu, G. Ma, Y. Peng, G. Xie, H. Zhan, B. Liu, *International Journal of Coal Preparation and Utilization* (2019).
7. X. Bu, Y. Chen, G. Ma, Y. Sun, C. Ni, G. Xie, *Advanced Powder Technology*, **30**, (2019).
8. D. W. Fuerstenau, P. B. Phatak, P. C. Kapur, A. Z. M. Abouzeid, *International Journal of Mineral Processing*, **99** (2011).
9. H. Shin, S. Lee, H. Jung, J. Kim, *Ceramics International*, **39** (2013).
10. C. Tangsathitkulchai, L. G. Austin, T. Singh, A. Awasthi, P. Tripathi, S. Gautam, A. Gautam, *International Journal of Coal Science and Technology*, **3**(2) (2016).
11. M. A. A. Tuzun, PhD Dissertation, Chemical Engineering Department, University of Kwazulu-Natal, 1994.
12. N. Aslan, Y. Cebeci, *Fuels*, **86** (2007).
13. A. Edadnejad, G. R. Karimi, H. Dehghani, *Powder Technology*, **245** (2013).

Reduction and biosorption of hexavalent chromium ions from wastewaters: a review

A. Pathania¹, D. Thapliyal², R. Kumar Arya^{2*}

¹Fuel Cell Department, Korea Institute of Energy Research (KIER), 152 Gajeong-ro, Yuseong-gu, Daejeon 34129, Korea

²Department of Chemical Engineering, Dr B R Ambedkar National Institute of Technology, Jalandhar, 144011, Punjab, India

Received: October 13, 2021; Revised: February 08, 2022

Chromium contamination is one of the most serious environmental concerns faced by the world today. Chromium contamination can cause a variety of health problems. Research focussing on the reduction or eradication of hexavalent chromium has evoked the interest of scientists in recent years. The applicability of several types of microorganisms for hexavalent chromium reduction and biosorption is highlighted in this review. The type of microorganism growth determines the optimal pH and temperature for Cr(VI) reduction. Culture medium for Cr(VI) reduction must be chosen carefully since it is significantly reliant on the functional group present; as with *Aspergillus niger* and *Aspergillus parasiticus*, culture with tannic acid has a lower Cr(VI) removal efficiency than culture for *Bacillus* sp. Having glucose, the Cr(VI) removal efficiency improves substantially. The application of dead cells is more efficient for reduction and biosorption of Cr(VI) as dead cells require less maintenance. A brief discussion of several types of chromium removal methods from wastewater streams is also included in the review.

Keywords: Biosorption; Chromium reduction; Hexavalent chromium; Microorganisms; Bioreduction; Wastewater treatment.

INTRODUCTION

Chromium (Cr) is found in abundance in the crust of the earth. Cr is mostly utilized in tanning of leather, dyes and paints, ceramic ware and glass, fungicides, for the manufacturing of several catalysts, in photography, chrome alloys, chrome plating, corrosion control, wood preservation and manufacturing of refractory materials. Chromium exists as Cr(III) and Cr(VI) in the aquatic environment. When compared to trivalent chromium, hexavalent chromium is hundred times more hazardous and transportable. Because it causes cancer and mutations in humans, Cr(VI) is one of the most dangerous environmental contaminants [1]. Contamination of underlying aquifers and vadose zones has resulted in improper Cr metal disposal at sites in semiarid and arid locations [2]. Most of the industrial effluents contain Cr(VI) and these effluents are almost impossible to be removed from wastewater using conventional wastewater treatment systems [3].

Methods including coagulation, precipitation, filtration, adsorption, ion exchange, membrane technology, electrodialysis, and biological removal are the few ways for removing chromium from wastewater. Majority of the traditional methods for the removal of Cr(VI) are not economically viable

and have certain difficulties in developing countries [4]. From the past research, it has been found that microorganisms can be used to reduce Cr(VI) to Cr(III) in an alternative approach. Bioaccumulation, chromate reduction, chromate efflux, and biosorption have all been ascribed to microorganisms such as bacteria, fungi, and yeast for chromium bioremediation [5]. This study focuses on reducing hexavalent chromium to trivalent chromium utilizing various microorganisms such as bacteria, fungi, and yeast, as well as hexavalent chromium biosorption.

Chromium removal techniques from contaminated wastewater

Human health is known to be jeopardized by Cr(VI) ions. Skin rashes, ulcers, respiratory difficulties, renal damage, liver dysfunction, cancer, and even death can be caused by these ions [6-8]. As a result, the removal of these ions is critical for maintaining human health. There are several techniques through which Cr(VI) is removed from contaminated wastewater like adsorption, coagulation, membrane technology, precipitation, filtration, ion exchange, electrodialysis and biological removal which are being summarized in Table 1 along with benefits and drawbacks of the main approaches for chromium removal from water.

* To whom all correspondence should be sent:

E-mail: aryark@nitj.ac.in; rajaryache@gmail.com

Table 1. Summary of different methods for Cr removal from water

Method	Advantages	Limitations	References
Adsorption	Depending on pH adsorption, media can adsorb either cationic or anionic Cr ions. Adsorbent can be regenerated. Activated carbon is effective in removing both Cr (III) and Cr (VI).	Difficult to get optimum pH to remove both cation and anion. Also, they have low capacity Activated carbon is expensive. Carbon nanotubes get disposed in water and pose a risk to aquatic life and humans.	[9-16]
Coagulation	Conventional coagulation is an efficient method for removing Cr (III) with a fast response time. Redox-assisted coagulation (RAC) with Fe (II) is >99% effective for removal of Cr (VI).	For the removal of Cr (VI), conventional coagulation uses a two-stage procedure that generates a large amount of sludge. RAC is affected by the settleability of the floc and filterability of the precipitated particles.	[17-19]
Membrane Filtration	Reverse osmosis is 90–100% effective for the removal of Cr (VI) and Cr (III). Polymer enhanced ultrafiltration has high removal efficiency and high binding selectivity.	Reverse osmosis needs high investment and operational costs. Difficult to find suitable polymers to achieve complexation with metal ions, in polymer enhanced ultrafiltration.	[20-24]
Chemical Precipitation	The solubilities of metal sulfide precipitates are lower than hydroxide precipitates and sulfide precipitates are not amphoteric. Sulfide potentially reduces Cr (VI) and precipitates Cr in one step.	Hydroxide precipitation generates large volumes of relatively low-density sludge Sulfide precipitants in acidic conditions can result in the evolution of toxic H ₂ S fumes. Also, the process is relatively expensive.	[25-28]
Ion Exchange	High treatment capacity and fast kinetics. Suitable for small and large installations. Variety of specific resins are available for removing specific contaminants	More research into the industrial application of zeolites is required. Resin fouling and removal efficiency is affected by the presence of other ions in water.	[29-33]
Biological Removal	Biosorbents are characteristic of broad sources, low cost and rapid adsorption.	The separation of biosorbents is difficult after adsorption At acidic pH, certain biological removal methods are not suitable for drinking water treatment applications.	[34, 35]

Reduction of hexavalent chromium by using microorganisms

Bacillus sp. isolation from chromium waste was investigated by Liu *et al.* [1] for its ability to reduce Cr(VI). Among the five isolated bacteria, two were recognized as *Bacillus* sp., namely XW-2 and XW-4. But XW-4 was selected for the Cr(VI) reduction experiments because XW-4 isolates have lower concentration as compared to XW-2 after 3 days.

They investigated the influence of Cr(VI) on cell growth and discovered that the higher the Cr(VI) concentration, the stronger is the effect on cell growth as compared with the lower concentration. They also examined the effects of pH and tempera-

ture and discovered that the best initial pH value was 9 when changing pH from 4 to 11. Three different temperatures, 37°C, 47°C, and 20°C, were used to reduce Cr(VI).

The absorption and reduction of Cr(VI) by two fungi were investigated by Shugaba *et al.* [2]. They used two fungi i.e, *Aspergillus niger* and *Aspergillus parasiticus* which are isolated from the landfill. It was shown that the Cr(VI) concentration decreases with growth time. The authors found that subsequent to the growth of 96 hours the solution became completely colourless and the removal of Cr(VI) was achieved at 96.3% and 91.6% after 96 hours in *Aspergillus niger* and *Aspergillus parasiticus* cultures.

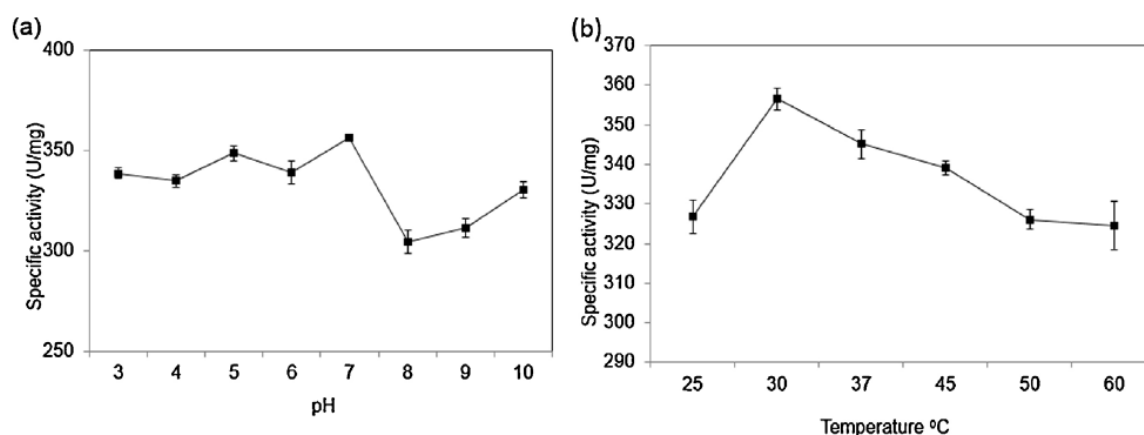


Figure 1. (a) Effect of pH on chromate reductase activity in *B. methylotrophicus*. (b) Effect of temperature on chromate reductase activity in *B. methylotrophicus* [5].

Donmez and Kocberber [3] used enhanced microbial cultures made from molasses and NaCl-containing medium to investigate the bioaccumulation of hexavalent chromium. They prepared the enriched cultures with the help of sodium chloride, molasses and Cr(VI) for better bioaccumulation efficiency. The authors found that the percentage of uptake yield of mixed cultures increased from 95 to 99 percent after 5 days for all samples of NaCl concentration and pH values. The optimum pH values were 7, 8 and 9 in a solution containing 2%, 4% and 6% NaCl, respectively. At pH 7, maximal Cr uptake was 87.5 mg/g at a higher NaCl concentration (6 percent w/v), whereas initial Cr concentration was 83.6 mg/L.

Mala *et al.* [5] investigated the chromium bioremediation potential of an inducible chromate reductase with extracellular activity in *Bacillus methylotrophicus*. The authors utilized four *Bacillus* strains for chromate reduction in various media, all of which were obtained from tannery sludge. *Bacillus methylotrophicus*, for example, reduced chromate 95 M Cr(VI) to 7.14 M Cr(VI) after 48 hours. They created five different assay mixtures, including the standard assay system, TCA (tricarboxylic acid) addition prior to incubation, heat-inactivated enzyme, no added enzyme, and no added NADPH (nicotinamide adenine dinucleotide phosphate), and discovered that the percentage of residual Cr(VI) in the standard assay system is significantly lower than in the other four systems. The authors studied the effect of pH and temperature, as shown in Figure 1. Except for Na⁺ and Ca²⁺, all metal ions enhanced chromate reductase activity which was estimated using a Lineweaver–Burk plot, and the values of K_m and V_{max} derived from the graph are 86.5 μM and 59.89 μM, respectively, which suggest that the reaction rate using K₂Cr₂O₇ as substrate is feasible. Fukuda *et*

al. [36] investigated the removal of Cr(VI) from chromium deposits by chromate-resistant fungi *in vitro* and in contaminated soils. Seven fungal isolates were used for reducing the chromium concentration at nearly neutral pH and strongly acidic pH. They identified only three fungal isolates by using a morphology study, i.e. *Aspergillus* sp. N2, *Penicillium* sp. N3 and *Penicillium* sp. N5. These three isolates reduced higher chromium concentrations as compared to others. In strongly acidic pH 3 *Aspergillus* sp. N2 and *Penicillium* sp. N3 are reducing 50% of chromium concentration and *Penicillium* sp. N5 is reducing chromium concentration by nearly 30%. The authors found that the higher the initial concentration of chromium in growth media the slower will be the Cr(VI) removal. Fernandez *et al.* [37] explored the removal efficiency of Cr⁶⁺ by indigenous yeasts, i.e. *Pichia jadinni* M9 and *Pichia anomala* M10 isolated from textile factory effluent. There is a very slight effect on the growth of cells at concentrations of 26, 52 and 78 μg mL⁻¹ and the indigenous yeasts survive the Cr⁶⁺ concentration 104 μg mL⁻¹ and have no effect on cells growth. They found that the optimum temperature is 30°C, optimum pH is 7, optimum agitation speed is 150 and 250 rpm and optimum initial Cr⁶⁺ concentration is 26 μg mL⁻¹ where the chromium is removed by both the cultures *Pichia jadinni* M9 and *Pichia anomala* M10.

The decrease of Cr(VI) by *Bacillus coagulans* isolated from polluted soils was investigated by Philip *et al.* [38]. They isolated *Bacillus coagulans* from contaminated soils and compared it with *Pseudomonas aeruginosa* and *Bacillus circulans* from garden soil and found that *Bacillus coagulans* (8.30 mg/L) showed the highest Cr(VI) reduction as compared to the *Pseudomonas aeruginosa* (20.48 mg/L) and *Bacillus circulans* (38.80 mg/L) when initial concentration was 104 mg/L. Malate showed

the highest Cr(VI) reduction as compared to the other three electron donors, i.e. citrate, succinate and glucose. Cr(VI) had an optimal pH of 7. The presence of nitrates and sulfates had no influence on the decrease of Cr(VI). Garbisu *et al.* [39] evaluated the aerobic chromate reduction by *Bacillus subtilis*. The latter have been cultured in agar media and were able to reduce Cr(VI) to Cr(III) at a concentration varying from 0.1 to 1 mM K_2CrO_4 . They studied the effect of sodium nitrate and metabolic poisons and found that chromate reduction was independent of sodium nitrate which had no effect on growth and reduction of chromate. Metabolic poisons had inhibited the growth and chromate reduction. Effects of kanamycin and low temperature were studied and it was found that kanamycin cultures have not reduced the chromate as fast as compared to the control cultures and at low temperature 4°C inhibited the chromate reduction, as shown in Figure 2.

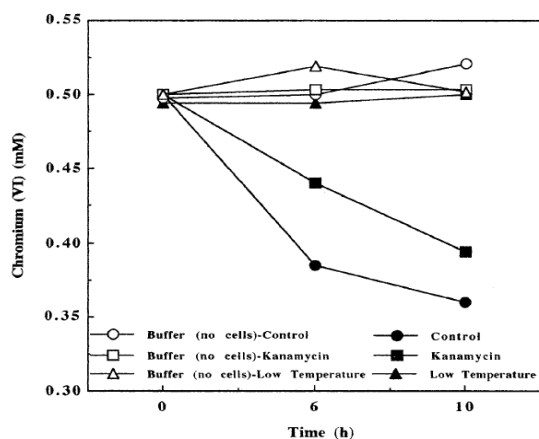


Figure 2. Effect of kanamycin and low temperature on the decrease in Cr(VI) in the supernatant fraction of cultures of *B. subtilis* resting cells [39].

Ganguli and Tripathi [40] used chromate-reducing *Pseudomonas aeruginosa* A2Chr to study the bioremediation of hazardous chromium from electroplating effluent in two bioreactors. In batch culture - dialysis bioreactor and rotating biological contactor, they compared *Pseudomonas aeruginosa* A2Chr's chromate-reducing capabilities. They had cultured two media, succinate minimal medium and electroplating effluent and varied the Cr(VI)

concentration 10-100 mg/L. The study found that the highest Cr(VI) reduction occurred at 10 mg/L and the rotating biological contractor showed the highest Cr(VI) reduction as compared to the batch culture and dialysis bioreactor at 100 mg/L Cr(VI) concentration. Park *et al.* [41] evaluated the elimination of Cr(VI) by *Aspergillus niger* dead fungal biomass. They found that Cr(VI) to Cr(III) reduction occurred when no Cr(III) was in the solution at first but gradually emerged in an aqueous solution when Cr(VI) was reduced to Cr(III). They investigated the X-ray photoelectron spectroscopy and desorption of this dead fungal biomass and discovered that much of the chromium linked to the biomass was trivalent. They also noticed that if the temperature increases then the percentage of adsorption increases but pH followed the opposite trend by increasing the pH then the percentage of adsorption decreases.

Biosorption of hexavalent chromium by using bioadsorbent

Bankar *et al.* [4] explored the adsorption of Cr(VI) ions from aqueous solution onto two *Yarrowia lipolytica* marine isolates, namely NCIM 3589 and NCIM 3590. They studied the effect of sea salt and cell biomass on Cr(VI) adsorption and noticed that adding sea salt decreases the adsorption capacity and increasing the biomass percentage it also starts decreasing the adsorption capacity. They also conducted a surface morphology study of cell loaded with Cr(VI) by SEM-EDS and ED-XRF to notice the presence of chromium (VI) as shown in Figure 3.

Bai and Abraham [42] investigated *Rhizopus nigricans*' capacity to biosorb Cr(VI) from aqueous solution. The highest adsorption capacity was achieved at optimum pH 2; that is 99.8%. Optimum agitation speed is 120 rpm for higher adsorption efficiency. By increasing the initial Cr(VI) ion concentration from 50 to 400 mg/L the adsorption efficiency starts decreasing. Adsorption capacity starts increasing by increasing the contact time but if more than 75% Cr(VI) is removed within 30 minutes then it takes a long time for complete removal of Cr(VI) which is approximately 8 hours.

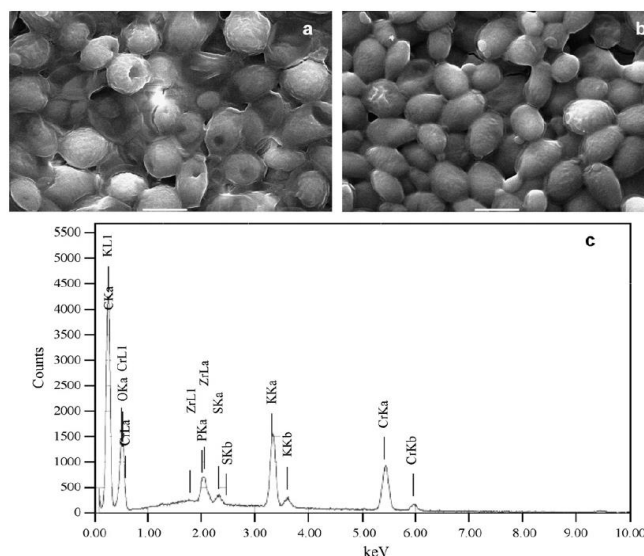
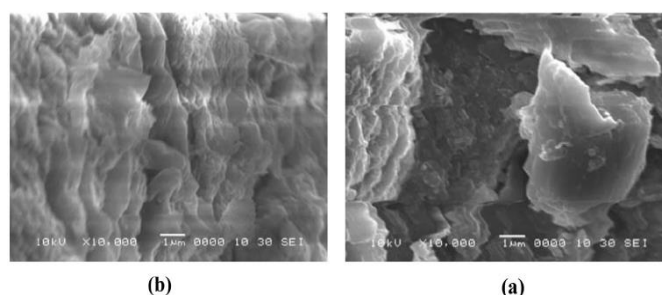


Figure 3. SEM analysis of *Y. lipolytica* (a) NCIM 3589 and (b) NCIM 3590 after Cr (VI) biosorption (c) Representative energy dispersive X-ray spectrum of SEM images indicating the presence of Cr [4].

Figure 4. SEM micrographs of the *Chlorella pyrenoidosa* before (b) and after (a) of biosorption [43] .



Rezaei [43] has studied the biosorption of chromium by using dried *Spirulina*. He observed that by increasing the contact time, adsorbent dose, agitation speed and temperature the percentage of biosorption also increases. Optimum contact time, adsorbent dose, agitation speed, temperature and pH are 120 min, 0.1 g, 120 rpm, 25°C and 5, respectively. He analyzed the Langmuir and Freundlich isotherms for adsorption and found that the results are in accordance with these two models. Kinetic modeling was studied by using pseudo-first and second order rate but adsorption of chromium by *Spirulina* followed second order kinetics. Finally, he also performed SEM analysis of bio-adsorbent as shown in Figure 4.

Balan *et al.* [44] conducted batch sorption studies with *Sphagnum* moss peat as a sorbent to investigate the elimination process of chromium(III) from aqueous solutions. They found that moss peat treated with sodium chloride showed a higher reduction of Cr(III) as compared to chromium nitrate. They

investigated the Langmuir model which shows a higher sorption capacity as compared to others. The sorption capacity of Langmuir is 18.62 mg Cr(III)/g of peat. Mean free sorption energy binding the Cr(III) on peat through an ion exchange mechanism is in the range of 10.9 to 12.9 kJ mol⁻¹. The production of varied metal ions based on alginate bentonite bio-composites for Cr(VI) sorption was investigated by Gopalakannan *et al.* [45]. They synthesized the bio-composites by dispersing bentonite in an alginate biopolymer and crosslinked with calcium chloride (Ca²⁺), cerium nitrate (Ce³⁺) and zirconium oxychloride (Zr⁴⁺). They also used SEM to characterize the synthesized biocomposites and noticed that some changes take place in the synthesized bio-composites after Cr(VI) is sorbed by bio-composites as shown in Figure 5. They have found that optimum contact time is 60 min, optimum dosage is 0.1 g, optimum pH is 2, the presence of co-ions shows less influence on sorption capacities except for HCO₃⁻.

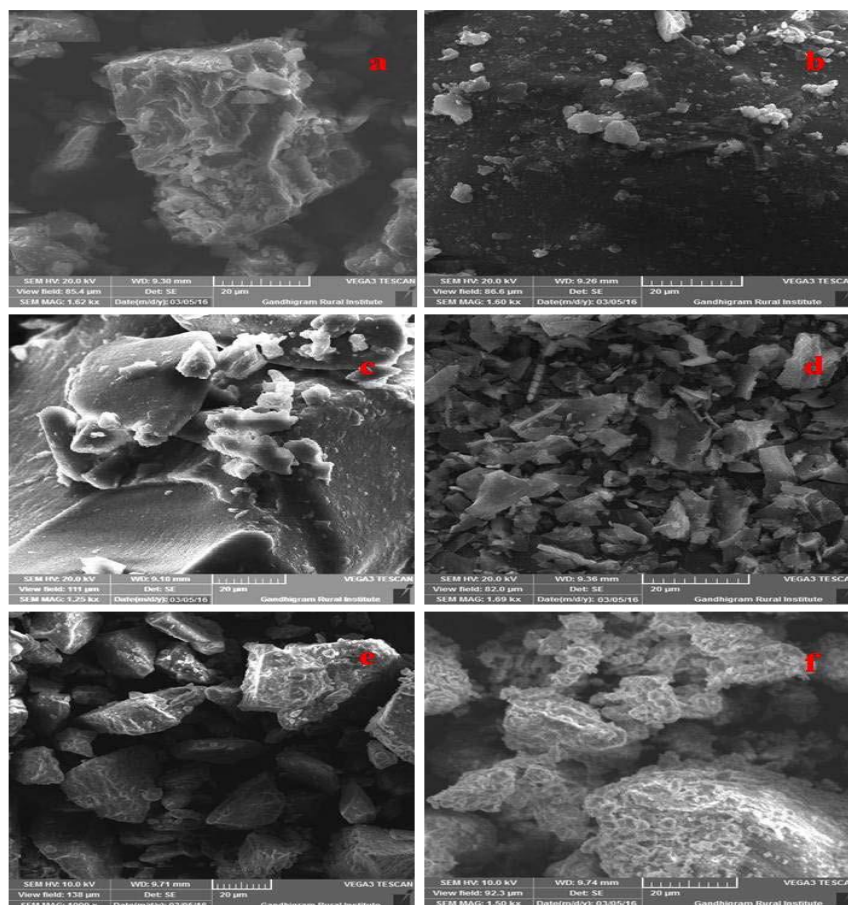


Figure 5. SEM images of (a) Calcium-alginate biopolymer, (b) Chromium sorbed calcium-alginate biopolymer composite, (c) Cesium-alginate biopolymer, (d) Chromium sorbed cesium-alginate biopolymer composite, (e) Zirconium-alginate biopolymer, (f) Chromium sorbed zirconium-alginate biopolymer composite [45].

The authors found that Langmuir isotherm best fits the Cr(VI) sorption and also noticed that all three bio-composites followed pseudo-second order kinetics. Pan *et al.* [46] investigated the use of amino-functionalized alkaline clay combined with a cationic polymer as adsorbent for removing Cr(VI) from aqueous solution. The cationic polymer was prepared through the method of atom transfer radical polymerization by using acrylamide (AM) and dimethyl aminoethyl methacrylate (DMAEMA) monomers and using CuBr/2,2'-bipyridine (BPY) and 4Br-PER as an initiator. According to the authors, the optimum value of pH is 4 which shows a high adsorption capacity, i.e. 102 mg/g and by increasing the contact time the adsorption capacity also starts increasing. Maximum adsorption capacity is 102 mg/g in 100 min. Then they fitted the equilibrium data in two isotherm models, i.e. Langmuir and Freundlich adsorption isotherm and noticed that Langmuir isotherm which is the best-fit isotherm, had an adsorption capacity of 137.9 mg/g at 30°C. Mala *et al.* [47] had studied the biosorption and bioaccumulation of chromium by *Aspergillus niger* MTCC 2594. They had taken a spent chrome

liquor from the leather industry. They identified the Cr(III) and Cr(VI) content in spent chrome liquor from two different processes. Similarly, they also prepared a biomass (*Aspergillus niger*) by harvesting for 72 hours at room temperature. The Cr(VI) and Cr(III) levels found in spent chrome liquor were higher and above the permissible limit. Then they studied the bioaccumulation of Cr(VI) and Cr(III) and found that 75%-78% accumulation takes place by the end of 24-36 hours. According to the research, in contrast to the Langmuir isotherm, the data matched better the Freundlich isotherm. Uzun *et al.* [48] examined the biosorption of Cr(VI) from aqueous solution by *Pinus sylvestris* cone biomass. They discovered that as pH decreases from 7 to 1, initial Cr(VI) concentration increases from 50 to 300 mg/L, the biosorption efficiency decreases. The research group also used the Freundlich isotherm to study the adsorption and discovered that the data fit well in this model, indicating a high adsorption capacity.

Soya cake was used to investigate Cr adsorption and Cr(VI) reduction to Cr(III) in aqueous solutions by Daneshvar *et al.* [49]. Adsorption and reduction

efficiency decreased as the pH increased. In the temperature parameter, adsorption and reduction efficiency is increasing as the temperature increased. The optimum condition for the reduction of Cr(VI) to Cr(III) is pH=1, T=25°C, time=5 h and soya mass is 0.7 g. The optimum condition for the adsorption of Cr(VI) is pH=1, T=20°C, time=1 h and soya mass is 30 g. They also concluded that the Langmuir and Freundlich isotherms did not explain the adsorption data well. Aksu *et al.* [50] explored the adsorption of Cr(VI) ions by dead cells of *C. Vulgaris* and *Z. Ramigera*. The study had shown that for the adsorption of Cr(VI) by dead cells, optimal temperature and pH range are 25-50°C and 1-2, respectively. The authors also found that when the metal ion concentration increases, the adsorption capabilities decrease. In case of cell concentration, efficiency of adsorption starts increasing by increasing the biomass concentration but the rate of adsorption is very slow.

The absorption of chromium cations and anions by milled peat was investigated by Dean and Tobin [51]. They looked at Cr(VI) and Cr(III) absorption by biomass at different pH levels, such as 2, 4, and 7, and used MINEQL to predict Cr(VI) and Cr(III) speciation. Finally, they compared both. The research group found that the uptake of Cr(VI) and Cr(III) increased by increasing the concentration of the solution and maximum uptake of Cr(VI) and Cr(III) is 0.58 and 0.27 mmol/g at pH 2 and 4. The researchers also found the speciation of Cr(VI) and Cr(III) by MINEQL at different pH 2, 4 and 7 and predominant species at pH 2, 4 and 7 in Cr(VI) is $HCrO_4^-$ at pH 2 and 4 but at pH 7 predominant species is CrO_4^{2-} . They also found that the predominant species at pH 4 for Cr(III) is 50% Cr^{3+} and 50% $Cr(OH)^{2+}$. Predominant species at pH 2 is Cr^{3+} and predominant species at pH 7 is $Cr(OH)^{2+}$. Prakasham *et al.* [52] explored how free and immobilized *Rhizopus arrhizus* adsorbed chromium (VI) from synthetic effluent and chromium solution. Immobilization of *Rhizopus arrhizus* was done with the help of alginate. All the experiments were conducted at pH 2. They discovered that the effectiveness of adsorption improved as contact time increased for both free and immobilised biomass. At 2-8 hours; 46.50-63.54% and 50.63-73.98% Cr(VI) was adsorbed for immobilized and free biomass. However, when the initial chromium ion concentration raises, the adsorption capacity of both free and immobilized biomass decreases. At 50-300 mg/L initial chromium concentration residual chromium left was 0.57-69.21 mg/L and 0.79-61.6 mg/L for free and immobilized biomass. They also studied the adsorption isotherm on these data and

found that the data showed a low intensity of biosorption less than 1, 0.187 and 0.23 for free and immobilized biomass.

Sag and Kutsal [53] investigated the need for adsorption of isotherms in the study of chromium adsorption on *Z. ramigera*. The research group explored the influence of pH and temperature isotherm in two models, i.e. Langmuir and Freundlich isotherm. The authors varied the pH from 0.5-4 and temperature 25-35°C and then finally found out that the optimum pH and the temperature is 2 and 25°C in the eradication process of chromium from aqueous solution. Dakiky *et al.* [54] researched on the selective adsorption of chromium (VI) in industrial wastewater using low-cost, widely available adsorbents. The authors used a variety of adsorbents such as wool, olive cake, sawdust, pine needles, almond shells, cactus leaves, and charcoal for the experiment. They discovered that as the adsorbent concentration and contact duration rose, so did the percentage of Cr(VI) removal. Wool showed the highest removal efficiency, that is 81.3% at 16 g/L concentration of adsorbent. Almond shell showed the lowest removal efficiency, that is 19.8% at 8 g/L adsorbent concentration. When the pH was raised from 1 to 8, the removal efficiency of Cr(VI) began to decline. The best pH, contact duration, temperature, and adsorbent dose were 2, 2 hours, 30°C, and 8 g/L, respectively. In comparison to the other adsorbents, it was apparent that wool is the best adsorbent for removing Cr(VI). Kiran *et al.* [55] researched the biosorption of Cr(VI) in the presence of salts by a natural isolate of *Lyngbya putealis* (HH-15). They noticed that by increasing the pH from 2 to 10, Cr(VI) uptake started decreasing. Cr(VI) uptake started increasing by increasing the contact time from 5-180 minutes and metal ion concentration from 10-100 mg/L. Optimum pH, contact time and metal ion concentration was 3, 120 min and 50 mg/L. They also found that their experimental data were in accordance with both pseudo-first and second order kinetics. Das and Guha [56] have studied the biosorption of chromium by *Termitomyces clypeatus*. They have tested different strains of fungi to eliminate chromium but *Termitomyces clypeatus* had shown a great potential for the elimination of chromium and adsorption percentage of live and dead *Termitomyces clypeatus* biomass is 91 ± 2.1 and 62 ± 2.0 . But they have taken live *Termitomyces clypeatus* biomass for further studies. They noticed that the adsorption value increased by increasing the pH of that solution from 2 to 3 but after that equilibrium was obtained, and the optimum value of pH was 3. They examined the adsorption isotherm

by using two models, i.e. Langmuir and Freundlich isotherm and noticed that Langmuir model fits better as compared to Freundlich. The coefficient of regression, r^2 value for Langmuir and Freundlich is 0.998 and 0.965, respectively. They also analyzed this model by using χ^2 -square test and found that χ^2 value for Langmuir and Freundlich is 5.03 and 18.53, respectively.

Park *et al.* [41] investigated the biosorption of Cr(VI) by chemically treated *Ecklonia* sp. biomass. They had taken *Ecklonia* sp. and treated it with various alkalis, acids, organic solvents, and other chemicals and noticed that the treatment of biomass with acids showed the best performance as compared to the other treatments like alkalis, organic solvents, etc. By using FTIR spectroscopy they discovered that carboxyl and amino groups were connected to chromium biosorption and that methylation of the amino group reduced the removal rate of Cr(VI) while amination of the carboxyl group enhances the removal rate of Cr(VI). Kratochvil *et al.* [57] investigated how seaweed biosorbent may remove trivalent and hexavalent chromium. They discovered that pH 4 and 2 are the best for removing Cr(III) and Cr(VI). They also studied the desorption mechanism, and found that after 2 to 24 hours, about 40 to 70 percent of the total chromium was recovered. Basha *et al.* [58] tested the biosorption of Cr(VI) by using *Cystoseira indica*, a scientifically formulated seaweed. They have used *Cystoseira indica* as a bioadsorbent and chemically modified it by oxidation with potassium permanganate (CB3), crosslinking agent epichlorohydrin (CB1, CB2) and distilled water (RB). The research group also noticed that by increasing the contact time and initial Cr(VI) ion concentration the Cr(VI) uptake started increasing. But they also found that the percentage of adsorption started decreasing in case of increasing the initial Cr(VI) ion concentration. They have found that by increasing the pH from 1 to 3 the Cr(VI) uptake started increasing but, above pH 3 Cr(VI) uptake started decreasing. Optimum pH, contact time, and solid/liquid ratio is 3, 180 min and 0.5 g/L.

Suksabye *et al.* [59] researched the use of coir pith to remove chromium from electroplating effluent. They used adsorbents made of coir pith and activated carbon to remove chromium from electroplating effluent. The authors have found that by increasing the contact time (5 min-24 hours), adsorbent dosage (5-45 g/L) and temperature (15-60°C) the efficiency of adsorption also increased in both cases, but coir pith had shown better result as compared to the activated carbon. They discovered that pH played a significant part in the adsorption of chromium, and that raising the pH from 2 to 10

decreased the effectiveness of adsorption in both situations. Coir pith had shown the maximum adsorption efficiency and chromium uptake - that is 99.99% and 317.65 mg/g at solution pH 2. Optimum contact time, adsorbent dosage, pH and temperature were 18 hours, 20 g/L, 2 and 30°C. The elimination of Cr(VI) from aqueous solutions by a surplus agricultural waste – rice straw was investigated by Gao *et al.* [60]. They discovered that raising the initial Cr(VI) ion concentration (40-200 mg/L) and temperature (27-47°C) increased the percentage of adsorption. At the same time, by increasing the pH (2-6) and straw particle sizes (150-380 μm) the removal percentage of Cr(VI) started decreasing. Optimum pH, temperature, initial Cr(VI) ion concentration and straw particle sizes were 2, 47°C, 100 mg/L, and less than 150 μm . They have also noticed that rice straw reduces the Cr(VI) to Cr(III) and studied the effect of NO_3^- and SO_4^{2-} on Cr(VI) removal. They had found that Langmuir data well fitted these experimental data and Langmuir showed the highest sorption capacity that is 3.15 mg/g as compared to the Freundlich model, 1.397 mg/g.

Han *et al.* [61] investigated the biosorption and bioreduction of Cr(VI) by *Chlorella miniata*, a microalgal isolate. The kinetics and equilibrium of Cr(VI) removal indicated that increasing Cr(VI) concentration from 50 to 200 g/L increases Cr(VI) absorption, whereas raising pH from 1-4 decreases Cr(VI) removal percentage. The amount of biomass present had an important impact on the decrease and adsorption of Cr(VI). As biomass concentration rises from 1 to 5 g/L, the percent of Cr(VI) removed rises as well. The ideal pH and biomass concentrations were 2 and 2 g/L, respectively. They also conducted a desorption study using 0.5 M NaOH, 0.5 M HCL, and deionized water, finding that the majority of the Cr(VI) was converted to Cr(III) and that 0.5 M NaOH had a better potential for total chromium recovery than 0.5 M HCL and deionized water. They have found that biosorption-bioreduction model had a higher value of R^2 as compared to the direct bioreduction model.

Using the green alga *Ulva Lactuca* and its activated carbon, EL-Sikaily *et al.* [62] researched the eradication of chromium from aqueous solution, wastewater, and saline water. They had found that by enhancing the biosorption time and adsorbent dose the removal efficiency of chromium also increases for both adsorbents and at the same time by increasing the pH and metal ion concentration the removal efficiency of chromium starts decreasing for both adsorbents. Optimum pH was 1. According to the authors the Langmuir model complemented the experimental data as compared to other models.

According to the Langmuir model, the highest adsorption capacity of activated carbon and green alga *Ulva Lactuca* was 112.36 and 10.61 mg/g, respectively. They also discovered that the pseudo-second order model matched the actual data. Activated carbon and green alga had shown the maximum removal and uptake of chromium which was 100 %, 59.55% and 96.52 mg/g, 10.5 mg/g from synthetic seawater. The biosorption of Cr(VI) from aqueous solutions by green algae *Spirogyra* species was tested by Gupta et al. [63]. They assessed pH, contact duration, and adsorbent dosage, as well as other variables in Cr(VI) adsorption. The initial concentration of Cr(VI) was changed from 1 to 25 mg/L. The authors have found that adsorption capacity basically depended upon the pH. They have

also noticed that by increasing the pH from 1-5 the removal of Cr(VI) started decreasing and at the same time by increasing the contact time (0-200 min) and adsorbent dose (1-25 g/L) the removal of Cr(VI) started increasing. The research group used the Langmuir model to study the adsorption isotherm and discovered that the maximum removal of Cr(VI) from aqueous solution was 14.7×10^3 mg/kg biomass at pH 2 with an initial Cr(VI) concentration of 5 mg/L and a contact duration of 120 minutes. *Spirogyra* species, a kind of green algae, showed the capacity to extract Cr(VI) from industrial wastewaters. Comparison of biosorption capacities of Cr(VI) removal with different adsorbents is being tabulated in Table 2.

Table 2. Comparison of biosorption capacities of Cr(VI) removal with different adsorbents

Adsorbent	Kinetics	Sorption-Isotherm Model	Optimum pH	Sorption Capacity, mg/g	Reference
<i>Tamarindus Indica</i>	First order	Freundlich	2	90	[64]
<i>Phanera vahilii</i> fruit biomass based activated carbon	Pseudo-second order	Freundlich	2	159.1-278.5	[10]
Heat-treated microalgae <i>Chlamydomonas reinhardtii</i>	Second order	Langmuir	2	25.6	[65]
<i>Rhizopus nigricans</i>	Langergren model	Langmuir and Freundlich	2	47	[66]
<i>Dunaliella</i> species	Pseudo-second order	Langmuir and Freundlich	2	45.5-58.3	[67]
<i>Spirulina platensis</i>	Initially zero order followed by first order	Langmuir and Freundlich	1.5	148.64	[68]
<i>Chlorella vulgaris</i>				140	
Acid-treated green alga <i>Oedogonium hatei</i>	Pseudo-first order	Langmuir and Freundlich	2	35.2	[69]
Date pit and olive stone	Pseudo-second order	Freundlich	2	82.63 and 53.31	[70]
Banana peel dust	Pseudo-first and pseudo-second order	Langmuir	1	26.46	[71]
<i>Bacillus cereus</i>	Pseudo-second order	Langmuir and Freundlich	2	86	[72]
<i>Luffa cylindrica</i> activated carbon	Pseudo-first order	Freundlich	8	188.50	[73]
Sulfuric acid activated strychnine tree fruit shell	Pseudo-second order	Langmuir and Freundlich	2	100	[74]
Phosphoric acid activated strychnine tree fruit shell				142.85	

CONCLUSION

Hexavalent chromium is a very lethal, known carcinogen that is classified as a major environmental contaminant. This review focuses on the chemistry of employing microbes to treat Cr(VI)-containing wastes. There is ample literature available to demonstrate the role of microbes in Cr(VI) biosorption and reduction. A broad range of microorganisms including bacteria, fungi, yeasts, and many more have demonstrated efficient reduction under a variety of conditions, including pH, temperature, contact time, agitation, nutritional medium, initial Cr concentration, adsorbent dose and many more, as described in the literature. Cr(VI) can be adsorbed by attaching to the functional mass of certain living or dead cells. Bacteria, fungi, plants, algae, and other microbes highlight the feasibility to bioreduce or biosorb Cr(VI) due to their diverse life cycles. In these findings with the removal of potentially hazardous metal such as Cr(VI), as presented in this review, the application of microbes to adsorb or reduce Cr(VI) is considered to be a developing, low-cost biotechnological approach.

Authors' contributions: Methodology and original draft preparation by Aman Pathania and Devyani Thapliyal, Supervision and formal analysis by Raj Kumar Arya.

Acknowledgement: The authors are very thankful to the authorities of Fuel Cell Department, Korea Institute of Energy Research (KIER), Daejeon and the Department of Chemical Engineering, Dr. B. R. Ambedkar National Institute of Technology, Jalandhar for necessary support to complete this review on time. Authors are highly thankful to Sarada Paul Roy for language proof reading, language editing, and restructuring the manuscript.

REFERENCES

1. Y.-G. Liu, W.-H. Xu, G.-M. Zeng, X. Li, H. Gao, *Process Biochemistry*, **41**, 1981 (2006).
2. A. Shugaba, F. Buba, B. Kolo, A. Nok, D. Ameh, J. Lori, *J. Pet. Environ. Biotechnol*, **3**, 119 (2012).
3. G. Dönmez, N. Koçberber, *Process Biochemistry*, **40**, 2493 (2005).
4. A.V. Bankar, A.R. Kumar, S.S. Zinjarde, *Journal of Hazardous Materials*, **170**, 487 (2009).
5. J.G.S. Mala, D. Sujatha, C. Rose, *Microbiological Research*, **170**, 235 (2015).
6. C.-H. Lin, C.-H. Lai, Y.-P. Peng, P.-C. Wu, K.-Y. Chuang, T.-Y. Yen, Y.-K. Xiang, *Environmental Science and Pollution Research*, **26**, 33906 (2019).
7. M. Junaid, M.Z. Hashmi, R.N. Malik, D.-S. Pei, *Environmental Science and Pollution Research*, **23**, 20151 (2016).
8. K. Oginawati, S.H. Susetyo, F.A. Rosalyn, S.B. Kurniawan, S.R.S. Abdullah, *Environmental Science and Pollution Research*, **28**, 14000 (2021).
9. J. Chen, Q. Liang, S. Ploychompoo, H. Luo, *Environmental Science and Pollution Research*, **27**, 10715 (2020).
10. . Ajmani, T. Shahnaz, S. Subbiah, S. Narayanasamy, *Environmental Science and Pollution Research*, **26**, 32137 (2019).
11. K. Pillay, E.M. Cukrowska, N.J. Coville, *Journal of Hazardous Materials*, **166**, 1067 (2009).
12. L. Jin, L. Chai, L. Ren, Y. Jiang, W. Yang, S. Wang, Q. Liao, H. Wang, L. Zhang, *Environmental Science and Pollution Research*, **26**, 31099 (2019).
13. X. Zhang, J. Gao, S. Zhao, Y. Lei, Y. Yuan, C. He, C. Gao, L. Deng, *Environmental Science and Pollution Research*, **26**, 32928 (2019).
14. F. Fu, Q. Wang, *Journal of Environmental Management*, **92**, 407 (2011).
15. A. Jusoh, L.S. Shiung, M. Noor, *Desalination*, **206**, 9 (2007).
16. K.C. Kang, S.S. Kim, J.W. Choi, S.H. Kwon, *Journal of Industrial and Engineering Chemistry*, **14**, 131 (2008).
17. G. Lee, J.G. Hering, *Journal of Water Supply: Research and Technology-Aqua*, **52**, 319 (2003).
18. A. Martin, R. Huerta, S. Pérez Castrejón, S. Hoyos, I. Villegas-Mendoza, S. Gelover, P. Drogui, G. Buelna, *Separation and Purification Technology*, **200**, 266 (2018).
19. A.K. Golder, A.N. Samanta, S. Ray, *Separation and Purification Technology*, **53**, 33 (2007).
20. A. Çimen, *Russian Journal of Physical Chemistry A*, **89**, 1238 (2015).
21. I. Korus, K. Loska, *Desalination*, **247**, 390 (2009).
22. A.M. Shahalam, A. Al-Harthy, A. Al-Zawhry, *Desalination*, **150**, 235 (2002).
23. P. Eriksson, *Environmental Progress*, **7**, 58 (1988).
24. M. Sadrzadeh, T. Mohammadi, J. Ivakpour, N. Kasiri, *Chemical Engineering and Processing: Process Intensification*, **48**, 1371 (2009).
25. L.K. Wang, D.A. Vaccari, Y. Li, N.K. Shammass, Chemical Precipitation, in: L.K. Wang, Y.-T. Hung, N.K. Shammass (eds.) *Physicochemical Treatment Processes*, Humana Press, Totowa, NJ, 2005, p. 141.
26. J.S. Whang, D. Young, M. Pressman, *Environmental Progress*, **1**, 110 (1982).
27. S.A. Mirbagheri, S.N. Hosseini, *Desalination*, **171**, 85 (2005).
28. Y. Ku, I.-L. Jung, *Water research*, **35**, 135 (2001).
29. A. Dąbrowski, Z. Hubicki, P. Podkościelny, E. Robens, *Chemosphere*, **56**, 91 (2004).
30. S. Rengaraj, K.-H. Yeon, S.-H. Moon, *Journal of Hazardous Materials*, **87**, 273 (2001).
31. M. Pansini, C. Colella, M. De Gennaro, *Desalination*, **83**, 145 (1991).
32. S.-Y. Kang, J.-U. Lee, S.-H. Moon, K.-W. Kim, *Chemosphere*, **56**, 141 (2004).
33. B. Alyüz, S. Veli, *Journal of Hazardous Materials*, **167**, 482 (2009).

34. A. Deepa, A. Singh, A. Singh, B.K. Mishra, *Environmental Science and Pollution Research*, **28**, 9864 (2021).
35. T.B. Ozer, I.A. Erkaya, A.U. Udoh, D.Y. Duygu, A. Akbulut, G. Bayramoglu, M.Y. Arica, *Environmental Science and Pollution Research*, **19**, 2983 (2012).
36. T. Fukuda, K. Tsutsumi, Y. Ishino, T. Satou, A. Ogawa, H. Morita, *Journal of Environmental Biotechnology*, **8**, 111 (2008).
37. P. Fernandez, M. Martorell, J. Farina, L. Figueroa, *The Scientific World Journal*, (2012).
38. L. Philip, L. Iyengar, C. Venkobachar, *Journal of Environmental Engineering*, **124**, 1165 (1998).
39. C. Garbisu, I. Alkorta, M.J. Llama, J.L. Serra, *Biodegradation*, **9**, 133 (1998).
40. A. Ganguli, A. Tripathi, *Applied Microbiology and Biotechnology*, **58**, 416 (2002).
41. D. Park, Y.-S. Yun, J.H. Jo, J.M. Park, *Water Research*, **39**, 533 (2005).
42. S. Bai, T.E. Abraham, *Bioresource Technology*, **79**, 73 (2001).
43. H. Rezaei, *Arabian Journal of Chemistry*, **9**, 846 (2016).
44. C. Balan, D. Bilba, M. Macoveanu, *Journal of the Serbian Chemical Society*, **74**, 953 (2009).
45. V. Gopalakannan, S. Periyasamy, N. Viswanathan, *Carbohydrate Polymers*, **151**, 1100 (2016).
46. Y. Pan, P. Cai, M. Farmahini-Farahani, Y. Li, X. Hou, H. Xiao, *Applied Surface Science*, **385**, 333 (2016).
47. J.G.S. Mala, B.U. Nair, R. Puvanakrishnan, *The Journal of General and Applied Microbiology*, **52**, 179 (2006).
48. H. Uzun, Y.K. Bayhan, Y. Kaya, A. Cakici, O.F. Algur, *Bioresource Technology*, **85**, 155 (2002).
49. N. Daneshvar, D. Salari, S. Aber, *Journal of Hazardous Materials*, **94**, 49 (2002).
50. Z. Aksu, Y. Sag, T. Kutsal, *Environmental Technology*, **11**, 33 (1990).
51. S.A. Dean, J.M. Tobin, *Resources, Conservation and Recycling*, **27**, 151 (1999).
52. R. Prakasham, J.S. Merrie, R. Sheela, N. Saswathi, S. Ramakrishna, *Environmental Pollution*, **104**, 421 (1999).
53. Y. Sağ, T. Kutsal, *Biotechnology Letters*, **11**, 141 (1989).
54. M. Dakiky, M. Khamis, A. Manassra, M. Mer'Eb, *Advances in Environmental Research*, **6**, 533 (2002).
55. B. Kiran, A. Kaushik, C. Kaushik, *Journal of Hazardous Materials*, **141**, 662 (2007).
56. S.K. Das, A.K. Guha, *Colloids and Surfaces B: Biointerfaces*, **60**, 46 (2007).
57. D. Kratochvil, P. Pimentel, B. Volesky, *Environmental Science & Technology*, **32**, 2693 (1998).
58. S. Basha, Z. Murthy, B. Jha, *Chemical Engineering Journal*, **137**, 480 (2008).
59. P. Suksabye, P. Thiravetyan, W. Nakbanpote, S. Chayabutra, *Journal of Hazardous Materials*, **141**, 637 (2007).
60. H. Gao, Y. Liu, G. Zeng, W. Xu, T. Li, W. Xia, *Journal of Hazardous Materials*, **150**, 446 (2008).
61. X. Han, Y.S. Wong, M.H. Wong, N.F.Y. Tam, *Journal of Hazardous Materials*, **146**, 65 (2007).
62. A. El-Sikaily, A. El Nemr, A. Khaled, O. Abdelwehab, *Journal of Hazardous Materials*, **148**, 216 (2007).
63. V. Gupta, A. Shrivastava, N. Jain, *Water Research*, **35**, 4079 (2001).
64. G.S. Agarwal, H.K. Bhuptawat, S. Chaudhari, *Bioresource Technology*, **97**, 949 (2006).
65. M.Y. Arica, İ. Tüzün, E. Yalçın, Ö. İnce, G. Bayramoğlu, *Process Biochemistry*, **40**, 2351 (2005).
66. S.B. R. T. E. Abraham, *Bioresource Technology*, **79**, 73 (2001).
67. G. Dönmez, Z. Aksu, *Process Biochemistry*, **38**, 751 (2002).
68. S. Gokhale, K. Jyoti, S. Lele, *Bioresource Technology*, **99**, 3600 (2008).
69. V. Gupta, A. Rastogi, *Journal of Hazardous Materials*, **163**, 396 (2009).
70. C. Mangwandi, T. Kurniaa, A. Albadarin, *Chemical Engineering Research and Design*, **156**, 251 (2020).
71. N.K. Mondal, A. Samanta, S. Chakraborty, W.A. Shaikh, *Sustainable Water Resources Management*, **4**, 489 (2018).
72. P.F. Nguema, Z. Luo, J. Lian, *Frontiers of Chemical Science and Engineering*, **8**, 454 (2014).
73. K. Nwosu-Obieogu, B.I. Okolo, *Environmental Quality Management*, **29**, 23 (2020).
74. E. Nakkeeran, N. Selvaraju, *International journal of Phytoremediation*, **19**, 1065 (2017).

Influence of the excessive use of fertilizer on the soil attributes: A case study

A. Gupta, M. Patel*, R. Singh

DR BR Ambedkar National Institute of Technology, Jalandhar, Punjab, India

Received: December 23, 2021; Revised: February 28, 2022

In the past few years, the increase in the population has also caused a significant increase in the demand for edible products such as cereals and vegetables. Therefore, in order to meet the demand, several types of fertilizers and pesticides have been considered in agricultural fields. The fertilizers and pesticides excel the growth of these products but at the same time, these chemical products also harm the soil characteristics such as the amount of organic matter, pH and electric conductivity, etc., due to their excessive application. By testing the soil characteristics of any agricultural field, the type and extent of treatment that is required can be evaluated. Therefore, an area of Lalri Village, Hamirpur, Himachal Pradesh has been selected to check the effects of fertilizer and pesticides on the fields of potato, peas and bitter gourd. The soil characteristics of the agricultural fields of these three crops were compared and found higher than the permissible limits. The present study aims to provide important information about the toxic effects of these chemicals on human health and the environment.

Keywords: Fertilizer, Soil, Hazardous, Organic content

INTRODUCTION

The demand of food production has been significantly increased in the past few years. More than one-third of the population of the world depends upon agriculture [1]. One-third of the world's cereal production rose from 1970 to 1980, with half of the rise in India's grain production due to greater fertilizer use [2]. It is expected that by year 2050, the consumption of nitrogen (N), phosphorus (P), and potassium (K) will grow by 172%, 175%, and 150%, respectively. Usually, fertilizers and pesticides are used to improve the growth and quality of any agricultural product, but, the uncontrolled and long-term use of fertilizers has become a major source of soil and water contamination in recent years [3, 4]. Over time, the soil of agricultural fields gets deteriorated because of the accumulation of heavy metals and other hazardous compounds as a result of excessive application of fertilizers. These toxic compounds have a greater affinity to cause harm to human health and environment [5]. It is estimated that over 10,000 casualties per year have been caused by the application of chemical fertilizers in the field in developing countries [6].

Currently, India is one of the largest producers of chemical fertilizers and pesticides with the production of 90,000 tons per year [7, 8]. Irritation to eyes and chronic health problems such as cancer, nervous system and reproductive disorders have been commonly observed in the spray workers [9, 10]. Besides the increase in the agricultural productivity, many direct and indirect negative effects have been caused by these toxic chemicals in the past few decades. In Himachal Pradesh, various

types of edible products such as tomato, potato, bitter gourd, cauliflower, cabbage, pea and capsicum are grown by the farmers [11, 12]. According to a report, the consumption of NPK in the Himachal Pradesh has been increased from 7.2 kg per hectare to 10.84 kg per hectare in the past 5 years [13]. Because of the incapability of soil to absorb more nutrients, the amount of fertilizer used to distribute in the field is usually increased by the farmers during its application [14–18].

Therefore, considering the problems caused by the chemical fertilizer on human health and environment, the current case study has been undertaken to assess its impact on the three edible products such as potato, peas, and bitter gourd. The agricultural fields of Lalri village of Himachal Pradesh have been considered to evaluate the soil parameters such as pH, organic carbon and NPK. The current study also aims to provide the relevant information to the local farmers and authorities about the presence and mitigation measures so as to prevent environmental and health problems.

METHODOLOGY

Study area

'Lalri' is a region in Hamirpur District that is part of the study area. Lalri village has a population of 2358 people and a land area of 109.18 hectares. Fig. 1 illustrates the area selected for the current study.

Cropping system and soil sampling analysis

Potatoes, peas, and bitter gourd were selected as the three cropping systems. The chosen cropping systems were replicated six times, and uncultivated land was used as a control group. Samples of soil

* To whom all correspondence should be sent:
E-mail: patelm@nitj.ac.in

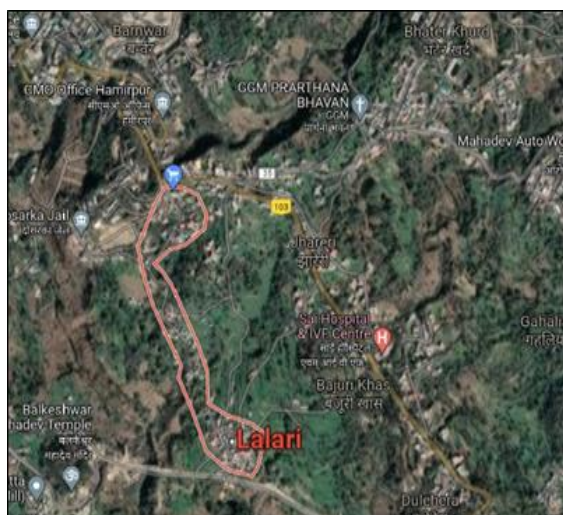


Fig 1. Study area selected in the study

electric conductivity and organic carbon concentration in the soil.

The analysis of the samples in the current research was conducted at the Chaudhary Sarwan Kumar Himachal Pradesh Krishi Vishwavidyalaya Agricultural University Palampur.

Sampling processing

To collect the soil samples, two depths were selected. The samples were collected from 0 to 15 cm of the surface and 15 to 30 cm of the subsurface. With the aid of a steel soil auger, soil samples were obtained from different depths. Using a wooden rod and a dryer, soil samples were pushed through a 2 mm sieve. After the collection, the samples were transported back to the lab for analysis. Table 1 and Fig. 2 lists the methodologies and tools utilized in this investigation.

were taken from a variety of locations in order to determine the effects of nutrient availability, pH,

Table 1. Equipment used to evaluate the different parameter in present study

Parameters	Instrument/Method used
pH	Glass electrode method (soil: water suspension 1:2.5)
Electrical conductivity	Soil water suspension (1:2)
Organic carbon	Walkey and Black (Rapid titration method)
Available nitrogen	Alkaline potassium permanganate method
Available phosphorus	Olsen's method (Ascorbic acid reductant method)
Available potassium	Flame photometer

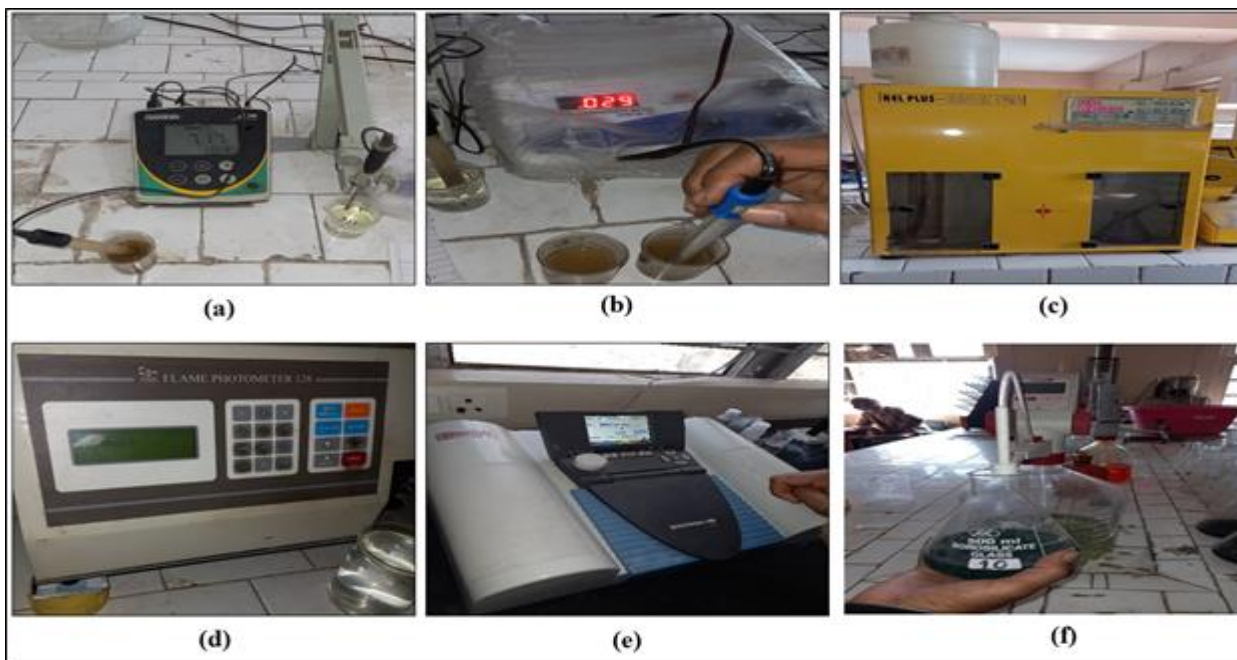


Fig. 2. (a) pH meter (b) Electrical conductivity meter (c) KEL Plus for available nitrogen (d) Flame photometer for potassium (e) Spectronic 200 for phosphorus (f) Rapid titration method for organic carbon

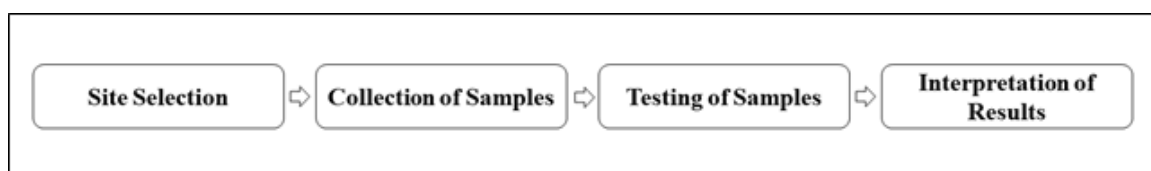


Fig. 3. Flowchart of the processes involved in the study

Sample testing

The analysis of the samples collected throughout the current study were conducted at the Chaudhary Sarwan Kumar Himachal Pradesh Krishi Vishwavidyalaya Agricultural University, Palampur. Fig. 3 represents the steps involved during the execution of the current study.

RESULTS AND DISCUSSION

Effect of pH

The pH values of the samples collected from the surface and subsurface layers ranged from 5.82-7.00 and 5.6-6.91, respectively. The pH of uncultivated agricultural soil has been reported to be around 6.34. The pH level of subsurface soil is lower than that of surface soil, although the overall systemic trend is the same. There is no correlation between soil pH and soil characteristics in different agricultural systems. Table 2 shows the findings of the pH of the soil at different sites.

Effect of electrical conductivity

Measured electrical conductivity in surface soil and subsurface soil was in the range of 0.024 to 0.070 ds m^{-1} and 0.018 to 0.051 ds m^{-1} , respectively. The electrical conductivity of crops is presented in sequence: Bitter gourd (0.070) > peas (0.055) > potatoes (0.041). Table 2 shows the findings of the electrical conductivity of soil at different locations. Electrical conductivity was found to be lower in subsurface soil than in surface soil. The samples from uncultivated agricultural soil shows electrical conductivity around 0.89 ds m^{-1} . The range of values for EC under different agricultural systems was typical and did not affect soil salinity concentrations. In the literature it has been stated by the researcher that the typical range of EC in agriculture soil can range from 0.05-0.7 ds m^{-1} [19].

Effect of organic carbon

For surface soil and subsurface soil, the organic carbon ranged from 1.99 to 2.53 % and 1.33 to 2.2%, respectively. Potatoes (2.533), peas (2.50), and bitter gourd (2.48) had the highest organic carbon values in soil. The control soil samples show organic carbon around 0.45% which is much less than the surface and subsurface values for all three edible products. Table 2 presents the organic carbon levels of soil

samples collected from the different locations. Compared to surface soil, subsurface soil has a lower organic carbon value. Potato-based cropping had a greater percentage of organic carbon than other cropping systems. The main reason behind this is higher carbon stock is due to the use of long-term organic manure [20–22].

Available NPK

A major effect on soil nutrient availability has occurred in the research area's agricultural system. The findings of the NPK analysis of soils from different locations are provided in Table 3. Subsurface soil has a lower nutritional value than surface soil, regardless of the cropping schemes. Potatoes have a substantially larger amount of accessible nutrients than other crops due to the usage of inorganic fertilizers [22–24]. It has also been observed that the values of NPK samples of all three edible products were significantly more than the permissible limits and control samples [25].

CONCLUSION

The cropping patterns in Himachal Pradesh had a substantial impact on nutrient availability, organic carbon, and physical and chemical characteristics, according to the research. It was reported that the values of these parameters were greater than the permitted limits. NPK fertilisers and insecticides are heavily employed in the agricultural systems of the research area. There are a number of harmful effects on human health and on the environment as a result of excessive fertiliser use. In order to prevent future degradation of soil properties, it is necessary to regulate sustainable methods of soil management. To effectively fertilise the soil, the soil must first be thoroughly analysed. Fertilizer consumption should be reduced by educating farmers about the negative effects of fertilisers and pesticides on human and environmental health. Agrochemicals can be reduced in the agricultural sector by using manures, composts, and vermicompost that are organic.

Acknowledgement: The authors of the study would like to acknowledge the staff of Chaudhary Sarwan Kumar, Himachal Pradesh Krishi Vishwavidyalaya Agricultural University, Palampur for providing assistance during the soil analysis.

Table 2. The values of pH, electrical conductivity and organic carbon in the surface and subsurface soils

Cropping systems	pH			EC			OC		
	Control	Surface	Subsurface	Control	Surface	Subsurface	Control	Surface	Subsurface
	6.34 ±0.43			0.089 ±0.002			0.45 ±0.06		
Potatoes:									
Site 1		5.82 ±0.54	5.6 ±0.8		0.029 ±0.002	0.024 ±0.001		1.756 ±0.92	1.33 ±0.62
Site 2		6.16 ±0.34	6.37 ±0.56		0.041 ±0.005	0.038 ±0.004		2.42 ±0.54	2.1 ±0.35
Site 3		7 ±0.31	6.91 ±0.41		0.03 ±0.004	0.034 ±0.001		2.533 ±0.86	2.13 ±0.74
Peas:									
Site 1		6.22 ±0.85	6.03 ±0.49		0.04 ±0.004	0.026 ±0.003		2.47 ±0.35	2.07 ±0.33
Site 2		5.79 ±0.56	5.66 ±0.62		0.025 ±0.001	0.018 ±0.005		2.39 ±0.54	2.19 ±0.02
Site 3		6.53 ±0.37	6.41 ±0.54		0.055 ±0.006	0.04 ±0.001		2.5 ±0.86	2.26 ±0.25
Bitter Gourd:									
Site 1		6.65 ±0.64	6.56 ±0.43		0.024 ±0.002	0.02 ±0.001		2.48 ±0.56	2.07 ±0.32
Site 2		6.42 ±0.07	6.27 ±0.34		0.07 ±0.008	0.051 ±0.001		2.19 ±0.24	1.63 ±0.28
Site 3		6.51 ±0.54	6.39 ±0.65		0.039 ±0.002	0.031 ±0.004		1.93 ±0.61	1.7 ±0.46

Table 3. Status of available nutrient availability under different cropping in Himachal Pradesh

Cropping systems	Nitrogen (kg ha ⁻¹)			Phosphorus (kg ha ⁻¹)			Potassium (kg ha ⁻¹)		
	Control	Surface	Subsurface	Control	Surface	Subsurface	Control	Surface	Subsurface
	260.87 ±12			16.7 ±2.28			206.08 ±2.9		
Potatoes:									
Site 1		445.52 ±12.3	381.79 ±2.5		26.9 ±2.53	18.53 ±1.75		416.05 ±5.4	348.48 ±5.644
Site 2		505.1 ±9.54	387.6 ±6.31		31.55 ±3.51	26.13 ±2.4		415.68 ±2.93	357.87 ±4.65
Site 3		538.7 ±13.2	518.6 ±9.14		30.3 ±2.4	27.76 ±2.3		422.28 ±2.23	396.79 ±4.87
Peas:									
Site 1		515.63 ±3.64	456.03 ±6.26		31.18 ±3.6	26.16 ±1.1		386.03 ±3.28	343.48 ±2.65
Site 2		521.66 ±4.1	477.92 ±3.5		28.53 ±2.2	24.28 ±1.97		419.32 ±2.92	357.76 ±6.2
Site 3		495.54 ±9.34	464.1 ±2.31		29.79 ±4.2	23.08 ±1.093		357.68 ±6.2	333.65 ±10.2
Bitter Gourd:									
Site 1		497.26 ±5.23	467.66 ±6.39		30.48 ±2.94	24.52 ±3.1		383.8 ±4.1	367.42 ±1.7
Site 2		515.73 ±3.63	463.34 ±2.4		27.4 ±2.34	19.66 ±0.63		364.8 ±7.63	365.76 ±3.3
Site 3		489.73 ±8.32	428.51 ±5.22		28.93 ±2.12	25.6 ±1.9		418.23 ±6.2	386.13 ±0.63

REFERENCES

1. P. Joshi, T. Trivedi, R. Sharma, S. Verma, V. Bharti, K. Gyota, ICAR's Vision 2030, 2011.
2. GRISP, Rice Almanac, 4th edn., International Rice Research Institute, Los Baños, Philippines, 2013.
3. M.N. Almasri, J.J. Kaluarachchi, *J. Hydrol.*, **295**, 225 (2004).
4. P.F. Hudak, *J. Hydrol.* **228**, 37 (2000).
5. S. Savci, *Int. J. Environ., Sci. Dev.*, **3**, 73 (2012).
6. L. Horrigan, R.S. Lawrence, P. Walker, *Environ. Health Perspect.*, **110**, 445 (2002).
7. *Planning Commission*, 2002, p. 1.
8. P.K. Gupta, *Toxicology*, **198**, 83 (2004).
9. WHO, Public Health Impact of Pesticides Used in Agriculture, 1990.
10. .R. Institute, Environmental Change and Human Health, World Resources 1998-1999, 1998.
11. *U. Seeds*, 2021.
12. ICAR, Indian Council. Agric. Res. (n.d.).
13. CEIC, Dep. Agric. Coop. (n.d.).
14. A.A. Al-Zaidi, E.A. Elhag, S.H. Al-Otaibi, M.B. Baig, *J. Anim. Plant Sci.*, **21**, 605 (2011).
15. K.A. da Silva, V.B. Nicola, R.T. Dudas, W.C. Demetrio, L. dos S. Maia, L. Cunha, M.L.C. Bartz, G.G. Brown, A. Pasini, P. Kille, N.G.C. Ferreira, C.M.R. de Oliveira, *Sci. Rep.*, **11**, 1 (2021).
16. Y.L. Wei, L.J. Bao, C.C. Wu, Z.C. He, E.Y. Zeng, *Sci. Total Environ.*, **514**, 409 (2015).
17. B. Yargholi, S. Azarneshan, *Int. J. Agric. Crop Sci.*, **7**, 518 (2014).
18. S. Kumari, H. Sharma, *Int. J. Sci. Res.*, **3** 144 (2014).
19. N. Loria, S.K. Bhardwaj, C.K. Ndungu, *J. Appl. Nat. Sci.*, **8**, 1479 (2016).
20. B.S. Brar, J. Singh, G. Singh, G. Kaur, *Agronomy*, 220 (2015).
21. L. Chen, X. Qi, X. Zhang, Q. Li, Y. Zhang, *Chinese Geogr. Sci.*, **21** 392 (2011).
22. J. Tian, M. Fan, J. Guo, P. Marschner, X. Li, Y. Kuzyakov, *Eur. J. Soil Biol.*, **52**, 67 (2012)
23. J. Kimigo, P. Gicheru, *Pedologist*, **55**, 326 (2012).
24. N. Nisar, F.A. Lone, *J. Res. Earth Environ. Sci.*, **1**, 13 (2013).
25. AgriTech, Rat. Chart Soil Test Data (n.d.).

BULGARIAN CHEMICAL COMMUNICATIONS

Instructions about Preparation of Manuscripts

General remarks: Manuscripts are submitted in English by e-mail or by mail (in duplicate). The text must be typed double-spaced, on A4 format paper using Times New Roman font size 12, normal character spacing. The manuscript should not exceed 15 pages (about 3500 words), including photographs, tables, drawings, formulae, etc. Authors are requested to use margins of 3 cm on all sides. For mail submission hard copies, made by a clearly legible duplication process, are requested. Manuscripts should be subdivided into labelled sections, e.g. **Introduction, Experimental, Results and Discussion, etc.**

The title page comprises headline, author's names and affiliations, abstract and key words.

Attention is drawn to the following:

a) **The title** of the manuscript should reflect concisely the purpose and findings of the work. Abbreviations, symbols, chemical formulas, references and footnotes should be avoided. If indispensable, abbreviations and formulas should be given in parentheses immediately after the respective full form.

b) **The author's** first and middle name initials, and family name in full should be given, followed by the address (or addresses) of the contributing laboratory (laboratories). **The affiliation** of the author(s) should be listed in detail (no abbreviations!). The author to whom correspondence and/or inquiries should be sent should be indicated by asterisk (*).

The abstract should be self-explanatory and intelligible without any references to the text and containing not more than 250 words. It should be followed by key words (not more than six).

References should be numbered sequentially in the order, in which they are cited in the text. The numbers in the text should be enclosed in brackets [2], [5, 6], [9–12], etc., set on the text line. References, typed with double spacing, are to be listed in numerical order on a separate sheet. All references are to be given in Latin letters. The names of the authors are given without inversion. Titles of journals must be abbreviated according to Chemical Abstracts and given in italics, the volume is typed in bold, the initial page is given and the year in parentheses. Attention is drawn to the following conventions:

a) The names of all authors of a certain publications should be given. The use of “*et al.*” in the list of references is not acceptable.

b) Only the initials of the first and middle names should be given.

In the manuscripts, the reference to author(s) of cited works should be made without giving initials, e.g. “Bush and Smith [7] pioneered...”. If the reference carries the names of three or more authors it should be quoted as “Bush *et al.* [7]”, if Bush is the first author, or as “Bush and co-workers [7]”, if Bush is the senior author.

Footnotes should be reduced to a minimum. Each footnote should be typed double-spaced at the bottom of the page, on which its subject is first mentioned.

Tables are numbered with Arabic numerals on the left-hand top. Each table should be referred to in the text. Column headings should be as short as possible but they must define units unambiguously. The units are to be separated from the preceding symbols by a comma or brackets.

Note: The following format should be used when figures, equations, etc. are referred to the text (followed by the respective numbers): Fig., Eqns., Table, Scheme.

Schemes and figures. Each manuscript (hard copy) should contain or be accompanied by the respective illustrative material as well as by the respective figure captions in a separate file (sheet). As far as presentation of units is concerned, SI units are to be used. However, some non-SI units are also acceptable, such as °C, ml, l, etc.

The author(s) name(s), the title of the manuscript, the number of drawings, photographs, diagrams, etc., should be written in black pencil on the back of the illustrative material (hard copies) in accordance with the list enclosed. Avoid using more than 6 (12 for reviews, respectively) figures in the manuscript. Since most of the illustrative materials are to be presented as 8-cm wide pictures, attention should be paid that all axis titles, numerals, legend(s) and texts are legible.

The authors are asked to submit **the final text** (after the manuscript has been accepted for publication) in electronic form either by e-mail or mail on a 3.5” diskette (CD) using a PC Word-processor. The main text, list of references, tables and figure captions should be saved in separate files (as *.rtf or *.doc) with clearly identifiable file names. It is essential that the name and version of the word-processing program and the format of the text files is clearly indicated. It is recommended that the pictures are presented in *.tif, *.jpg, *.cdr or *.bmp format, the equations are written using “Equation Editor” and chemical reaction schemes are written using ISIS Draw or ChemDraw programme.

The authors are required to submit the final text with a list of three individuals and their e-mail addresses that can be considered by the Editors as potential reviewers. Please, note that the reviewers

should be outside the authors' own institution or organization. The Editorial Board of the journal is not obliged to accept these proposals.

EXAMPLES FOR PRESENTATION OF REFERENCES

REFERENCES

1. D. S. Newsome, *Catal. Rev.–Sci. Eng.*, **21**, 275 (1980).
2. C.-H. Lin, C.-Y. Hsu, *J. Chem. Soc. Chem. Commun.*, 1479 (1992).
3. R. G. Parr, W. Yang, *Density Functional Theory of Atoms and Molecules*, Oxford Univ. Press, New York, 1989.
4. V. Ponec, G. C. Bond, *Catalysis by Metals and Alloys* (Stud. Surf. Sci. Catal., vol. 95), Elsevier, Amsterdam, 1995.
5. G. Kadinov, S. Todorova, A. Palazov, in: *New Frontiers in Catalysis* (Proc. 10th Int. Congr. Catal., Budapest, 1992), L. Guzzi, F. Solymosi, P. Tetenyi (eds.), Akademiai Kiado, Budapest, 1993, Part C, p. 2817.
6. G. L. C. Maire, F. Garin, in: *Catalysis. Science and Technology*, J. R. Anderson, M. Boudart (eds), vol. 6, Springer-Verlag, Berlin, 1984, p. 161.
7. D. Pocknell, *GB Patent 2 207 355* (1949).
8. G. Angelov, PhD Thesis, UCTM, Sofia, 2001.
9. JCPDS International Center for Diffraction Data, Power Diffraction File, Swarthmore, PA, 1991.
10. *CA* **127**, 184 762q (1998).
11. P. Hou, H. Wise, *J. Catal.*, in press.
12. M. Sinev, private communication.
13. <http://www.chemweb.com/alchem/articles/1051611477211.html>.

Texts with references which do not match these requirements will not be considered for publication!!!

CONTENTS

Selected papers from the International Chemical Engineering Conference 2021 “100 Glorious Years of Chemical Engineering & Technology”, Department of Chemical Engineering, Dr. B. R. Ambedkar National Institute of Technology, Jalandhar, Punjab, India, September 16 to 19, 2021

<i>M. Gupta, A. Kumar, S. Kumar</i> , Review of lead flows in the anthropogenic environment.....	5
<i>J. N. Srivastava, S. K. Gupta</i> , Enhancement of low-temperature impact toughness of polycarbonate by hydroxyl terminated siloxanes and its concomitant effects on other properties.....	11
<i>J. Srivastava, T. Nandi, R. K. Trivedi</i> , Comparative study of castor oil and dehydrated castor oil as lubricants.....	18
<i>M. Hanief, K. Zaman, S. Ul Bashir, J. Showkat, M. Zubair</i> , Investigation on cypress wood membrane for water filtration	25
<i>M. Gupta, A. Kumar, S. Kumar, M. K. Jat</i> , Substance flow analysis of lead and chromium through wastewater management system in a region.....	32
<i>S. Mahaboob Subhani, S. Altaf Hussain, P. D. Sankar Reddy</i> , Comparison of particle size distribution estimated by Rosin-Rammler equation vs Malvern particle size analyzer for different brands of PPC cement.....	40
<i>A. Ghosh</i> , Application of <i>Cocos nucifera</i> 's husk to remove Malachite green dye and response surface modelling.....	44
<i>Sh. Gautam, A. Gautam, M. Patel, H. Parmar, K. Patel</i> , A statistical analysis and optimization of Indian coal grinding in a laboratory ball mill: dry & wet method.....	51
<i>A. Pathania, D. Thapliya, R. Kumar Arya</i> , Reduction and biosorption of hexavalent chromium ions from wastewaters: a review.....	62
<i>A. Gupta, M. Patel, R. Singh</i> , Influence of the excessive use of fertilizer on the soil attributes: A case study.....	73
<i>INSTRUCTIONS TO AUTHORS</i>	78